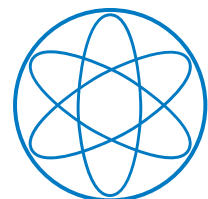
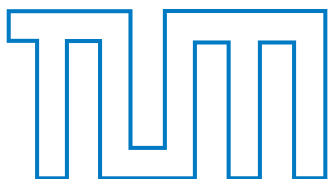
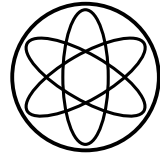

Chiral Dynamics of Heavy-Light Mesons

by

Michael Altenbuchinger

December, 2013





Physik Department
Institut für Theoretische Physik T39
Univ.-Prof. Dr. Wolfram Weise

Chiral Dynamics of Heavy-Light Mesons

Dipl.-Phys. (Univ.) Michael Christoph Altenbuchinger

Vollständiger Abdruck der von der Fakultät für Physik der Technischen Universität München zur Erlangung des akademischen Grades eines

Doktors der Naturwissenschaften (Dr. rer. nat.)

genehmigten Dissertation.

Vorsitzender: Univ.-Prof. Dr. Stephan Paul
Prüfer der Dissertation: 1. Univ.-Prof. Dr. Wolfram Weise
2. Univ.-Prof. Dr. Nora Brambilla

Die Dissertation wurde am 02.01.2014 bei der Technischen Universität München eingereicht und durch die Fakultät für Physik am 21.01.2014 angenommen.

Abstract

This thesis focuses on the physics of heavy-light mesons, i.e. quark-antiquark systems composed of a heavy (c or b) and a light (u , d or s) quark. The light-quark sector is treated within the framework of chiral effective field theory. Recent lattice QCD computations have progressed in determining the decay constants of charmed mesons and the scattering lengths of Nambu-Goldstone bosons (pions, kaons) off D mesons. These computations are performed for light quark masses larger than the physical ones. A chiral extrapolation down to physical masses is necessary. It is commonly performed using chiral perturbation theory. The related systematical uncertainties have to be examined carefully. In this thesis it is shown how these uncertainties can be reduced significantly by taking into account relativistic effects in the chiral extrapolations. As a byproduct, estimates are presented for several physical quantities that are related by heavy-quark spin and flavor symmetry. Furthermore, the investigation of the light-quark mass dependence of the scattering lengths of Nambu-Goldstone bosons off D mesons provides important information on the nature of one of the intriguing newly discovered resonances, the $D_{s_0}^*(2317)$. It is shown that this resonance can be dynamically generated from the coupled-channels DK interaction without a priori assumption of its existence. Finally we demonstrate how the underlying framework, unitarized chiral perturbation theory, can be improved by the inclusion of intermediate states with off-the-mass-shell kinematics.

Zusammenfassung

Diese Arbeit befasst sich mit der Physik von so genannten Heavy-Light Mesonen. Dabei handelt es sich um Quark-Antiquark Systeme, die sich aus einem schweren (c oder b) und einem leichten (u , d oder s) Quark zusammensetzen. Die leichten Quarks lassen sich im Rahmen der Chiralen Effektiven Theorie beschreiben. Aktuelle Gitter QCD Simulationen haben in den letzten Jahren große Fortschritte gemacht. Sie bieten Ergebnisse für Zerfallskonstanten von D Mesonen sowie für die Streuung von Nambu-Goldstone Bosonen (Pionen, Kaonen) an D Mesonen. Diese Simulationen werden für u und d Quarks durchgeführt, die deutlich schwerer sind als die tatsächlichen physikalischen Quarks. Dies erfordert eine chirale Extrapolation zu physikalischen Quarkmassen, was üblicherweise im Rahmen der Chiralen Effektiven Theorie durchgeführt wird. Die damit verbundenen systematischen Unsicherheiten müssen jedoch gründlich untersucht werden. In dieser Arbeit wird gezeigt, wie sie sich im Rahmen einer relativistischen Theorie signifikant reduzieren lassen. Ausserdem ist es uns möglich für mehrere physikalische Größen, unter Verwendung der Spin- und Flavor-Symmetrie des schweren Quarks, Vorhersagen zu treffen. Angewendet auf die Streuung von Nambu-Goldstone Bosonen an D Mesonen geben diese Rechnungen wichtige Hinweise auf die Zusammensetzung einer der meist diskutierten neu entdeckten Resonanzen, bezeichnet als $D_{s0}^*(2317)$. Es wird gezeigt, dass sie dynamisch generiert werden kann durch die DK Wechselwirkung in gekoppelten Kanälen, wobei keine Annahmen über die Existenz dieser Resonanz erforderlich sind. Abschließend wird demonstriert wie die zugrundeliegende Theorie, die Unitarisierte Chirale Störungstheorie, verbessert werden kann. Dabei werden Zwischenzustände berücksichtigt, die sich nicht auf der Massenschale befinden.

Contents

1	Introduction	11
2	Heavy-quark symmetry	15
2.1	The physical picture	15
2.2	The heavy-quark limit of QCD	16
2.3	Spectroscopical implications	18
3	The chiral effective Lagrangian	19
3.1	Chiral perturbation theory	19
3.2	Representation of heavy-light meson fields	20
3.3	Covariant Lagrangian for heavy-light mesons	22
4	SU(3) breaking corrections to the D, D*, B, and B* decay constants	25
4.1	Light quark mass dependence of the D and D_s decay constants	25
4.1.1	Theoretical framework	27
4.1.2	The extended-on-mass-shell (EOMS) scheme	31
4.1.3	Results and discussion	33
4.2	Predictions on $f_{D_s^*}/f_{D^*}$, f_{B_s}/f_B , and $f_{B_s^*}/f_{B^*}$ in NNLO covariant ChPT	36
5	Scattering of Nambu-Goldstone bosons off heavy-light mesons	45
5.1	Introduction	45
5.2	The T-matrix, unitarity, and the Bethe-Salpeter equation	47
5.2.1	The S- and T-matrix	47
5.2.2	The Bethe-Salpeter equation	48
5.2.3	Partial-wave and isospin decomposition	51
5.3	Chiral potentials	53
5.3.1	Off-shell potentials	53
5.3.2	Partial-wave projected on-shell potentials	57
5.4	The scattering of Nambu-Goldstone bosons off heavy-light mesons in the HQS scheme	62
5.4.1	Renormalization scheme motivated by heavy-quark symmetry	62
5.4.2	Results and discussions	65

5.5	Off-shell effects on the light-quark mass evolution of scattering lengths	78
5.5.1	Framework	78
5.5.2	Results and discussions	84
6	Summary and conclusions	87
7	Acknowledgements	89
A	Appendix	91
A.1	Loop functions	91
A.2	Partial wave decomposition for $P^*\phi$ scattering	93
A.3	“Renormalization” of the BS equation	98
A.4	Charmed and bottomed mesons from PDG [1]	99

Chapter 1

Introduction

The study of charm and bottom hadrons has provided numerous constraints on the parameters of the Standard Model. Their weak decays offer the most direct way to determine the weak mixing angles, to test the unitarity of the Cabibbo-Kobayashi-Maskawa (CKM) matrix and to study CP violation. Furthermore, they have constrained many scenarios of physics beyond the Standard Model and hopefully they will give some hints for new physics in ongoing or upcoming experiments. For a review see [1] and references therein.

The elements of the CKM matrix are fundamental parameters of the Standard Model. A few of them are determined to high accuracy, as for instance $|V_{ud}|$, $|V_{us}|$ and $|V_{cs}|$, with errors mainly governed by our knowledge of form factors. For $|V_{ud}|$, this is $g_A = G_A/G_V$, known to high precision [2]. For $|V_{cs}|$, it is the D_s meson decay constant f_{D_s} , and for $|V_{us}|$ it is the form factor entering the semi-leptonic decays of kaons to pions. Those form factors can be calculated accurately in unquenched Lattice Quantum Chromodynamics (LQCD) computations [2, 3]. On the other hand, CKM matrix elements involving top or bottom quarks are less certain. The extraction of $|V_{ub}|$ requires an accurate knowledge of the B meson decay constant, f_B , or of some form factors in semi-leptonic decays of bottomed hadrons. The matrix elements $|V_{ts}|$ and $|V_{td}|$ are extracted from $B^0 - \bar{B}^0$ mixing, which requires a good knowledge of $f_{B_s}\sqrt{\hat{B}_{B_s}}$ and $f_{B_d}\sqrt{\hat{B}_{B_d}}$, where \hat{B} is the non-perturbative QCD bag parameter. All these quantities are difficult to determine in experiment and input from LQCD is needed. This, however, has significant statistical and systematical errors and accounts for the main uncertainty of these CKM matrix elements. Several supplementary methods further constrain the CKM matrix. For instance, taking the ratio $|V_{ts}|/|V_{td}|$, depending on $\xi = (f_{B_s}\sqrt{\hat{B}_{B_s}})/(f_{B_d}\sqrt{\hat{B}_{B_d}})$, reduces errors from LQCD significantly. A comprehensive review can be found in [1].

LQCD calculations obviously play a key role in constraining the Standard Model. Their uncertainties, however, have to be examined carefully. Lattice QCD calculations are performed on a discrete Euclidean lattice in a finite box. They need to be translated to Minkowski space, infinite volume and infinitesimally small lattice spacings. Additionally, most of the calculations are performed for larger than physical light-quark masses. This reduces computation costs but requires a chiral extrapolation to physical masses. A very powerful tool employed in this context is chiral effective theory, c.f. [4] for an overview. Investigating the dependence of LQCD results on pion mass, volume and lattice spacing, offers a unique opportunity to constrain many unknown low-energy constants (LECs) of chiral effective field theory. This enables us to be predictive. In

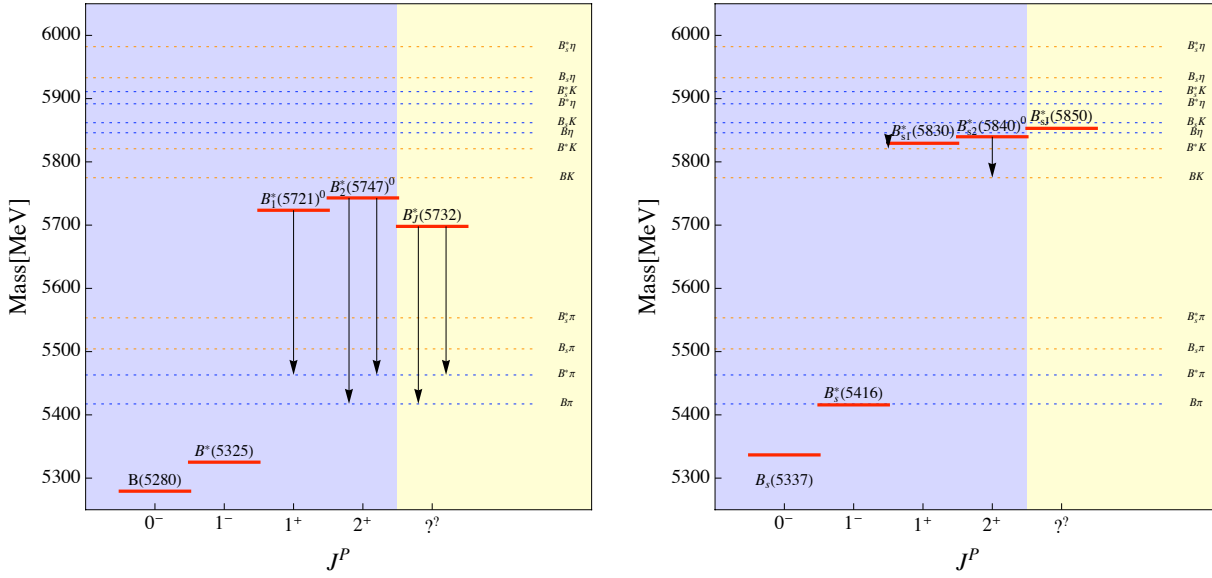


FIGURE 1.2: Bottomed mesons listed in Particle Data Group (PDG) [1]. The arrows indicate decay modes [1] and the dashed blue and orange lines show thresholds with strangeness $S = 0$ and $S = 1$.

Among the most controversially discussed states are the charmed-strange positive parity scalar and vector mesons $D_{s0}^*(2317)$ and $D_{s1}(2460)^\pm$. The $D_{s0}^*(2317)$ was first discovered in 2003 by the BaBar collaboration as a very narrow resonance in the $D_s \pi$ channel [6]. Later in 2003, it was confirmed by CLEO [7], where in addition the $D_s^* \pi$ channel was measured. This channel has resolved a narrow resonance, now known as $D_{s1}(2460)^\pm$. Since both states lie below the DK and D^*K thresholds, respectively, their S-wave decay modes $D_{s0}^*(2317) \rightarrow DK$ and $D_{s1}(2460)^\pm \rightarrow D^*K$ are kinematically forbidden. Hence, they dominantly decay either isospin violating or radiative. For this reason both resonances are very narrow. From the constituent quark model, these states might be most reasonably identified with the P-wave $c\bar{s}$ states with $J^P = 0^+$ and $J^P = 1^+$. Due to heavy-quark symmetry, it is then very natural to combine $D_{s0}^*(2317)$ and $D_{s1}(2460)^\pm$ in a doublet with $J_{s_l}^P = (0^+, 1^+)_{1/2}$, where $s_l = 1/2$ is the spin of the light degrees of freedom. However, in the constituent quark models [8], the masses of these states are about 100 MeV higher than those measured in experiment. This was the reason for numerous, still ongoing, discussions in the literature.

These two states are only a small sample of the huge number of charmed meson states discovered in recent years, c.f. Figure 1.1. A more comprehensive discussion is postponed to Chapter 5. The significant progress in the charmed meson spectroscopy came along with a few newly observed states in the bottom meson sectors, c.f. Fig. 1.2. From a theoretical point of view, the bottom mesons are of particular interest. Here arguments from heavy-quark spin symmetry can be applied to better accuracy and hence a stringent classification is easier. However, concerning spectroscopy of heavy-light mesons, the most attention is devoted to the charmed sector, simply due to the number of recently observed open charm states at Belle [9] and Babar [10, 11].

This thesis is organized as follows. In Chapter 2, the basic idea of heavy-quark symmetry and its implications on the spectrum of heavy-light mesons is investigated. Chapter 3 presents chiral effective field theory for Nambu-Goldstone bosons and heavy-light mesons together with the relevant Lagrangians. In Chapter 4, this

theory is applied. In the first part of this chapter, it is demonstrated how covariant calculations can significantly improve chiral extrapolations. The second part is devoted to predictions on the ratios $f_{D_s^*}/f_{D^*}$, f_{B_s}/f_B , and $f_{B_s^*}/f_{B^*}$. Chapter 5 investigates the scattering of Nambu-Goldstone bosons off heavy-light mesons. In this chapter we first present the prerequisites of unitarized chiral perturbation theory in Section 5.2. These are the unitarity conditions for the T matrix, the Bethe-Salpeter equation and partial-wave projections. The chiral potentials up to next-to-leading order are presented in Section 5.3. Finally, unitarized chiral perturbation theory is applied starting from Section 5.4 in combination with recent lattice computations [12]. This allows us to predict numerous states of charm and bottom mesons by use of heavy-quark spin and flavor symmetry. The next part, Section 5.5, shows some alternative results, obtained by solving the Bethe-Salpeter equation for fully momentum dependent potentials, i.e. without employing the on-shell approximation. This is shown to improve the leading order resummations significantly. A short conclusion and summary is given in Chapter 6.

Chapter 2

Heavy-quark symmetry

2.1 The physical picture

Among the six different quark flavors, three can be identified as heavy compared to the fundamental scale of Quantum Chromodynamics (QCD), $\Lambda_{\text{QCD}} \sim 0.3 \text{ GeV}$. These are c, b, t with masses of roughly 1.5 GeV, 5 GeV and 175 GeV. We concentrate on heavy-light hadrons, which are composed of one heavy quark surrounded by light (anti-)quarks and gluons. Such systems exhibit additional symmetries in the limit $\Lambda_{\text{QCD}}/m_Q \rightarrow 0$, where m_Q is the mass of the heavy quark Q . These are the heavy-quark flavor and heavy-quark spin symmetry. There are numerous review articles and lecture notes investigating these symmetries, c.f. [13–17], to name just the few of which this section did benefit most.

The physical picture of heavy-light hadrons is similar to the hydrogen atom. There the proton acts in a first approximation as a static source of electromagnetic fields: it emits and absorbs photons, whereas all recoil effects are negligible. In heavy-light hadrons, the role of the proton is played by the heavy quark and the role of the electron cloud by the light degrees of freedom of QCD¹. The light degrees of freedom carry momenta of the order of Λ_{QCD} and the momenta transferred to the heavy quark are therefore of the same order of magnitude. The momentum of the heavy quark can be decomposed as

$$p_Q = m_Q v + k, \tag{2.1}$$

where v is the velocity of the heavy quark, with $v^2 = 1$, and k is a small residual momentum of the order of Λ_{QCD} . Even if the momentum of the heavy quark can be changed by orders of Λ_{QCD} , its velocity v is only altered by orders $\Lambda_{\text{QCD}}/m_Q \ll 1$. Hence, in the limit $m_Q \rightarrow \infty$, the heavy quark becomes a static color source, where all recoil effects from the emission or absorption of gluons can be neglected. The dynamics of the surrounding cloud is still governed by non-perturbative interactions among its constituents, but its interaction with the heavy quark has simplified tremendously. From this picture it becomes clear that in this limit, the light degrees of freedom do not see the exact mass of the heavy quark (since it is static), i.e. their wave-function does not depend on the heavy-quark mass. This is heavy-quark flavor symmetry.

¹By “light degrees of freedom” we mean the complex many-body system, consisting of the light quarks and antiquarks, and gluons, that surrounds the heavy quark. Frequently, the notation “brown muck” is used in this context [13, 14].

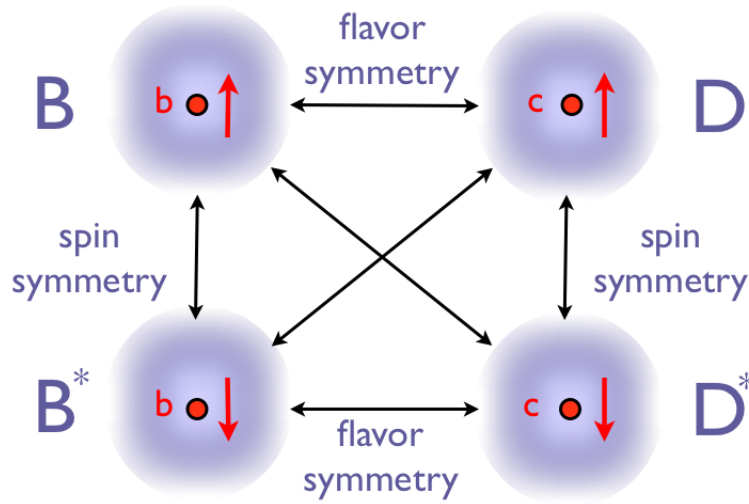


FIGURE 2.1: Visualization of heavy-quark spin and flavor symmetry for charmed and bottomed mesons.

Heavy-quark spin symmetry, on the other hand, is the statement that for $m_Q \rightarrow \infty$ the wave-function of the light degrees of freedom does not depend on the orientation of the spin of the heavy quark. The analogous situation is encountered in the hydrogen atom, where the spin dependent interaction, the spin-orbit term, enters as a relativistic correction.

A simplified visualization of how heavy-quark spin and flavor symmetry relates different kind of charm and bottom mesons can be found in Figure 2.1. Since charm and bottom quarks can be seen only approximately as infinitely heavy, these relations are valid up to corrections in $1/m_Q$, where $Q = c, b$.

2.2 The heavy-quark limit of QCD

Heavy-quark symmetries can also be understood directly from QCD. Consider the QCD Lagrangian for a heavy quark, as it can be found in a number of textbooks and review articles, [15–18],

$$\mathcal{L}_Q = \bar{Q}(i\not{D} - m_Q)Q, \quad (2.2)$$

where the heavy quark field is denoted as Q and its mass as m_Q . The gauge covariant derivative is defined as $D_\mu = \partial_\mu - igT_a A_\mu^a$, with the generators T_a of color $SU(3)$, normalized according to $\text{Tr}[T_a T_b] = \frac{1}{2}\delta_{ab}$, and the gluon field A_μ^a . Using Eq. (2.1) gives the heavy-quark propagator expanded in powers of k/m_Q ,

$$\frac{i}{\not{p}_Q - m_Q + i\epsilon} = \frac{i}{v \cdot k + i\epsilon} \frac{\not{p} + 1}{2} + \mathcal{O}(k/m_Q) \rightarrow \frac{i}{v \cdot k + i\epsilon} P_+, \quad (2.3)$$

where the projection operator $P_+ = (1 + \not{v})/2$ has been introduced. In the rest frame P_+ becomes $(1 + \gamma^0)/2$, which projects on the quark component of the Dirac spinor. The projection operator for the antiquark component is defined as $P_- = (1 - \not{v})/2$. From these definitions one obtains immediately $P_\pm P_\mp = 0$ and $P_\pm P_\pm = P_\pm$, and $P_+ \gamma_\mu P_+ = P_+ v_\mu P_+$. The last identity implies that the quark gluon vertex $igT_a \gamma^\mu$ can be

replaced by

$$igT_a v^\mu \quad (2.4)$$

at leading order in $1/m_Q$. One notices that both limits, Eq. (2.3) and Eq. (2.4), do not refer to the mass of the heavy quark, in accordance with our intuitive picture of heavy-quark flavor symmetry. The coefficient P_+ in Eq. (2.3) projects on the upper (quark) component of the spinor, whereas the remaining part of the propagator is diagonal in spin, i.e. it does not depend on the spin of the quark or antiquark field. Obviously, Eq. (2.4) is diagonal in spin space, too. Therefore the interaction does not depend on the spin orientation of the heavy quark, in accordance with heavy-quark spin symmetry.

Heavy-quark symmetries can be implemented at the Lagrangian level. This is done in the language of heavy-quark-effective theory (HQET), which is directly derived from the generating functional of QCD. There the heavy degrees of freedom can be identified and integrated out, resulting in a non-local action. Expanding in a series of local terms gives the Lagrangian of HQET [19]. Equivalently, one can perform a number of field redefinitions, Foldy-Wouthuysen transformations, to transform away the couplings to the small components of the spinors, as described in [20]. At leading order the Lagrangian of HQET can be also obtained directly from Eq. (2.2) by redefining the heavy-quark field,

$$Q(x) = \exp(-im_Q v \cdot x) (h_v(x) + H_v(x)), \quad (2.5)$$

with

$$\begin{aligned} h_v(x) &= \exp(im_Q v \cdot x) \frac{1 + \not{v}}{2} Q(x), \\ H_v(x) &= \exp(im_Q v \cdot x) \frac{1 - \not{v}}{2} Q(x), \end{aligned} \quad (2.6)$$

where the quark component is denoted by $h_v(x)$ and the antiquark component by $H_v(x)$. The exponential factor ensures that derivatives applied to $h_v(x)$ produce only momenta of the order k . Inserting Eq. (2.5) into the QCD lagrangian Eq. (2.2), and retaining only the quark component $h_v(x)$, gives the leading order lagrangian of HQET,

$$\mathcal{L}_{\text{eff}} = \bar{h}_v i v \cdot D h_v = \bar{h}_v (i v_\mu \partial^\mu + g T_a v_\mu A_a^\mu) h_v. \quad (2.7)$$

Taking into account also the antiquark part $H_v(x)$ produces corrections of higher order in $1/m_Q$, as can be shown by employing the equations of motion to express $H_v(x)$ in terms of $h_v(x)$. The Feynman rules derived from this Lagrangian are in accordance with Eq. (2.3) and Eq. (2.4). The Lagrangian (2.7) does not have a heavy-quark mass term, as a manifestation of heavy-quark flavor symmetry. Further, one notices that the Lagrangian is invariant under spin rotations,

$$h_v(x) \rightarrow (1 + i\epsilon \cdot \mathbf{S}) h_v(x), \quad \text{with} \quad S_i = \frac{1}{2} \begin{pmatrix} \sigma_i & 0 \\ 0 & \sigma_i \end{pmatrix}, \quad (2.8)$$

where σ_i are the Pauli matrices, i.e. it possesses heavy-quark spin symmetry. Breaking effects to these symmetries start at order $1/m_Q$.

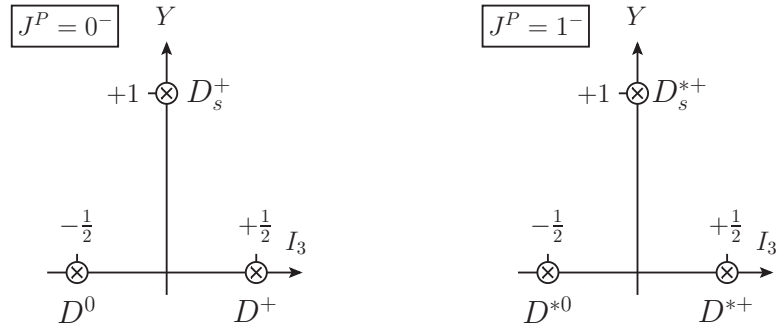


FIGURE 2.2: Weight diagrams of the ground state charmed mesons with valence quark content $c\bar{q}$ and $J^P = 0^-$ and $J^P = 1^-$.

2.3 Spectroscopical implications

Consider a general heavy-light meson with valence quark content $Q\bar{q}$. The total angular momentum \mathbf{J} of the meson is a conserved quantity. As already explained in detail, this is also the case for spin of the heavy quark, \mathbf{S}_Q , in the limit $m_Q \rightarrow \infty$. Hence,

$$\mathbf{S}_l = \mathbf{J} - \mathbf{S}_Q \quad (2.9)$$

has to be conserved in the heavy-quark limit, too. The operator \mathbf{S}_l is denoted as spin of the light degrees of freedom and represents the total angular momentum contribution of the complex many-body system, consisting of the valence antiquark \bar{q} , gluons and $q\bar{q}$ pairs, that surrounds the heavy quark Q . The associated quantum numbers are j , s_Q and s_l , entering the eigenvalues $j(j+1)$, $s_Q(s_Q+1)$ and $s_l(s_l+1)$ of the operators \mathbf{J}^2 , \mathbf{S}_Q^2 and \mathbf{S}_l^2 , respectively. The light quark with spin $s_l = \frac{1}{2}$ and the heavy-quark with spin $s_Q = \frac{1}{2}$ form a doublet with $j = \frac{1}{2} \otimes \frac{1}{2} = 0 \oplus 1$, that becomes degenerate as $m_Q \rightarrow \infty$. This doublet has negative parity, due to the opposite parity of quark and antiquark. Since heavy-quark spin symmetry is only realized approximately in charmed and bottomed hadrons, the degeneracy is lifted. For charmed mesons, this produces mass splittings between the $J^P = 0^-$ and $J^P = 1^-$ states, i.e. D and D^* mesons, of about 140 MeV. Due to the significantly larger mass of the bottom quark, the mass splitting between B and B^* is only about 50 MeV. The weight diagrams of the D meson ground state doublet is shown in Figure 2.2. The masses of bottomed and charmed mesons are listed in Table A.1 to A.4.

Chapter 3

The chiral effective Lagrangian

3.1 Chiral perturbation theory

The three quark flavors u , d and s , can be considered as light compared to the fundamental scale of QCD, $\Lambda_{\text{QCD}} \sim 0.3 \text{ GeV}$. This classification is obvious for u and d , whereas the mass of the strange quark s is almost of the same order of magnitude as Λ_{QCD} , but still reasonably small. In the limit of vanishing light quark masses, $m_u = m_d = m_s = 0$, the Lagrangian of QCD possesses the symmetries $SU(3)_L \otimes SU(3)_R \otimes U(1)_V$. These are spontaneously broken down to $SU(3)_V \otimes U(1)_V$, leading to eight massless Nambu-Goldstone bosons which correspond to eight broken generators. As a consequence of the explicit chiral symmetry breaking, $m_{u,d,s} \neq 0$, these bosons acquire a mass and can be identified with the light pseudoscalar meson octet consisting of pions, kaons and the eta meson. The theory describing the interaction of these low-energy degrees of freedom is called chiral effective field theory [21, 22]. In the following we summarize the most important ingredients of this theory and refer to [23] and the references therein for more details.

The most general Lagrangian describing the interaction of Nambu-Goldstone bosons consists of an infinite amount of terms. To be predictive anyway, we have to specify power counting rules: the masses m_ϕ of the Nambu-Goldstone bosons ϕ and the field gradients $\partial_\mu \phi$ are counted as $\mathcal{O}(p)$, where p is a small momentum compared to the characteristic scale of the theory, $4\pi f_0 \approx 1.2 \text{ GeV}$. To given chiral order only a finite number of terms enters the Lagrangian and therefore the theory becomes predictive. In our analysis it is sufficient to consider only the leading chiral order.

We introduce the field $\Sigma = \exp\left(\frac{i\Phi}{f_0}\right) \in SU(3)$, where f_0 is the pion decay constant in the chiral limit and Φ collects the light pseudoscalar meson octet,

$$\Phi = \Lambda_\alpha \phi_\alpha = \sqrt{2} \begin{pmatrix} \frac{\pi^0}{\sqrt{2}} + \frac{\eta}{\sqrt{6}} & \pi^+ & K^+ \\ \pi^- & -\frac{\pi^0}{\sqrt{2}} + \frac{\eta}{\sqrt{6}} & K^0 \\ K^- & \bar{K}^0 & -\frac{2}{\sqrt{6}}\eta \end{pmatrix}. \quad (3.1)$$

This field transforms under flavor $SU(3)_L \times SU(3)_R$ as

$$\Sigma \rightarrow L\Sigma R^\dagger, \quad (3.2)$$

where $L \in SU(3)_L$ and $R \in SU(3)_R$.

We use the field ξ defined by $\xi^2 = \Sigma = \exp\left(\frac{i\Phi}{f_0}\right)$. As can be seen from (3.2), it has to transform as

$$\xi \rightarrow L\xi U^\dagger = U\xi R^\dagger \quad (3.3)$$

under $SU(3)_L \times SU(3)_R$, where U is a unitary matrix depending on L , R and the meson fields $\Phi(x)$. With these ingredients, the most general Lagrangian consistent with the symmetries of the theory is [23]

$$\mathcal{L}^{(2)} = \frac{f_0^2}{4} \langle \partial_\mu \Sigma \partial^\mu \Sigma^\dagger \rangle + \frac{f_0^2}{4} \langle \chi_+ \rangle, \quad (3.4)$$

at leading chiral order. The brackets $\langle \dots \rangle$ stand for the trace over flavor indices. The superscript (2) gives the order of the Lagrangian and $\chi_+ = \xi^\dagger \mathcal{M} \xi^\dagger + \xi \mathcal{M} \xi$. The light-quark mass matrix, responsible for explicit chiral symmetry breaking, is defined as $\mathcal{M} = 2B_0 \text{Diag}(m_u, m_d, m_s)$, where the new parameter B_0 can be related to the chiral quark condensate by $3f_0^2 B_0 = -\langle \bar{q}q \rangle = -\langle \bar{u}u + \bar{d}d + \bar{s}s \rangle$. For exact isospin symmetry, $m \equiv m_u = m_d$, the masses of the Nambu-Goldstone bosons can be expressed in terms of the light quark masses by

$$m_\pi^2 = 2B_0 m, \quad (3.5)$$

$$m_K^2 = B_0(m + m_s), \quad (3.6)$$

$$m_\eta^2 = \frac{2}{3}B_0(m + 2m_s), \quad (3.7)$$

at leading chiral order. These equations, together with their relation to the chiral quark condensate, are known as the Gell-Mann, Oakes, and Renner relations [24]. As a direct consequence, one obtains the Gell-Mann-Okubo relation

$$4m_K^2 = 3m_\eta^2 + m_\pi^2, \quad (3.8)$$

which is used throughout our analysis to express the mass of the η meson. The mass matrix can be written as $\mathcal{M} = (m_\pi^2, m_\pi^2, 2m_K^2 - m_\pi^2)$, where equations (3.5) to (3.7) have been used.

3.2 Representation of heavy-light meson fields

It is convenient to impose heavy-quark spin symmetry on the level of the Lagrangian. This is done by representing the $Q\bar{q}$ mesons by a field H , that contains both, pseudoscalar and vector meson ground states. These ground states become degenerate as the mass of the heavy quark goes to infinity, $m_Q \rightarrow \infty$.

The field H has to transform as a bispinor under Lorentz transformations [17],

$$H'(x') = D(\Lambda)H(x)D(\Lambda)^{-1}, \quad x' = \Lambda x, \quad (3.9)$$

where $D(\Lambda)$ is the Lorentz transformation for spinors and Λ for coordinates. Equivalently,

$$H(x) \rightarrow H'(x) = D(\Lambda)H(\Lambda^{-1}x)D(\Lambda)^{-1}. \quad (3.10)$$

This field can be expressed as a linear combination of a pseudoscalar meson field P and a vector meson field $P^{*\mu}$,

$$H = \frac{i\mathcal{D} + m_P}{2m_P}(\gamma^\mu P_\mu^* + iP\gamma^5), \quad (3.11)$$

where m_P is the characteristic mass of the heavy-light meson. The field H is a scalar under Lorentz transformations since γ_5 multiplies the pseudoscalar meson field P and γ_μ the vector field $P^{*\mu}$. The phase between P and $P^{*\mu}$ is arbitrary. Under parity, H transforms as

$$H(x) \rightarrow \gamma^0 H(x_P) \gamma^0, \quad \text{with} \quad x_P = (x^0, -\mathbf{x}). \quad (3.12)$$

The covariant derivative \mathcal{D}_μ in Eq. (3.11) has been introduced with respect to triplets under flavor $SU(3)$. For D mesons ($Q = c$), they are $P = (D^0, D^+, D_s^+)$ and $P_\mu^* = (D^{*0}, D^{*+}, D_s^{*+})_\mu$ and for \bar{B} mesons ($Q = b$), they are $P = (B^-, \bar{B}^0, \bar{B}_s^0)$ and $P_\mu^* = (B^{*-}, \bar{B}^{*0}, \bar{B}_s^{*0})_\mu$. Then, H transforms as

$$H_a \rightarrow H_b U_{ba}^\dagger \quad (3.13)$$

under $SU(3)_L \times SU(3)_R$, where $a(b)$ are the flavor indices. This transformation is not the only possible choice. It has, however, the advantage that the transformation under parity takes the simple form of Eq. (3.12)¹. For more details we refer to [17]. The covariant derivative is defined as

$$\mathcal{D}_\mu P_a = \partial_\mu P_a - \Gamma_\mu^{ba} P_b, \quad \mathcal{D}^\mu P_a^\dagger = \partial^\mu P_a^\dagger + \Gamma_{ab}^\mu P_b^\dagger, \quad (3.14)$$

with the vector current $\Gamma_\mu = \frac{1}{2}(\xi^\dagger \partial_\mu \xi + \xi \partial_\mu \xi^\dagger)$. With this definition

$$\mathcal{D}_\mu H_a \rightarrow (\mathcal{D}_\mu H_b) U_{ba}^\dagger \quad (3.15)$$

under $SU(3)_L \times SU(3)_R$. In the limit $m_P \rightarrow \infty$, the coefficient $(i\mathcal{D} + m_P)/(2m_P)$ in Eq. (3.11) becomes a projection operator, as can be understood by decomposing the momentum of the heavy-light meson as $p_P^\mu = m_P v^\mu + k^\mu$, with the static part $m_P v^\mu$ and the small residual momentum k^μ . The velocity is normalized as $v^2 = 1$. In the static limit $(i\mathcal{D} + m_P)/(2m_P) \rightarrow (1 + \not{v})/2$, where the interaction terms with Nambu-Goldstone

¹This ambiguity can be translated to the freedom of choosing different interpolating fields H . Therefore, physical predictions are still unique.

bosons are neglected. The operators $P_+ = (1 + \not{\psi})/2$ and $P_- = (1 - \not{\psi})/2$ project on quark and antiquark component of the heavy quark [17], respectively. Their properties are summarized in Section 2.2.

With respect to rotations of the spins, the field H transforms as a $(1/2, 1/2)$ representation under $S_Q \otimes S_l$. Under finite rotations of the heavy-quark spin, this field transforms as

$$H \rightarrow D(R)_Q H, \quad (3.16)$$

where $D(R)_Q$ is a rotation matrix in the spinor representation for a rotation R , applied to the heavy quark Q . As for the Lorentz transformations, the relation $\gamma^0 D(R)_Q^\dagger \gamma^0 = D(R)_Q^{-1}$ holds.

In the heavy-quark flavor space, the field H transforms as

$$\sqrt{m_{P_i}} H^{(Q_i)} \rightarrow U_Q^{ij} \sqrt{m_{P_j}} H^{(Q_j)}, \quad (3.17)$$

with the unitary transformation U_Q . The superscript (Q_i) has been added to indicate the heavy quark of flavor Q_i . The characteristic mass of the $Q_i \bar{q}$ meson is denoted by m_{P_i} . One should notice that our convention deviates from standard heavy meson chiral perturbation theory, where the pre-factors $\sqrt{m_{P_i}}$ in (3.17) are not present. This is due to our definition of fields, which are chosen to carry mass dimension 1, in contrast to the standard choice $3/2$.

The conjugate field is introduced as

$$\bar{H} = \gamma^0 H^\dagger \gamma^0 = (\gamma^\mu P_\mu^{*\dagger} + iP^\dagger \gamma^5) \frac{\overleftarrow{\not{D}} + m_P}{2m_P}, \quad (3.18)$$

with $P_a^\dagger \overleftarrow{\mathcal{D}}^\mu \equiv \mathcal{D}^\mu P_a^\dagger$. The field \bar{H} transforms also as a bispinor under Lorentz transformations

$$\bar{H}'(x) = D(\Lambda) \bar{H}(\Lambda^{-1}x) D(\Lambda)^{-1}, \quad (3.19)$$

since $\gamma_0 D(\Lambda)^\dagger \gamma_0 = D(\Lambda)^{-1}$. Under chiral $SU(3)_L \times SU(3)_R$ it transforms as

$$\bar{H}_a \rightarrow U_{ab} \bar{H}_b \quad \text{and} \quad \mathcal{D}_\mu \bar{H}_a \rightarrow U_{ab} (\mathcal{D}_\mu \bar{H}_b). \quad (3.20)$$

3.3 Covariant Lagrangian for heavy-light mesons

In this section we construct the chiral effective Lagrangian describing the interaction of Nambu-Goldstone bosons with heavy-light pseudoscalar and vector mesons. The power-counting rules from Section 3.1 are supplemented by field gradients $\partial_\mu P$, $\partial_\mu P_\nu^*$ and masses m_P and m_{P^*} , both counted as $\mathcal{O}(1)$. Employing these rules together with Lorentz covariance, hermiticity, chiral symmetry and invariance under parity and charge

conjugation, gives the leading order (LO) Lagrangian

$$\begin{aligned} \mathcal{L}_A^{(1)} = & \mathcal{D}_\mu P \mathcal{D}^\mu P^\dagger - m_P^2 P P^\dagger - \mathcal{D}_\mu P^{*\nu} \mathcal{D}^\mu P_\nu^{*\dagger} + m_{P^*}^2 P^{*\nu} P_\nu^{*\dagger} \\ & + i\tilde{g}_{PP^*\phi} \left(P_\mu^* u^\mu P^\dagger - P u^\mu P_\mu^{*\dagger} \right) + \frac{g_{P^*P^*\phi}}{2} \left(P_\mu^* u_\alpha \partial_\beta P_\nu^{*\dagger} - \partial_\beta P_\mu^* u_\alpha P_\nu^{*\dagger} \right) \epsilon^{\mu\nu\alpha\beta}. \end{aligned} \quad (3.21)$$

The masses of the P and P^* mesons in the chiral limit are denoted as m_P and m_{P^*} and the axial current is defined as $u_\mu = i(\xi^\dagger \partial_\mu \xi - \xi \partial_\mu \xi^\dagger)$. The coupling constant $\tilde{g}_{PP^*\phi}$ has mass dimension 1, whereas $g_{P^*P^*\phi}$ is dimensionless. As described in Section 3.2, heavy-quark spin symmetry can be imposed by use of the combined field H . In terms of this field, the LO Lagrangian is given by

$$\mathcal{L}^{(1)} = -\frac{1}{2} \text{Tr}[\mathcal{D}_\mu \bar{H}_a \mathcal{D}^\mu H_a] + \frac{1}{2} m_P^2 \text{Tr}[\bar{H}_a H_a] + \frac{\tilde{g}}{2} \text{Tr}[\bar{H}_b H_a \psi_{ab} \gamma_5], \quad (3.22)$$

where the trace $\text{Tr}[\dots]$ is taken in Dirac space and the indices $a(b)$ are flavor indices which are summed over implicitly. As previously, this form is restricted by the symmetries of the theory. The corresponding transformation properties were summarized in Section 3.2. Evaluating the traces in (3.22) gives a number of terms which are partially of higher order in $1/m_P$. These terms can be easily identified by integrating by parts and using the equations of motion. Neglecting these terms gives the LO Lagrangian (3.21) with $m_P = m_{P^*}$ and $\tilde{g} = \tilde{g}_{PP^*\phi} = m_P g_{P^*P^*\phi}$. These identities hold up to corrections in $1/m_P$.

The coupling $\tilde{g}_{DD^*\phi}$ is known from experiment. It can be determined from the decay width $\Gamma_{D^{*+}} = (96 \pm 22) \text{ keV}$ together with the branching ratio $BR_{D^{*+} \rightarrow D^0 \pi^+} = (67.7 \pm 0.5)\%$. At tree level, we obtain $\Gamma_{D^{*+} \rightarrow D^0 \pi^+} = \frac{1}{12\pi} \frac{\tilde{g}_{DD^*\phi}^2 |q_\pi|^3}{f_0^2 m_{D^{*+}}^2}$, which gives $\tilde{g}_{DD^*\phi} = (1177 \pm 137) \text{ MeV}$. Since not much information is available on $g_{D^*D^*\phi}$, we use throughout our analysis its relation to the coupling $\tilde{g}_{DD^*\phi}$, keeping in mind that there could be sizable deviations of higher order in $1/m_D$. The couplings $g_{BB^*\phi}$ and $g_{B^*B^*\phi}$ can be related to their D counterparts through heavy-quark flavor symmetry. On the other hand, the masses of both, P and P^* mesons, are known to high accuracy. Therefore we use physical masses for m_P and m_{P^*} , wherever we are working at sufficient order.

In a similar way, we can construct the covariant next-to-leading-order (NLO) Lagrangian

$$\begin{aligned} \mathcal{L}^{(2)} = & -2[c_0 P P^\dagger \langle \chi_+ \rangle - c_1 P \chi_+ P^\dagger - c_2 P P^\dagger \langle u^\mu u_\mu \rangle - c_3 P u^\mu u_\mu P^\dagger \\ & + \frac{c_4}{m_P^2} \mathcal{D}_\mu P \mathcal{D}_\nu P^\dagger \langle \{u^\mu, u^\nu\} \rangle + \frac{c_5}{m_P^2} \mathcal{D}_\mu P \{u^\mu, u^\nu\} \mathcal{D}_\nu P^\dagger + \frac{c_6}{m_P^2} \mathcal{D}_\mu P [u^\mu, u^\nu] \mathcal{D}_\nu P^\dagger \\ & + 2[\tilde{c}_0 P_\mu^* P^{*\mu\dagger} \langle \chi_+ \rangle - \tilde{c}_1 P_\mu^* \chi_+ P^{*\mu\dagger} - \tilde{c}_2 P_\mu^* P^{*\mu\dagger} \langle u^\mu u_\mu \rangle - \tilde{c}_3 P_\nu^* u^\mu u_\mu P^{*\nu\dagger} \\ & + \frac{\tilde{c}_4}{m_{P^*}^2} \mathcal{D}_\mu P_\alpha^* \mathcal{D}_\nu P^{*\alpha\dagger} \langle \{u^\mu, u^\nu\} \rangle + \frac{\tilde{c}_5}{m_{P^*}^2} \mathcal{D}_\mu P_\alpha^* \{u^\mu, u^\nu\} \mathcal{D}_\nu P^{*\alpha\dagger} \\ & + \frac{\tilde{c}_6}{m_{P^*}^2} \mathcal{D}_\mu P_\alpha^* [u^\mu, u^\nu] \mathcal{D}_\nu P^{*\alpha\dagger}], \end{aligned} \quad (3.23)$$

where we have introduced the low energy constants c_i and \tilde{c}_i with $i = 0, \dots, 6$. These constants have to be determined by comparison with experiment or lattice QCD. In the limit of exact heavy-quark spin symmetry,

the Lagrangian is written in terms of the combined field H as

$$\begin{aligned}
\mathcal{L}^{(2)} = & c_0 \text{Tr}[\bar{H}_a H_a](\chi_+)_{bb} - c_1 \text{Tr}[\bar{H}_a H_b](\chi_+)_{ba} - c_2 \text{Tr}[\bar{H}_a H_a](u^\mu u_\mu)_{bb} \\
& - c_3 \text{Tr}[\bar{H}_a H_b](u^\mu u_\mu)_{ba} + \frac{c_4}{m_P^2} \text{Tr}[\mathcal{D}_\mu \bar{H}_a \mathcal{D}_\nu H_a](\{u^\mu, u^\nu\})_{bb} \\
& + \text{Tr}[\mathcal{D}_\mu \bar{H}_a \mathcal{D}_\nu H_b] \left(\frac{c_5}{m_P^2} (\{u^\mu, u^\nu\})_{ba} + \frac{c_6}{m_P^2} ([u^\mu, u^\nu])_{ba} \right). \tag{3.24}
\end{aligned}$$

Evaluating the traces and removing terms suppressed in $1/m_P$, gives Lagrangian (3.23) with $c_i = \tilde{c}_i$ for $i = 0, \dots, 6$ and $m_P = m_{P^*}$. As a first estimate of the size of spin-symmetry breaking effects, we can determine the constants c_1 and \tilde{c}_1 from the masses of strange and non-strange D and D^* mesons. At next-to-leading chiral order, the masses of the D , D_s , D^* and D_s^* meson are given by

$$m_D^2 = m_{D,0}^2 + 4c_0(m_\pi^2 + 2m_K^2) - 4c_1 m_\pi^2, \tag{3.25}$$

$$m_{D_s}^2 = m_{D,0}^2 + 4c_0(m_\pi^2 + 2m_K^2) + 4c_1(m_\pi^2 - 2m_K^2), \tag{3.26}$$

$$m_{D^*}^2 = m_{D^*,0}^2 + 4\tilde{c}_0(m_\pi^2 + 2m_K^2) - 4\tilde{c}_1 m_\pi^2, \tag{3.27}$$

$$m_{D_s^*}^2 = m_{D^*,0}^2 + 4\tilde{c}_0(m_\pi^2 + 2m_K^2) + 4\tilde{c}_1(m_\pi^2 - 2m_K^2), \tag{3.28}$$

where the $D(D^*)$ meson mass in the chiral limit is denoted as $m_{D,0}(m_{D^*,0})$. Inserting the physical masses listed in Table 4.1 leads to $c_1 = -0.214$ and $\tilde{c}_1 = -0.236$. Repeating the same argument for the \bar{B} mesons, we obtain $c_1(B) = -0.513$ and $\tilde{c}_1(B) = -0.534$. The heavy-quark flavor symmetry dictates that $c_1(\tilde{c}_1)/M_{\text{HL}} = \text{const}$. Using an SU(3) averaged mass for M_{HL} for each sector, we find $c_1/\bar{M}_D = -0.113 \text{ GeV}^{-1}$, $\tilde{c}_1/\bar{M}_{D^*} = -0.116 \text{ GeV}^{-1}$, $c_1(B)/\bar{M}_B = -0.097 \text{ GeV}^{-1}$, and $\tilde{c}_1(B)/\bar{M}_{B^*} = -0.100 \text{ GeV}^{-1}$. These numbers provide a hint about the expected order of magnitude for the breaking of heavy-quark spin and flavor symmetry: about 3% between D vs. D^* and B vs. B^* , whereas it amounts to about 16% between D vs. B and D^* vs. B^* .

Chapter 4

SU(3) breaking corrections to the D , D^* , B , and B^* decay constants

4.1 Light quark mass dependence of the D and D_s decay constants

In this section, we study the light-quark mass dependence of the D and D_s meson decay constants, f_D and f_{D_s} , using a covariant formulation of chiral perturbation theory (ChPT). Using the HPQCD lattice results for the $D(D_s)$ decay constants as a benchmark we show that covariant ChPT can describe the HPQCD results [25] better than heavy meson ChPT (HMChPT).

The decay constants of charged pseudoscalar mesons π^\pm , K^\pm , D^\pm , D_s^\pm and B^\pm play an important role in our understanding of strong interaction physics, e.g., in measurements of the Cabibbo-Kobayashi-Maskawa (CKM) matrix elements [1] and in the search for signals of physics beyond the Standard Model (SM). At lowest order, the decay width of a charged pseudoscalar P^\pm with valence quark content $q_1\bar{q}_2$ decaying into a charged lepton pair ($\ell^\pm\nu_\ell$) via a virtual W^\pm meson is given by [26]

$$\Gamma(P^\pm \rightarrow \ell^\pm\nu_\ell) = \frac{G_F^2}{8\pi} f_P^2 m_\ell^2 M_P \left(1 - \frac{m_\ell^2}{M_P^2}\right)^2 |V_{q_1q_2}|^2, \quad (4.1)$$

where m_ℓ is the ℓ^\pm mass, $|V_{q_1q_2}|$ is the CKM matrix element between the constituent quarks $q_1\bar{q}_2$ in P^\pm , and G_F is the Fermi constant. The parameter f_P is the decay constant, related to the wave function overlap of the $q_1\bar{q}_2$ pair. Measurements of purely leptonic decay branching fractions and lifetimes allow an experimental determination of the product $|V_{q_1q_2}f_P|$. A good knowledge of the value of either $|V_{q_1q_2}|$ or f_P can then be used to determine the value of the other.

These decay constants can be accessed both experimentally and through Lattice Quantum Chromodynamics (LQCD) simulations. While for f_π , f_K , f_D , experimental measurements agree well with lattice QCD calculations, a discrepancy is seen for the value of f_{D_s} : The 2008 PDG average for f_{D_s} is 273 ± 10 MeV [27], about 3σ larger than the most precise $N_f = 2 + 1$ LQCD result from the HPQCD/UKQCD collaboration [25], 241 ± 3 MeV. On the other hand, experiments and LQCD calculations agree very well with each other on the value of f_D , $f_D(\text{expt}) = 205.8 \pm 8.9$ MeV and $f_D(\text{LQCD}) = 207 \pm 4$ MeV. The discrepancy concerning f_{D_s}

is quite puzzling because whatever systematic errors have affected the LQCD calculation of f_D , they should also be expected for the calculation of f_{D_s} . In this context, constraints imposed by this discrepancy on new physics were seriously discussed (see, e.g., Ref. [34]).

However, the situation has changed recently. With the new (updated) data from CLEO [35–37] and Babar [38], together with the Belle measurement [39], the latest PDG average is $f_{D_s} = 257.5 \pm 6.1$ MeV [40]¹. The discrepancy is reduced to 2.4σ . Lately the HPQCD collaboration has also updated its study of the D_s decay constant [42]. By including additional results at smaller lattice spacing along with improved determinations of the lattice spacing and improved tuning of the charm and strange quark masses, a new value for the D_s decay constant has been reported²: $f_{D_s} = 248.0 \pm 2.5$ MeV. With the updated results from both the experimental side and the HPQCD collaboration, the window for possible new physics in this quantity is significantly reduced [42].

An important part of the uncertainties in heavy quark LQCD simulations comes from chiral extrapolations that are needed in order to extrapolate LQCD simulations, performed with larger-than-physical light-quark masses, down to the physical point. Recent LQCD studies of the D (D_s) decay constants, both for $N_f = 2 + 1$ [25, 44] and $N_f = 2$ [45], have adopted the one-loop heavy-meson chiral perturbation theory (HMChPT) (including its partially-quenched and staggered counterparts) to perform chiral extrapolations. In particular, the HPQCD collaboration has used the standard continuum chiral expansions through first order but augmented by second- and third-order polynomial terms in $x_q = B_0 m_q / 8(\pi f_\pi)^2$ where $B_0 \equiv m_\pi^2 / (m_u + m_d)$ to leading order in ChPT, arguing that the polynomial terms are required by the precision of the data. It is clear that the NLO HMChPT alone fails to describe its data.

HMChPT [33, 46, 47] has been widely employed not only in extrapolating LQCD simulations but also in phenomenology studies and has been remarkably successful over the decades (see Ref. [48] for a partial review of early applications). In Ref. [49], it was argued that a covariant formulation of ChPT may be a better choice for studying heavy-meson phenomenology and LQCD simulations. This was based on the observation that the counterpart in the SU(3) baryon sector, heavy baryon ChPT, converges very slowly and often fails to describe both phenomenology and lattice data (particularly the latter), e.g., in the description of the lattice data for the masses of the lowest-lying baryons [50, 51]. On the other hand, covariant baryon ChPT was shown to provide a much improved description of the same data [52]. Indeed, in Ref. [49] it was shown that for the scattering lengths of light pseudoscalar mesons interacting with D mesons, recoil corrections are non-negligible. Given the important role played by f_D (f_{D_s}) in our understanding of strong-interaction physics and the importance of chiral extrapolations in LQCD simulations, it is timely to examine how covariant ChPT works in conjunction with the HPQCD f_D (f_{D_s}) data.

In this section we study the light quark mass dependence of the HPQCD f_D and f_{D_s} results [25]³ using a covariant formulation of ChPT. It is not our purpose to reanalyze the raw LQCD data because the HPQCD

¹The October 2010 average from the Heavy Flavor Averaging Group (HFAG) is similar: $f_{D_s} = 257.3 \pm 5.3$ MeV [41].

²A slightly different but less precise value of $f_{D_s} = 250.2 \pm 3.6$ MeV was obtained in Ref. [43] as a byproduct from the study of the $D \rightarrow K \ell \nu$ semileptonic decay scalar form factor by the same collaboration.

³Although the HPQCD collaboration has updated its study of the f_{D_s} decay constant, it has not done the same for the f_D decay constant, and therefore its f_{D_s}/f_D ratio remains the same but with a slightly larger uncertainty. For our purposes, it is enough to study the HPQCD 2007 data [25].

collaboration has performed a comprehensive study. Repeating such a process using a different formulation of ChPT will not likely yield any significantly different results. Instead, we will focus on their final results in the continuum limit as a function of m_q/m_s , with m_q the average of up and down quark masses and m_s the strange quark mass. These results can be treated as quasi-original lattice data because, for chiral extrapolations, the HPQCD collaboration has used the NLO HMChPT result plus two polynomials of higher chiral order. Therefore, any inadequacy of the NLO HMChPT should have been remedied by fine-tuning the two polynomials. Accordingly the extrapolations should be reliable, apart from the fact that the connection with an order-by-order ChPT analysis is lost. This section tries to close this gap. Using the HPQCD continuum limits as a benchmark instead of the raw data not only greatly simplifies our analysis but also highlights the point we wish to make, namely that the covariant formulation of ChPT is more suitable for chiral extrapolations of LQCD data than the HMChPT, at least in the present case.

4.1.1 Theoretical framework

The decay constants of heavy-light pseudoscalar and vector mesons with quark content $\bar{q}Q$, with q one of the u , d , and s quarks and Q either the c or b quark, are defined by

$$\langle 0 | \bar{q} \gamma^\mu \gamma_5 Q(0) | P_q(p) \rangle = -i f_{P_q} p^\mu, \quad (4.2)$$

$$\langle 0 | \bar{q} \gamma^\mu Q(0) | P_q^*(p, \epsilon) \rangle = F_{P_q^*} \epsilon^\mu, \quad (4.3)$$

where P_q denotes a pseudoscalar meson and P_q^* a vector meson. In this convention, f_{P_q} has mass dimension one and $F_{P_q^*}$ has mass dimension two [17]. From now on, we concentrate on the charm sector, D , D_s , D^* , and D_s^* . The formalism can easily be extended to the bottom sector.

The coupling of the D (D_s) mesons to the vacuum or to Nambu-Goldstone bosons through the left-handed current is described by the following leading order chiral Lagrangian:

$$\mathcal{L}_{\text{source}}^{(1)} = \alpha (c' P_\mu^* - \frac{\partial_\mu P}{m_P}) \xi^\dagger J^\mu, \quad (4.4)$$

where α is a normalization constant with mass dimension two, $J_\mu = (J_\mu^{cu}, J_\mu^{cd}, J_\mu^{cs})^T$ with the weak current $J_\mu^{cq} = \bar{c} \gamma_\mu (1 - \gamma_5) q$, and $P = (D^0, D^+, D_s^+)$, $P_\mu^* = (D^{*0}, D^{*+}, D_s^{*+})$, where m_P is the characteristic mass of the P triplet introduced to conserve heavy-quark spin symmetry in the $m_Q \rightarrow \infty$ limit, i.e., \hat{m}_D at NLO and m_D at NNLO (see Table 4.1). We have introduced a dimensionless coefficient c' to distinguish the vector and pseudoscalar fields, which is 1 if heavy-quark spin symmetry is exact. We need to stress that in our covariant formulation of ChPT we do not keep track of explicit $1/m_Q$ corrections that break heavy-quark spin and flavor symmetry, instead we focus on SU(3) breaking. This implies that different couplings have to be used for $D(D^*)$ and $B(B^*)$ mesons. In this section we only need to make such a differentiation in calculating diagram Fig. (4.1d). In Eq. (4.25) we have therefore explicitly pointed out that c' may be different from 1. In all the other places, we will simply set c' equal to 1.

The leading-order (LO) SU(3) breaking of the D meson decay constants is described by the following

next-to-leading order (NLO) chiral Lagrangian

$$\mathcal{L}^{(3)} = -\frac{\alpha}{2\Lambda_\chi} \left[b_D \left(P_\mu^* - \frac{\partial_\mu P}{m_P} \right) (\chi_+ \xi^\dagger) J^\mu + b_A \left(P_\mu^* - \frac{\partial_\mu P}{m_P} \right) \xi^\dagger J^\mu \langle \chi_+ \rangle \right], \quad (4.5)$$

where b_D and b_A are two LECs.

To study the NLO SU(3) breaking, one has to take into account the DD^* ($D_s D_s^*$) and DD_s ($D^* D_s^*$) mass splittings. Experimentally the DD^* and $D_s D_s^*$ splittings are similar:

$$\Delta_{DD^*} = 141.4 \text{ MeV} \quad \text{and} \quad \Delta_{D_s D_s^*} = 143.8 \text{ MeV}. \quad (4.6)$$

Therefore in our calculation we will take an average of these two splittings, i.e., $\Delta = (\Delta_{DD^*} + \Delta_{D_s D_s^*})/2 = 142.6 \text{ MeV}$. It should be noted that the DD^* mass splitting is of sub-leading order in the $1/m_Q$ expansion of heavy quark effective theory. The numbers above show that SU(3) breaking of this quantity is less than 2%. The mass splitting in principle can also depend on the light-quark masses but we expect that the dependence of this ‘‘hyperfine’’ splitting should be much weaker than that of the D mass⁴, m_D , which we discuss below.

At NLO, the following Lagrangian is responsible for generating SU(3) breaking between the D and D_s masses [49]:

$$\mathcal{L}^{(2)} = -2c_0 P P^\dagger \langle \chi_+ \rangle + 2c_1 P \chi_+ P^\dagger, \quad (4.7)$$

which yields the NLO mass formulas Eq. (3.25) and (3.26). One may implement this mass splitting in two different ways by either using the HPQCD continuum limits on the D and D_s masses [25] to fix the three LECs: $m_{D,0}$, c_0 , and c_1 , or taking into account only the DD_s mass splitting

$$-8c_1(m_K^2 - m_\pi^2) = (m_{D_s}^2 - m_D^2 + m_{D_s^*}^2 - m_{D^*}^2)/2 \approx \Delta_s(m_D + m_{D_s} + m_{D^*} + m_{D_s^*})/2, \quad (4.8)$$

where we have introduced $\Delta_s \equiv m_{D_s} - m_D \approx m_{D_s^*} - m_{D^*} \approx (m_{D_s} - m_D + m_{D_s^*} - m_{D^*})/2$. In the second approach, using the experimental data for m_D , m_{D_s} , m_{D^*} , and $m_{D_s^*}$, one obtains $c_1 = -0.225$. We found that the HPQCD continuum limits on the D and D^* masses can be described very well using Eqs. (3.25,3.26). We also found that using Eqs. (3.25,3.26) or Eq. (4.8) gives very similar results in our analysis of the D (D_s) decay constants. The results shown below are obtained using Eq. (4.8) to implement the SU(3) breaking and light-quark mass evolution of the D (D_s) masses.

In order to calculate loop diagrams contributing to the decay constants one needs to know the coupling, $g_{DD^*\phi}$, with ϕ denoting a Nambu-Goldstone boson. This is provided at the leading chiral order by the following part of Lagrangian (3.21):

$$\mathcal{L}^{(1)} = ig \hat{m}_D \left(P_\mu^* u^\mu P^\dagger - P u^\mu P_\mu^{*\dagger} \right) \quad (4.9)$$

where $u_\mu = i(\xi^\dagger \partial_\mu \xi - \xi \partial_\mu \xi^\dagger)$ and \hat{m}_D is the average of D , D_s , D^* , and D_s^* masses. The dimensionless coupling $g \equiv \tilde{g}/\hat{m}_D$, determined from the $D^{*+} \rightarrow D^0 \pi^+$ decay width, is $g_{DD^*\pi} = 0.60 \pm 0.07$ [49]. At the chiral order we are working, one can take $g_{DD^*\phi} = g_{DD^*\pi}$. If heavy-quark flavor symmetry is exact, we expect

⁴This seems to be supported by quenched LQCD calculations, see, e.g., Refs. [53,54].

TABLE 4.1: Numerical values of the isospin-averaged masses [40] and decay constants (in units of MeV) used in the present study. The eta meson mass is calculated using the Gell-Mann-Okubo mass relation: $m_\eta^2 = (4m_K^2 - m_\pi^2)/3$. F_0 is the average of physical f_π , f_K and f_η .

\dot{m}_D	$m_{D_s^*}$	m_{D^*}	m_{D_s}	m_D	m_π	m_K	Δ_s	Δ
1972.1	2112.3	2008.6	1968.5	1867.2	138.0	495.6	102.5	142.6
\dot{m}_B	$m_{B_s^*}$	m_{B^*}	m_{B_s}	m_B	$\Delta_s(B)$	$\Delta(B)$	f_π	F_0
5331.9	5415.4	5325.2	5366.8	5279.4	88.7	47.5	92.4	$1.15 f_\pi$

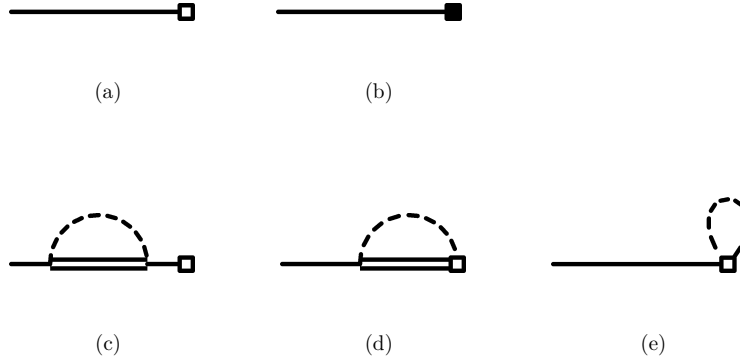


FIGURE 4.1: Feynman diagrams contributing to the calculation of f_D and f_{D_s} up to next-to-leading order (NLO): (a) and (b) are LO and NLO tree level diagrams, loop diagrams (c), (d), and (e) contribute at NLO. The dashed lines correspond to Nambu-Goldstone bosons and the single and double solid lines to pseudoscalar and vector heavy-light mesons.

$g_{BB^*\pi} = g_{DD^*\pi}$. Otherwise deviations are expected. We will come back to this later.

Up to NLO⁵, the $D(D_s)$ decay constants receive contributions from the Feynman diagrams shown in Fig. 4.1. Studies of these decay constants within the framework of HMChPT have a long history [55–57]. Here we are going to present the first covariant ChPT calculation. Insertion of the mass splittings between D , D_s , D^* , and D_s^* in the loop diagrams shown in Fig. 4.1 generates the NNLO contributions which are implemented in the present case by making the following replacements in the NLO results:

$$m_{D_s} \rightarrow m_D + \Delta_s, \quad m_{D^*} \rightarrow m_D + \Delta, \quad \text{and} \quad m_{D_s^*} \rightarrow m_D + \Delta + \Delta_s, \quad (4.10)$$

with the values of these quantities given in Table 4.1.

Computation of the tree-level diagrams Figs. (4.1a,4.1b) is trivial. Fig. (4.1a) gives $\hat{\alpha} = \alpha/m_P$ with mass dimension one for both D and D_s . Fig. (4.1b) yields

$$\delta_1 = \hat{\alpha} \left[-\frac{1}{16\pi^2 F_0^2} (b_A(2m_K^2 + m_\pi^2) + b_D m_\pi^2) \right], \quad (4.11)$$

$$\delta_2 = \hat{\alpha} \left[-\frac{1}{16\pi^2 F_0^2} (b_A(2m_K^2 + m_\pi^2) + b_D(2m_K^2 - m_\pi^2)) \right], \quad (4.12)$$

⁵The chiral order of a properly renormalized diagram with L loops, N_M (N_H) Nambu-Goldstone boson (HL meson) propagators and V_k vertices from k th-order Lagrangians is $n_\chi = 4L - 2N_M - N_H + \sum_k kV_k$.

where δ_1 is for D and δ_2 for D_s .

Diagram Fig. (4.1c) represents the wave function renormalization, from which one can calculate the wave function renormalization constants, which can be written as

$$Z_i = \sum_{j,k} \xi_{i,j,k} \frac{d\phi_w(p_i^2, m_j^2, m_k^2)}{dp_i^2} \Big|_{p_i^2=m_i^2}, \quad (4.13)$$

where p_i denotes the four-momentum of D (D_s), m_i the mass of D (D_s), m_j the mass of D^* (D_s^*), and m_k the mass of π , η , and K . The coefficients $\xi_{i,j,k}$ are given in Table 4.2. The function ϕ_w is defined as⁶

$$\begin{aligned} \phi_w(p_i^2, m_V^2, m_M^2) &= \frac{(g\hat{m}_D)^2}{4F_0^2 m_V^2} \left[(-2m_M^2 (p_i^2 + m_V^2) + (m_V^2 - p_i^2)^2 + m_M^4) B_0(p_i^2, m_M^2, m_V^2) \right. \\ &\quad \left. + A_0(m_V^2) (-p_i^2 + m_M^2 - m_V^2) + A_0(m_M^2) (-p_i^2 + 3m_M^2 + m_V^2) \right], \quad (4.14) \end{aligned}$$

where the functions A_0 and B_0 are defined in the Appendix A.1.

Diagram Fig. (4.1d) provides current renormalization, which has the following form

$$C_i = \hat{\alpha} c' \sum_{j,k} \xi_{i,j,k} \phi_c(m_i^2, m_j^2, m_k^2), \quad (4.15)$$

where $\xi_{i,j,k}$ are given in Table 4.2 with i running over D and D_s , j over D^* and D_s^* , and k over π , η , K . The function ϕ_c is defined as

$$\begin{aligned} \phi_c(m_i^2, m_V^2, m_M^2) &= -\frac{(g\hat{m}_D)m_P}{8F_0^2 m_i^2 m_V^2} \left[(m_M^2 - m_V^2) (m_i^2 - m_M^2 + m_V^2) B_0(0, m_M^2, m_V^2) - 2m_i^2 A_0(m_M^2) \right. \\ &\quad \left. + (-2m_i^2 (m_M^2 + m_V^2) + m_i^4 + (m_M^2 - m_V^2)^2) B_0(m_i^2, m_M^2, m_V^2) \right]. \quad (4.16) \end{aligned}$$

It should be noted that C_i vanishes in NLO HMChPT but plays an important role in covariant ChPT.

Diagram Fig. (4.1e) also provides current correction

$$T_i = \hat{\alpha} \sum_{j=\pi,\eta,K} \zeta_{i,j} A_0(m_j^2)/F_0^2, \quad (4.17)$$

with $\zeta_{i,j}$ given in Table 4.3.

The total results are then

$$f_i = \hat{\alpha}(1 + Z_i/2) + \delta_i + T_i + C_i. \quad (4.18)$$

⁶To be consistent, the product $g\hat{m}_D$ is only appropriate for NLO. At NNLO, it has to be replaced by $g'm_D$ with $g' = g\hat{m}_D/m_D \approx 0.63$ before performing expansions in terms of $1/m_D$ either to obtain the HMChPT results or to remove the power-counting-breaking pieces. The same applies to the calculation of C_i [see Eq. (4.15)].

TABLE 4.2: Coefficients, $\xi_{i,j,k}$, appearing in Eqs. (4.13,4.15).

	D^*			D_s^*		
	π	η	K	π	η	K
D	3	$\frac{1}{3}$	0	0	0	2
D_s	0	0	4	0	$\frac{4}{3}$	0

TABLE 4.3: Coefficients, $\zeta_{i,j}$, appearing in Eq. (4.17).

	π	η	K
D	$-\frac{3}{8}$	$-\frac{1}{24}$	$-\frac{1}{4}$
D_s	0	$-\frac{1}{6}$	$-\frac{1}{2}$

4.1.2 The extended-on-mass-shell (EOMS) scheme

Because of the large D meson masses, C_i and Z_i contain so-called power-counting-breaking (PCB) terms. As explained in detail in Ref. [49] one can simply expand these functions in terms of $1/\hat{m}_D$ at NLO or $1/m_D$ at NNLO and then remove the PCB pieces. This procedure is in fact the same as the extended-on-mass-shell (EOMS) scheme. This scheme was first developed for baryon chiral perturbation theory [58, 59] and has been shown to be superior to heavy baryon ChPT in a number of cases, see, e.g., Refs. [52, 60, 61]. Here, we want to elaborate on this scheme.

The basic idea behind the EOMS scheme is to restore the naive power counting of a loop diagram by a redefinition of the involved low-energy constants. This idea can be understood as an extension to the minimal subtraction (MS) scheme employed in [62]. As explained in detail in a number of textbooks the minimal subtraction scheme is a prescription to absorb divergent parts that emerge in dimensionally regularized loop diagrams, see for instance [63]. In the EOMS scheme, one absorbs in addition to these infinite terms also finite parts that break the power counting. The final, subtracted diagram is then in accordance with the chiral counting, i.e. with the chiral order n_χ . To illustrate this, we present the PCB terms explicitly for the final result Eq. (4.18), where we employ the renormalized one and two-point functions of Appendix A.1. Only the loop diagrams Figure (4.1c) and (4.1d) break the chiral power counting. The remaining diagrams are already of the correct chiral order. Both diagrams are naively counted as $n_\chi = 3$. We use the replacements $m_D^2 = m_{D,0}^2 + 2m_{D,0}\Delta_{s,1}$ and $m_{D_s}^2 = m_{D,0}^2 + 2m_{D,0}\Delta_{s,2}$, where $\Delta_{s,1}$ and $\Delta_{s,2}$ are determined from Eq. (3.25) and (3.26). Further we fix $\tilde{c}_0 = c_0$ and $\tilde{c}_1 = c_1$, and use $m_{D^*,0}^2 \equiv m_{D,0}^2 + 2m_{D,0}\Delta$. This gives

$m_{D^*}^2 = m_{D,0}^2 + 2m_{D,0}(\Delta + \Delta_{s,1})$ and $m_{D_s^*}^2 = m_{D,0}^2 + 2m_{D,0}(\Delta + \Delta_{s,2})$. Expanding finally in $1/m_{D,0}$ gives

$$\begin{aligned}
C_1 &= \frac{\hat{\alpha}c'g}{24\pi^2 f_0^2} \left[c_1 \left(3(m_K^2 - m_\pi^2) \log \left(\frac{\mu^2}{m_{D,0}^2} \right) - 2(3m_K^2 + m_\pi^2) \right) + 4m_{D,0} \Delta \right. \\
&\quad \left. - m_{D,0} (2m_{D,0} + 2\Delta) \log \left(\frac{\mu^2}{m_{D,0}^2} \right) + 8c_0 (2m_K^2 + m_\pi^2) \right] + \mathcal{O}(n_\chi = 3) \\
C_2 &= \frac{\hat{\alpha}c'g}{24\pi^2 f_0^2} \left[-2c_1 \left(3(m_K^2 - m_\pi^2) \log \left(\frac{\mu^2}{m_{D,0}^2} \right) + 2(m_K^2 + m_\pi^2) \right) + 4m_{D,0} \Delta \right. \\
&\quad \left. - m_{D,0} (2m_{D,0} + 2\Delta) \log \left(\frac{\mu^2}{m_{D,0}^2} \right) + 8c_0 (2m_K^2 + m_\pi^2) \right] + \mathcal{O}(n_\chi = 3) \\
\hat{\alpha}Z_{1/2} &= \frac{\hat{\alpha}g^2}{24\pi^2 f_0^2} \left[c_1 \left(6(m_\pi^2 - m_K^2) \log \left(\frac{\mu^2}{m_{D,0}^2} \right) - 3m_K^2 + 7m_\pi^2 \right) + 2m_{D,0} \Delta \right. \\
&\quad \left. + m_{D,0} (m_{D,0} + 4\Delta) \log \left(\frac{\mu^2}{m_{D,0}^2} \right) - 4c_0 (2m_K^2 + m_\pi^2) \right] + \mathcal{O}(n_\chi = 3) \\
\hat{\alpha}Z_{2/2} &= \frac{\hat{\alpha}g^2}{24\pi^2 f_0^2} \left[2c_1 \left(6(m_K^2 - m_\pi^2) \log \left(\frac{\mu^2}{m_{D,0}^2} \right) + 7m_K^2 - 5m_\pi^2 \right) + 2m_{D,0} \Delta \right. \\
&\quad \left. + m_{D,0} (m_{D,0} + 4\Delta) \log \left(\frac{\mu^2}{m_{D,0}^2} \right) - 4c_0 (2m_K^2 + m_\pi^2) \right] + \mathcal{O}(n_\chi = 3) \tag{4.19}
\end{aligned}$$

where we have inserted the explicit form of $\Delta_{s,1}$ and $\Delta_{s,2}$.

These terms are the PCB terms, depending on three parameters, b_A , b_D and $\hat{\alpha}$. If only the NLO result is considered, the mass $m_{D,0}$ has to be replaced by \hat{m}_D in the previous expansion. The terms that do not depend on m_π and m_K are equal for $i = 1$ and $i = 2$ and can therefore be directly absorbed into the low-energy constant $\hat{\alpha}$. The terms that are proportional to c_0 and c_1 , on the other hand, require a redefinition of the low-energy constants b_D and b_A . Introducing new constants $b_{A,r}$ and $b_{D,r}$ by the replacements

$$\begin{aligned}
b_A &\rightarrow -c_1 g \left[-c' \left(\log \left(\frac{\mu^2}{m_{D,0}^2} \right) - 2 \right) + 2g \log \left(\frac{\mu^2}{m_{D,0}^2} \right) + g \right] + b_{A,r} - \frac{8}{3} c_0 g (g - 2c') , \\
b_D &\rightarrow \frac{1}{3} c_1 g \left[c' \left(2 - 9 \log \left(\frac{\mu^2}{m_{D,0}^2} \right) \right) + g \left(18 \log \left(\frac{\mu^2}{m_{D,0}^2} \right) + 17 \right) \right] + b_{D,r} , \tag{4.20}
\end{aligned}$$

removes the remaining PCB terms. Equivalently, we have expanded the results by use of equation (4.10) in powers of $1/m_D$ and have removed the PCB terms directly from C_i and Z_i , keeping in mind that the low-energy-constants b_A , b_D and $\hat{\alpha}$ are now to be understood as the renormalized constants. These subtracted functions are denoted by \tilde{C}_i and \tilde{Z}_i and have a proper power-counting as described in Ref. [49]. At the end one finds

$$\tilde{f}_i = \hat{\alpha} (1 + \tilde{Z}_i/2) + \delta_i + T_i + \tilde{C}_i, \tag{4.21}$$

the expression that is used in the actual calculations. By expanding Z_i and C_i in terms of $1/\hat{m}_D$ at NLO or $1/m_D$ at NNLO and keeping the lowest order in $1/\hat{m}_D$ ($1/m_D$) one can easily obtain the corresponding HMChPT results.

4.1.3 Results and discussion

Before presenting the numerical results, we should make it clear that in our present formulation of ChPT we have focused on SU(3) breaking in the context of the chiral expansions but we have not utilized explicitly heavy quark symmetry that relates the couplings of the D mesons with those of the D^* , B , and B^* mesons.

In the present case, we encounter three LECs: a , b_D , and b_A . At this point, light-quark mass dependent LQCD results are extremely useful. By a least-squares fit to the HPQCD results, one can fix those three LECs appearing in our calculation.

First we treat the D , D_s , D^* , and D_s^* mesons as degenerate, i.e., we work up to NLO. The corresponding results are shown in Fig. 4.2, where the HMChPT results are obtained by expanding our covariant results in terms of $1/\hat{m}_D$ and keeping only the lowest-order terms. It is clear that the covariant results (with $\chi^2=41$) are in much better agreement with the HPQCD continuum limits than the HMChPT results (with $\chi^2 = 201$)⁷. This is not surprising because as we mentioned earlier the HPQCD collaboration has added second and third order polynomial terms in x_q to perform their extrapolation. Furthermore one can notice that at larger light quark masses the difference between the covariant ChPT and the HMChPT results becomes larger. This highlights the importance of using a covariant formulation of ChPT in order to make chiral extrapolations if lattice simulations are performed with relatively large light quark masses. Similar conclusions have been reached in studying the light quark mass dependence of the lowest-lying octet and decuplet baryon masses [52].

Taking into account the mass splittings between D , D_s , D^* , and D_s^* as prescribed by Eq. (4.10) one obtains the NNLO ChPT results. Fitting them to the HPQCD extrapolations, one finds the results shown in Fig. 4.3. Compared to Fig. 4.2, it is clear that the agreement between the covariant ChPT results with the HPQCD extrapolations becomes even better. Furthermore the covariant χ PT results (with $\chi^2 = 16$) is still visibly better than the HMChPT results (with $\chi^2 = 59$), but now the difference between the covariant and the HMChPT results becomes smaller. The three LECs in the NNLO covariant ChPT have the following values: $\hat{a} = 208$ MeV, $b_D = 0.318$, $b_A = 0.166$.

If we had fitted the HPQCD extrapolations by neglecting the loop contributions, we would have obtained a even better agreement ($\chi^2 = 9$). In Ref. [52] we also found that the lattice baryon mass data could be fitted better with the LO (linear in m_q) chiral extrapolation. But there we found that the NLO chiral results in fact describe the experimental data better than the LO (linear) chiral extrapolation. This just shows that the lattice baryon mass data behave more linearly as a function of light quark masses at large light quark masses and chiral logarithms play a more relevant role at smaller light quark masses, as one naively expects.

Another way of understanding the importance of chiral logarithms is to perform separate fits for lattice simulations obtained at different light quark masses. One expects that at smaller light quark masses (e.g., $m_\pi < 300$ MeV) covariant ChPT and HM ChPT results should perform more or less similarly. On the other hand, if the light quark masses are larger, covariant ChPT should be a better choice. In Fig. 4.4, we show the fitted results obtained from fitting the HPQCD extrapolations in two different regions of light quark masses, $m_q/m_s \leq 0.2$ (left panel) and $m_q/m_s > 0.2$ (right panel). It is clearly seen that fitting lattice data with

⁷It should be noted that the absolute value of χ^2 as defined here does not have a clear-cut physical meaning. It only reflects to what extent the chiral results agree with the HPQCD extrapolations.

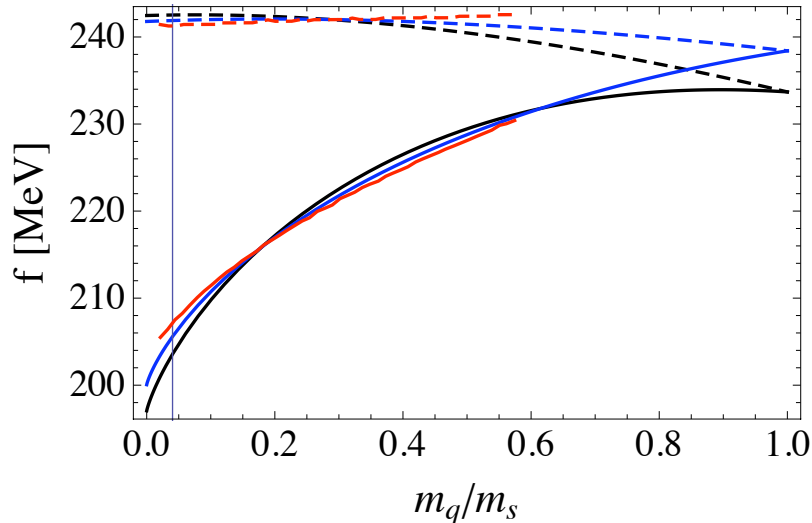


FIGURE 4.2: Light quark mass dependence of f_D (solid lines) and f_{D_s} (dashed lines). The black lines show the results of the NLO HMChPT and the blue lines the results of the covariant NLO ChPT. The red lines are the continuum extrapolations of the HPQCD collaboration [25]. The ratio $r = m_q/m_s$ is related to the pseudoscalar meson masses at leading chiral order through $m_\pi^2 = 2B_0m_s r$ and $m_K^2 = B_0m_s(r+1)$ with $B_0 = m_\pi^2/(m_u + m_d)$ and $m_q = (m_u + m_d)/2$, where m_u , m_d , and m_s are the physical up, down, and strange quark mass.

large light quark masses using the HMChPT results may give unreliable extrapolations. Here we have used the NNLO HMChPT and covariant ChPT results for comparison. The difference will become even larger if the NLO ChPT results are used. We should also mention that even for $m_q/m_s \leq 0.2$ ($m_\pi \leq 307$ MeV) the HPQCD extrapolations are better described by covariant ChPT than by HMChPT judging from the χ^2 analysis (although the difference is so small that it can hardly be appreciated by just looking at the left panel of Fig. 4.4).

We have checked that our covariant results are stable with respect to variations of certain input parameters within reasonable ranges, e.g., $m_\rho < \mu < 2$ GeV and $0.53 < g < 0.67$, where μ is the renormalization scale and g the $DD^*\pi$ coupling defined in Eq. (4.9). With our standard choice: $g = 0.6$ and $\mu = 1$ GeV, we have also noticed that for the NNLO covariant ChPT to produce a smaller χ^2 than the linear chiral extrapolation, c' has to be larger than 1.23. If we use the quenched LQCD result, $c' = 1.35 \pm 0.06$ [64], the fit is even better⁸. On the other hand, our results remain qualitatively the same with either $c' = 1$ or $c' = 1.35$. Therefore we have presented the results obtained with $c' = 1$.

Chiral perturbation theory not only helps extrapolating LQCD simulations to the physical light quark masses. It also benefits from this process because once the values of the relevant LECs are fixed by fitting the IQCD data, ChPT predicts observables involving the same set of LECs. In the present case, assuming that the $1/m_Q$ corrections to the values of the three LECs b_D , b_A , and g are small, we can calculate the ratio of f_{B_s}/f_B by making the following replacements in our NNLO covariant ChPT results:

$$m_D \rightarrow m_B, \quad \Delta \rightarrow \Delta(B), \quad \text{and} \quad \Delta_s \rightarrow \Delta_s(B). \quad (4.22)$$

⁸Using the results from a more recent calculation by the UKQCD collaboration [65], one obtains $c' \approx 1.18 \pm 0.13$, which is compatible with the result of Ref. [64] but with larger uncertainties.

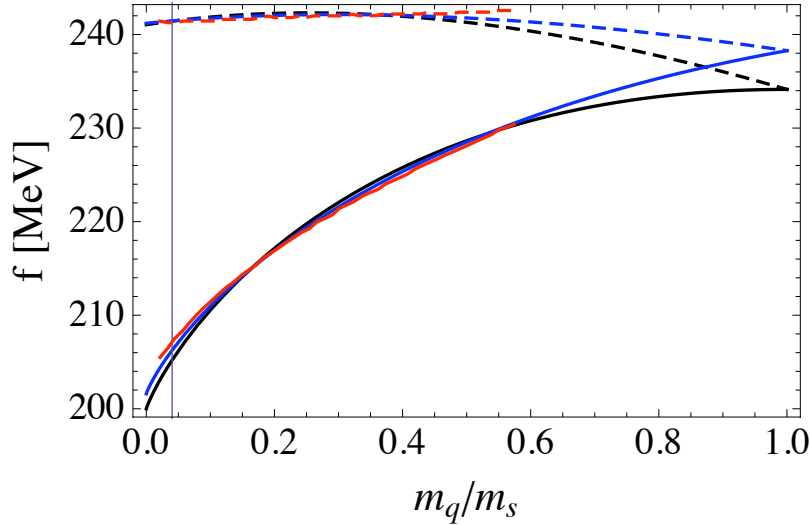
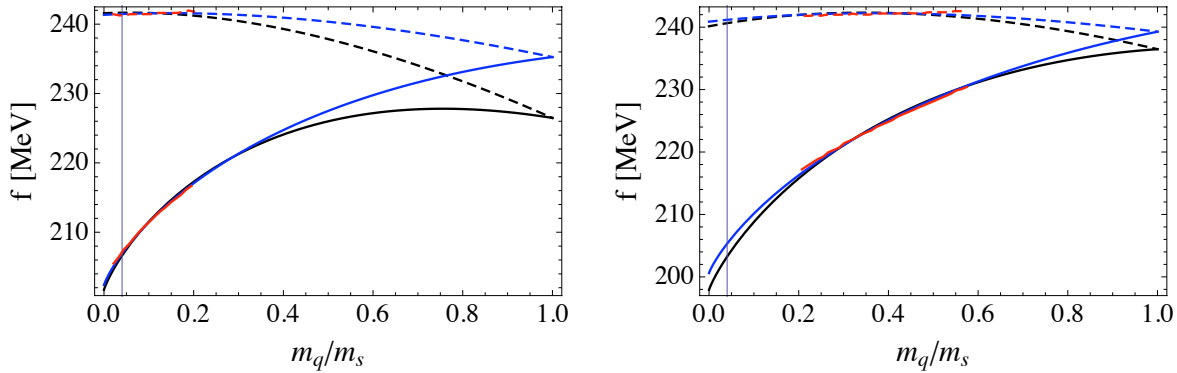


FIGURE 4.3: Same as Fig. 4.2, but the chiral expansions are calculated up to NNLO.

FIGURE 4.4: Same as Fig. 4.3, but on the left panel only the lattice extrapolations with $m_q/m_s \leq 0.2$ are fitted while on the right panel only those with $m_q/m_s > 0.2$ are fitted.

It is found that deviations of b_D and b_A from those determined from the $D(D^*)$ mesons affect the f_{B_s}/f_B ratio only by small amounts. Changing b_D and b_A by $\sim 15\%$ changes f_{B_s}/f_B ratio by only about 1%. On the other hand, the effect of $g_{BB^*\pi}$ is much larger. If heavy quark flavor symmetry were exact, one would have $g_{BB^*\pi} = g_{DD^*\pi} = 0.6$. However, lattice QCD simulations indicate that $g_{BB^*\pi}$ is most likely smaller than $g_{DD^*\pi}$. For instance, two most recent $N_f = 2$ studies give $g_{BB^*\pi} = 0.516(5)(33)(28)(28)$ [66] and $g_{BB^*\pi} = 0.44 \pm 0.03^{+0.07}_{-0.00}$ [67]. Using 0.516 as the central value and 0.60 (0.44) as the upper(lower) bounds for $g_{BB^*\pi}$, we find:

$$f_{B_s}/f_B = 1.22^{+0.05}_{-0.04}, \quad (4.23)$$

which agrees very well with the most precise result from the HPQCD collaboration: $f_{B_s}/f_B = 1.226(26)$ [68]. The uncertainty of ~ 0.05 does not take into account all sources of uncertainties⁹, but nevertheless it represents a reasonable estimate by covering a range of $g_{BB^*\pi}$ values suggested by the two recent LQCD calculations and possible $1/m_Q$ corrections to b_D and b_A .

⁹For instance, the small uncertainties propagated from the LQCD results of f_D (f_{D_s}).

4.2 Predictions on $f_{D_s^*}/f_{D^*}$, f_{B_s}/f_B , and $f_{B_s^*}/f_{B^*}$ in NNLO covariant ChPT

The decay constants of the ground-state D (D^*) and B (B^*) mesons have been subjects of intensive study over the past two decades. Assuming exact isospin symmetry, there are eight independent heavy-light (HL) decay constants: f_D (f_{D^*}), f_{D_s} ($f_{D_s^*}$), f_B (f_{B^*}), f_{B_s} ($f_{B_s^*}$). In the static limit of infinitely heavy charm (bottom) quarks, the vector and pseudoscalar D (B) meson decay constants become degenerate, and in the chiral limit of massless up, down and strange quarks, the strange and non-strange D (B) meson decay constants become degenerate. In the real world, both limits are only approximately realized and, as a result, the degeneracy disappears.

The gluonic sector of Quantum ChromoDynamics (QCD) is flavor blind, so the non-degeneracy between the HL decay constants must be entirely due to finite values of the quark masses in their hierarchy. A systematic way of studying the effects of finite quark masses is the heavy-meson chiral perturbation theory (HMChPT) [33, 46, 47]. The HL decay constants have been calculated up to next-to-leading order (NLO) in the chiral expansion, and to leading-order (LO) [55, 56] and NLO [57, 69] in $1/m_H$ expansion, where m_H is the generic mass of the HL systems. In the previous section, the covariant formulation of ChPT has been employed to study the pseudoscalar decay constants, where faster convergence compared to HMChPT was observed.

Lattice QCD (LQCD) provides an ab initio method for calculating the HL decay constants. There exist many $n_f = 2 + 1$ computations of the pseudoscalar decay constants, f_{D_s} and f_D [25, 42, 70–72], and f_{B_s} and f_B [68, 71, 73], motivated by the important role they play in determinations of the CKM matrix elements and in tests of the Standard Model (see, e.g., Ref. [34]). On the other hand, for the vector meson decay constants, most existing simulations are quenched [65, 74, 75], except for Ref. [76] where $n_f = 2$. Simulations with $n_f = 2 + 1$ are underway [77].

In this section, we present a next-to-next-to-leading order (NNLO) covariant ChPT study of the HL pseudoscalar and vector meson decay constants. We will show that heavy-quark spin-flavor symmetry breaking effects only lead to small deviations of the ratios f_{B_s}/f_B , $f_{D_s^*}/f_{D^*}$, and $f_{B_s^*}/f_{B^*}$, from f_{D_s}/f_D . Utilizing the latest HPQCD data on f_{D_s} and f_D [25], and taking into account heavy-quark spin-flavor symmetry breaking corrections to the relevant low-energy constants (LECs), we are able to make some highly nontrivial predictions on the other three ratios. The predicted light-quark mass dependencies of the HL decay constants are also of great value for future lattice simulations.

The decay constants of the D and D^* mesons with quark content $\bar{q}Q$, with $q = u, d, s$, are defined in Eq. (4.2) and (4.3). For the sake of comparison with other approaches, we introduce $f_{P^*} = F_{P^*}/m_{P^*}$, which has mass dimension one. Our formalism can be trivially extended to the B meson decay constants and therefore in the following we concentrate on the D mesons, therefore we take $Q = c$ in Eq. (4.2) and (4.3).

To construct the relevant Lagrangians in a compact manner, one uses the fields¹⁰ Eq. (3.11) and the current as in Ref. [47]:

$$J = \frac{1}{2}\gamma^\mu(1 - \gamma_5)J_\mu, \quad (4.24)$$

¹⁰It should be noted that the heavy-light states in the relativistic formalism have mass dimension of 1 instead of $3/2$ as in the HM formulation.

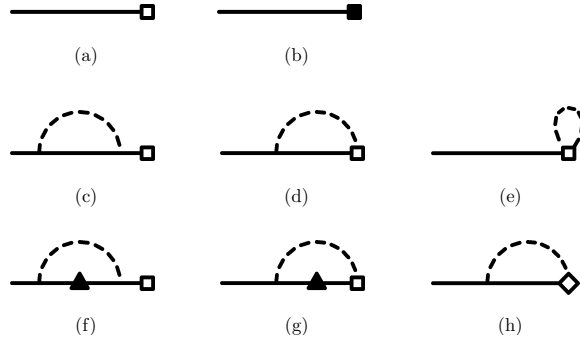


FIGURE 4.5: Feynman diagrams contributing to the heavy-light (HL) decay constants up to NNLO: (a) and (b) are LO and NLO tree level diagrams, loop diagrams (c), (d) and (e) contribute at NLO while diagrams (f), (g) and (h) contribute at NNLO. The solid lines denote either HL pseudoscalar or HL vector mesons and combinations thereof, dashed lines represent Nambu-Goldstone bosons, the empty (solid) squares and empty diamond denote currents from the first (third) and second order Lagrangians, and the solid triangles denote mass insertions of second chiral order (see Ref. [78]).

where $J_\mu = (J_\mu^{cu}, J_\mu^{cd}, J_\mu^{cs})^T$ with the weak current $J_\mu^{cq} = \bar{c}\gamma_\mu(1 - \gamma^5)q$. The weak couplings have the following form [47]:

$$\mathcal{L}_w^{(1)} = \alpha \text{Tr}[J_b H_a] \xi_{ab}^\dagger, \quad (4.25)$$

$$\mathcal{L}_w^{(2)} = \frac{\alpha}{\Lambda_\chi} \left\{ i\beta_1 \text{Tr}[J_b H_a \phi_{ab}] + \frac{\beta_2}{m_P} \text{Tr}[J_b \partial_\nu H_a] \omega_{ab}^\nu \right\}, \quad (4.26)$$

$$\begin{aligned} \mathcal{L}_w^{(3)} = & -\frac{\alpha}{2\Lambda_\chi^2} \left\{ b_D \text{Tr}[J_b H_a] (\chi_+ \xi^\dagger)_{ab} \right. \\ & \left. + b_A \text{Tr}[J_b H_a] \xi_{ab}^\dagger (\chi_+)_{cc} \right\}, \end{aligned} \quad (4.27)$$

where α is a normalization constant of mass dimension two, $\omega_\mu = \xi \partial_\mu \Sigma^\dagger$, $\Lambda_\chi = 4\pi F_0$ is the scale of spontaneous chiral symmetry breaking, and χ_+ is defined as in Section 3.1. Here we have counted the axial current, the derivative on the NG boson fields, and their masses as $\mathcal{O}(p)$, as usual.

To calculate chiral loops, the LO Lagrangian is introduced as in Section 3.3, which we cite here for convenience (in this section, only the relevant terms are explicitly shown):

$$\mathcal{L}^{(1)} = \frac{gm_P}{2} \text{Tr}[\bar{H}_b H_a \not{\psi}_{ab} \gamma_5]. \quad (4.28)$$

It describes the interactions between a pair of HL mesons (PP^* or P^*P^*) with a Nambu-Goldstone boson $\phi = \pi, K, \eta$. In Eq. (4.25) to (4.28), we have introduced m_P for the sake of convenience. It should be taken as \hat{m}_D (\hat{m}_B) at NLO and m_D (m_B) at NNLO. In the D meson sector, $g_{DD^*\pi} \equiv g = 0.60 \pm 0.07$ [49], while $g_{D^*D^*\pi} \equiv g^*$ is not precisely known. At the chiral order we are working, one can take $g_{DD^*\phi} = g_{DD^*\pi}$. If heavy quark spin-flavor symmetry is exact, $g_{BB^*\phi} = g_{B^*B^*\phi} = g_{D^*D^*\phi} = g_{DD^*\phi}$, otherwise deviations are expected.

The Feynman diagrams contributing to the decay constants up to NNLO¹¹ are shown in Fig. 4.5. For the HL pseudoscalar meson decay constants, diagrams (a-g) have been calculated in the previous section. However, diagram (h) that contains two new LECs β_1 and β_2 was not considered there. Its contribution to the pseudoscalar decay constant is

$$R_i^h = \frac{\hat{\alpha}}{\Lambda_\chi} \sum_{j,k} \xi_{i,j,k} \left(\frac{gm_P}{16F_0^2 m_i^2} \right) \left(\frac{-1}{16\pi^2} \right) \phi^h(m_i^2, m_k^2)$$

with

$$\begin{aligned} \phi^h = & 4\beta_1 \left[m_k^2 ((4m_i^2 - m_k^2) \bar{B}_0(m_i^2, m_i^2, m_k^2) + \bar{A}_0(m_k^2)) \right. \\ & \left. + (2m_i^2 - m_k^2) \bar{A}_0(m_i^2) \right] + \frac{\beta_2}{m_i^2} \left[-2m_k^4 (m_k^2 - 4m_i^2) \right. \\ & \times \bar{B}_0(m_i^2, m_i^2, m_k^2) - m_i^6 + (4m_i^2 m_k^2 + 6m_i^4 - 2m_k^4) \\ & \left. \times \bar{A}_0(m_i^2) + 2(5m_i^2 m_k^2 + m_k^4) \bar{A}_0(m_k^2) + m_i^2 m_k^4 \right], \end{aligned}$$

where $\xi_{i,j,k}$ can be found in Table 4.2 with i running over D and D_s , j over D^* and D_s^* , and k over π , η , and K . The functions $\bar{A}_0 = (-16\pi^2)A_0$ and $\bar{B}_0 = (-16\pi^2)B_0$ with A_0 and B_0 defined in Appendix A.1. It should be noted that at NNLO the HL meson masses appearing here are the average of the vector and pseudoscalar heavy-light mesons, i.e. \hat{m}_D and \hat{m}_B in Table 4.1. For the diagrams contributing to the HL vector meson decay constants, the computation of the corresponding diagrams (a, b, e) is the same as in the case of the pseudoscalar decay constants, keeping in mind that now α , b_D , and b_A are all understood to be different from those in the pseudoscalar sector by heavy-quark spin symmetry breaking corrections.

The loop diagrams for vector mesons fall into two categories, depending on whether a HL vector meson (class I) or a HL pseudoscalar meson (class II) propagates in the loop. For vector mesons, the wave function renormalization diagrams (f) yield:

$$R_i^{f^{I,II}} = \sum_{j,k} \xi_{i,j,k} \left(\frac{1}{18F_0^2} \right) \left(\frac{-1}{16\pi^2} \right) \frac{d\phi^{f^{I,II}}(p_i^2, m_j^2, m_k^2)}{dp_i^2} \Big|_{p_i^2=m_i^2},$$

with

$$\begin{aligned} \phi^{f^I} = & (g^*)^2 \left[3(-p_i^2 + (m_j - m_k)^2)(-p_i^2 + (m_j + m_k)^2) \right. \\ & \times \bar{B}_0(p_i^2, m_k^2, m_j^2) + 3\bar{A}_0(m_j^2)(-p_i^2 + m_k^2 - m_j^2) \\ & \left. - 3\bar{A}_0(m_k^2)(p_i^2 + m_k^2 - m_j^2) + p_i^2(-p_i^2 + 3m_k^2 + 3m_j^2) \right], \end{aligned}$$

¹¹The chiral order of a properly renormalized diagram with L loops, N_M (N_H) Nambu-Goldstone boson (HL meson) propagators and V_k vertices from k th-order Lagrangians is $n_\chi = 4L - 2N_M - N_H + \sum_k kV_k$.

$$\begin{aligned}\phi^{f^{II}} &= -\frac{m_P^2}{2p_i^2}g^2 \left[-3(-2m_k^2(p_i^2 + m_j^2) + (m_j^2 - p_i^2)^2 + m_k^4) \right. \\ &\quad \times \bar{B}_0(p_i^2, m_k^2, m_j^2) + 3\bar{A}_0(m_k^2)(p_i^2 + m_k^2 - m_j^2) \\ &\quad \left. + 3\bar{A}_0(m_j^2)(p_i^2 - m_k^2 + m_j^2) + 6p_i^2(m_k^2 + m_j^2) - 2p_i^4 \right],\end{aligned}$$

where i denotes (D^*, D_s^*) and j denotes either (D^*, D_s^*) or (D, D_s) .

Diagrams (g) yield $R^{g^I} = 0$ and

$$R^{g^{II}} = \sum_{j,k} \xi_{i,j,k} \left(\frac{\alpha g}{72F_0^2 m_i^2} \right) \left(\frac{-1}{16\pi^2} \right) \phi^{g^{II}}(m_i^2, m_j^2, m_k^2)$$

with

$$\begin{aligned}\phi^{g^{II}} &= -3((m_i - m_k)^2 - m_j^2)((m_i + m_k)^2 - m_j^2) \\ &\quad \times \bar{B}_0(m_i^2, m_j^2, m_k^2) + 3\bar{A}_0(m_j^2)(m_i^2 + m_j^2 - m_k^2) \\ &\quad + 3\bar{A}_0(m_k^2)(m_i^2 - m_j^2 + m_k^2) - 2m_i^2(m_i^2 - 3(m_j^2 + m_k^2)).\end{aligned}$$

Diagrams (h) give

$$R^{h^{I,II}} = \frac{\alpha}{\Lambda_\chi} \sum_{j,k} \xi_{i,j,k} \left(\frac{gm_P}{144F_0^2 m_i^2} \right) \left(\frac{-1}{16\pi^2} \right) \phi^{h^{I,II}}(m_i^2, m_k^2)$$

with

$$\begin{aligned}\phi^{h^I} &= 8\beta_1 \frac{m_i^2}{m_P^2} \frac{g^*}{g} \left[(6m_i^2 - 3m_k^2)\bar{A}_0(m_i^2) - 3m_i^2 m_k^2 - 2m_i^4 \right. \\ &\quad \left. + 3m_k^2[(4m_i^2 - m_k^2)\bar{B}_0(m_i^2, m_i^2, m_k^2) + \bar{A}_0(m_k^2)] \right],\end{aligned}$$

$$\begin{aligned}\phi^{h^{II}} &= 4\beta_1 \left[3m_k^2((4m_i^2 - m_k^2)\bar{B}_0(m_i^2, m_i^2, m_k^2) \right. \\ &\quad \left. + \bar{A}_0(m_k^2)) + (6m_i^2 - 3m_k^2)\bar{A}_0(m_i^2) + 6m_i^2 m_k^2 \right. \\ &\quad \left. + 4m_i^4 \right] + \frac{\beta_2}{m_P^2} \left[-6m_k^4(m_k^2 - 4m_i^2)\bar{B}_0(m_i^2, m_i^2, m_k^2) \right. \\ &\quad \left. + 6(3m_i^2 - m_k^2)(m_i^2 + m_k^2)\bar{A}_0(m_i^2) + 8m_i^4 m_k^2 \right. \\ &\quad \left. + 21m_i^2 m_k^4 + 9m_i^6 + 6(3m_i^2 m_k^2 + m_k^4)\bar{A}_0(m_k^2) \right].\end{aligned}$$

As explained in Section 4.1, mass insertions in diagrams (c, d) generate NNLO contributions. Therefore, using $m_{D_s} \rightarrow m_D + \Delta_s$, $m_{D^*} \rightarrow m_D + \Delta$, and $m_{D_s^*} \rightarrow m_D + \Delta + \Delta_s$ for the HL meson masses in diagrams (f, g), one obtains the full NNLO results of these diagrams. The complete NNLO results for the pseudoscalar

and vector HL decay constants are

$$\begin{aligned} f_i &= \hat{\alpha}(1 + \tilde{Z}_i/2) + \delta_i + T_i + \tilde{C}_i + \tilde{R}_i^h, \\ F_i^* &= \alpha(1 + (\tilde{R}_i^{fI} + \tilde{R}_i^{fII})/2) + m_P \delta_i^* + R_i^e + \tilde{R}_i^{gII} + \tilde{R}_i^{hI} + \tilde{R}_i^{hII}, \end{aligned}$$

where $\hat{\alpha} = \alpha/m_P$ and Z_i , T_i , and C_i can be found in Section 4.1 and $R_i^e = m_P T_i$. The NLO tree level δ_i^* equals δ_i , where b_A and b_D are replaced by the low-energy constants from the vector meson sector of the theory b_A^* and b_D^* . The Lagrangian Eq. (4.27) implies $b_A = b_A^*$ and $b_D = b_D^*$, which has to be modified by finite subtractions, as explained in the following. As previously, the “tilde” indicates that one has to perform a subtraction to remove the power-counting-breaking terms that are inherent of covariant ChPT involving heavy hadrons whose masses do not vanish at the chiral limit (for details see Refs. [49, 78]). Furthermore, a second subtraction is needed to ensure that heavy-quark spin symmetry is exact in the limit of infinite heavy quark masses. This means $F_i^* = m_P f_i$ should hold for $m_P \rightarrow \infty$. In order to achieve this, the NNLO low-energy constants b_A^* and b_D^* have to be shifted by finite parts (equivalently one can also shift b_A and b_D). We impose at order $n_\chi = 3$ for $m_P \rightarrow \infty$:

$$m_P \delta_i^* + \alpha(\tilde{R}_i^{fI} + \tilde{R}_i^{fII})/2 + \tilde{R}_i^{gII} - m_P \delta_i - \alpha(\tilde{Z}_i/2) - m_P \tilde{C}_i \stackrel{!}{=} 0 \quad (4.29)$$

This can be achieved by shifting the NNLO low-energy constant b_A^* and b_D^* according to

$$\begin{aligned} b_A^* &\rightarrow \frac{1}{72} \left(11(g-2)g \log \left(\frac{m_{D,0}^2}{\mu^2} \right) + 72 b_A - 22(g-1)g \right) \\ b_D^* &\rightarrow \frac{1}{24} \left(5(g-2)g \log \left(\frac{m_{D,0}^2}{\mu^2} \right) + 24 b_D - 10(g-1)g \right) \end{aligned} \quad (4.30)$$

After these subtractions (or redefinition of low-energy constants) the results can be expanded in the inverse heavy-light meson mass. In the limit $m_P \rightarrow \infty$ the lowest order HMChPT results are recovered. The covariant approach, being fully relativistic, sums all powers of contributions in $1/m_P$, which are of higher order in HMChPT. Such a relativistic formulation is not only formally appealing. It also converges faster than non-relativistic formulations, such as HMChPT and HBChPT. This has been recently demonstrated in the one-baryon sector and in heavy-light systems for a number of observables (see, e.g., Refs. [49, 78]). It should be stressed that the loop functions are divergent and the infinities have been removed as previously or as in Ref. [78].

Now we are in a position to perform numerical studies. We first fix the five LECs, α , b_D , b_A , β_1 , and β_2 , by fitting the HPQCD f_{D_s}/f_D extrapolations [25]. The results are shown in Fig. (4.6a). The NNLO ChPT fits the chiral and continuum extrapolated lattice QCD results remarkably well, keeping in mind that the HPQCD extrapolations were obtained using the NLO HMChPT results supplemented with higher-order analytical terms [25].

In addition to providing the NNLO ChPT results that should be useful for future lattice simulations of the HL decay constants, a primary aim of the present study is to predict quantitatively the SU(3) breaking

corrections to $f_{D_s^*}/f_{D^*}$, f_{B_s}/f_B , and $f_{B_s^*}/f_{B^*}$ from that of the f_{D_s}/f_D . To achieve this, one must take into account heavy-quark spin-flavor symmetry breaking corrections to the LECs: α , b_D , b_A , β_1 , β_2 , and $g_{PP^*\phi}$ ($g_{P^*P^*\phi}$).

The LEC α is only relevant for the absolute value of the decay constants, therefore it does not appear in the SU(3) breaking ratios. However, in the Lagrangian of Eqs. (4.25,4.26), one implicitly assumes heavy-quark spin symmetry, i.e., $c' = \frac{f_{P^*}\sqrt{m_{P^*}}}{f_P\sqrt{m_P}} = 1$, which affects the computation of loop diagrams (g) for pseudoscalars and (g, h) for vector mesons (see Ref. [78] for details). Recent quenched LQCD simulations suggest that c' is within the range of $1.0 \sim 1.2$ [65, 74]. To be conservative we allow c' to vary within $0.8 \sim 1.2$. For b_D , b_A , β_1 , and β_2 , no LQCD data are available. However, the corrections to those constants from heavy-quark spin-flavor symmetry breaking are expected to be $\lesssim 20\%$.

The LECs that affect the predicted ratios most prominently turn out to be g and g^* , which determine the size of chiral loop contributions. In the present case $g_{DD^*\pi}$ is determined by reproducing the D^* meson decay width. Recent $n_f = 2$ LQCD simulations suggest that $g_{BB^*\pi}$ is in the range of $0.4 \sim 0.6$ [66, 67, 79]. We therefore take the central value of 0.516 from Ref. [66] and assign a 20% uncertainty. Studies based on QCD sum rules indicate that g and g^* could differ by $10 \sim 20\%$ [80, 81]. We take this into account in our study.

With heavy-quark spin-flavor symmetry breaking effects on the relevant LECs taken into account as described above, we can now make predictions for the ratios of f_{B_s}/f_B , $F_{D_s^*}/F_{D^*}$, and $F_{B_s^*}/F_{B^*}$ and their light-quark mass dependencies. The results are shown in Figs. (4.6b,4.6c,4.6d). The differences between the four ratios are small, at the order of a few percent. Interestingly, the ratios of the B meson decay constants are found to be larger than those of their D counterparts, in agreement with the HPQCD results [25, 68]. Fully dynamical lattice simulations of the vector meson decay constants should provide a stringent test of our predictions. It should be stressed that the bands shown in Fig. 4.6 reflect the estimated effects of heavy-quark spin-flavor symmetry breaking from the change of the relevant LECs, in addition to those induced by the covariant formulation of ChPT, the use of physical mass splittings and different $g_{DD^*\phi}$ ($g_{BB^*\phi}$). The same is true for the uncertainties of our results given in Table 4.4.

Our predicted ratios at the physical point are compared in Table 4.4 with the results from a number of other approaches, including the lattice simulations [65, 74, 76], the relativistic quark model (RQM) [83], the light-front quark model (LFQM) [84], and the field correlator method (FCM) [82].¹² Our predictions for the relative magnitude of the $f_{P_s^*}/f_{P^*}$ vs. f_{P_s}/f_P ratios agree with those of the FCM [82], the RQM [83] and LFQM [84]. It should be noted that the results in Fig. 4.6 are obtained with a renormalization scale of 1 GeV [78]. Uncertainties have been estimated changing this scale between $\mu = m_D$ and $\mu = m_B$ for the calculation of D and B decay constants, respectively. The changes turn out to be small and are taken into account in the results shown in Table 4.4.

In summary, we have calculated the pseudoscalar and vector decay constants of the B and D mesons using a covariant formulation of chiral perturbation theory up to next-to-next-to-leading order and found that it can describe well the HPQCD $n_f = 2 + 1$ data on f_{D_s}/f_D . Taking into account heavy-quark spin-flavor symmetry breaking effects on the relevant LECs, we have made predictions for the ratios of f_{B_s}/f_B , $f_{D_s^*}/f_{D^*}$, and

¹²It should be mentioned that the NNLO ChPT predictions cover the NLO predictions within uncertainties.

TABLE 4.4: Ratios of f_{D_s}/f_D , $f_{D_s^*}/f_{D^*}$, f_{B_s}/f_B , and $f_{B_s^*}/f_{B^*}$ from different approaches. The $f_{D_s}/f_D = 1.164$ from the HPQCD collaboration [25] is used as input in our approach.

Ref.	f_{D_s}/f_D	$f_{D_s^*}/f_{D^*}$	f_{B_s}/f_B	$f_{B_s^*}/f_{B^*}$
PDG [40]	1.25(6)	-	-	-
FCM [82]	1.24(4)	1.12	1.19(3)	1.15
RQM [83]	1.15	1.02	1.15	1.15
LFQM [84]	1.18(1.20)	1.14(1.18)	1.24(1.32)	1.23(1.32)
QLQCD [74]	1.10(2)	1.11(3)	1.14(3)(1)	1.17(4)(3)
QLQCD [65]	1.11(1)(1)	1.09(1)(2)	1.13(1)(1)	1.14(2)(2)
LQCD [76]			1.14(2)(2)	1.14(2)(2)
HPQCD [25, 68]	1.164(11)		1.226(26)	
NNLO ChPT	1.17	1.10(5)	1.24(4)	1.20(4)

$f_{B_s^*}/f_{B^*}$ and their light quark mass dependencies that should be testable in the near future. Our results show that $f_{B_s}/f_B > f_{D_s}/f_D$ and $f_{D_s^*}/f_{D^*} < f_{D_s}/f_D$ in a large portion of the allowed parameter space.

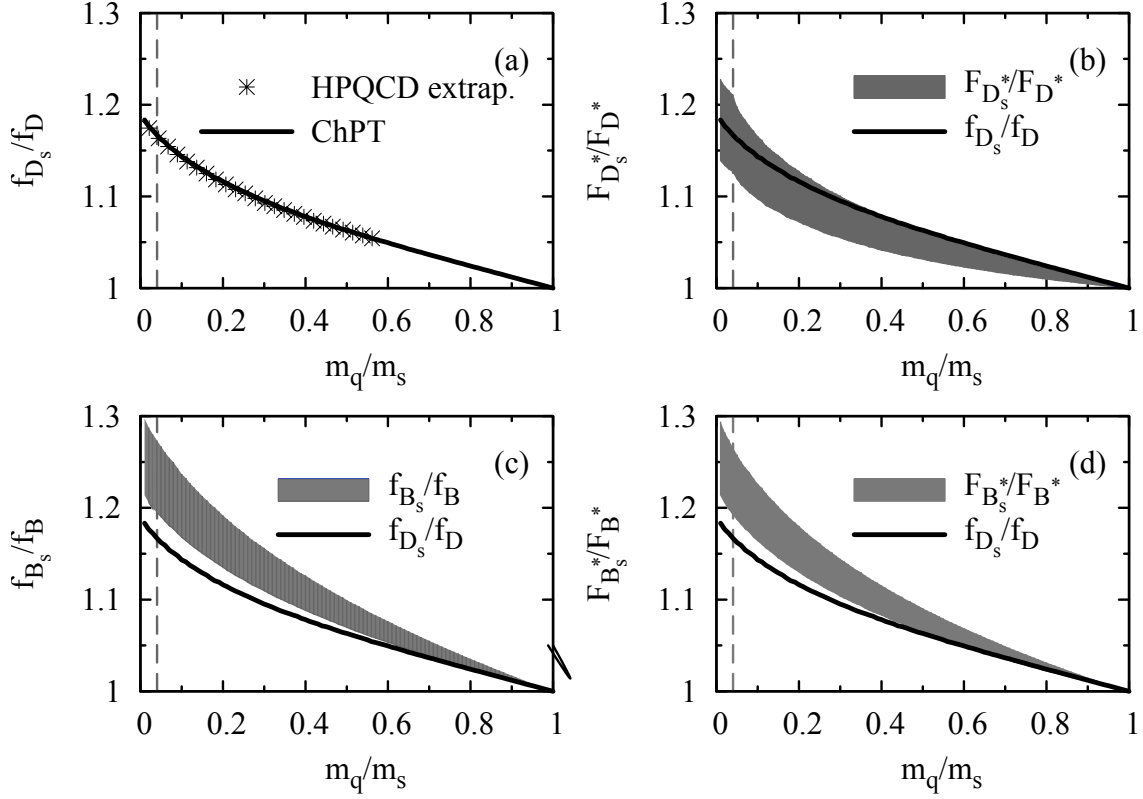


FIGURE 4.6: Light-quark mass evolution of f_{D_s}/f_D , $F_{D_s^*}/F_{D^*}$, f_{B_s}/f_B , and $F_{B_s^*}/F_{B^*}$. The ratio $r = m_q/m_s$ is related to the pseudoscalar meson masses at leading chiral order through $m_\pi^2 = 2B_0m_s r$ and $m_K^2 = B_0m_s(r+1)$ with $B_0 = m_\pi^2/(2m_q)$, where m_s is the physical strange quark mass and m_q the average of up and down quark masses. The vertical dotted lines denote physical m_q/m_s .

Chapter 5

Scattering of Nambu-Goldstone bosons off heavy-light mesons

5.1 Introduction

Measurements of hadronic states with charm quarks such as the $D_{s0}^*(2317)$ have led to extensive and still ongoing discussions about our deeper understanding of mesons and baryons [6, 7, 85], traditionally thought to be composed of a pair of quark and anti-quark or three quarks in the naive quark model. With its mass ($M = 2317.8 \pm 0.6$ MeV) about 100 MeV lower than the lowest $c\bar{s}$ scalar state in the naive quark model, the $D_{s0}^*(2317)$ cannot be a conventional $q\bar{q}$ state [86–99]. One possible interpretation is that of a compound dynamically generated by the strong DK interaction in coupled-channels dynamics [96–98]. Such approaches have provided many useful insights into the nature of some most intriguing new resonances (see, e.g., Refs. [100, 101] for some recent applications).

In order to clarify the nature of the $D_{s0}^*(2317)$, or of any other meson of similar kind, it is useful to study such objects from various perspectives and compare the results with experimental and lattice QCD (LQCD) data. In this respect, it has been argued that the isospin-breaking decay width $D_{s0}^*(2317) \rightarrow D_s\pi$ [102, 103], the light-quark mass dependence [104], and the volume dependence [105] of $D_{s0}^*(2317)$ properties can provide valuable information on its nature. At the same time it should also be noted that, in addition to the $D_{s0}^*(2317)$, coupled-channels unitary dynamics predicts several other states in sectors/channels related to the $D_{s0}^*(2317)$ by heavy-quark spin and flavor symmetry and (approximate) chiral symmetry (or broken SU(4) symmetry) [96–98, 106, 107]. Once the mass and width of the $D_{s0}^*(2317)$ are fixed, so are those of the other related states. Future experiments in search for those resonances in the predicted energy regions are therefore strongly encouraged.

All these predictions are subject to potentially sizable symmetry breaking corrections. In particular, a comprehensive study is necessary to estimate the impact of recoil corrections. For the scattering Length of the Nambu-Goldstone bosons off the D mesons, such a study was performed in [49], showing that these effects are sizable¹. In Chapter 4, or Refs. [78, 109], covariant chiral perturbation theory (ChPT), supplemented with the extended-on-mass-shell (EOMS) scheme, was applied to study the decay constants of the $D(D^*)/B(B^*)$

¹See Ref. [108] for a related discussion on the scattering lengths of the pseudoscalar mesons off the heavy-light vector mesons.

mesons. It was shown that the covariant ChPT converges faster than its non-relativistic (heavy-meson) counterpart. These findings can, to some extent, be deemed as repercussions of the one-baryon sector. For instance, it has been shown that the EOMS formulation of the baryon ChPT is capable of better describing three-flavor observables and their light-quark mass evolutions than its non-relativistic (heavy-baryon) counterpart, see, e.g., Refs. [52, 60, 110] and references cited therein.

In the present chapter we study the interactions of the heavy-light mesons (D , D^* , B , B^* and their strange counterparts) with Nambu-Goldstone bosons (the octet of the lightest pseudoscalar mesons) in covariant ChPT and its unitary version. We calculate the interaction potentials up to next-to-leading order (NLO) and perform an iteration of these potentials to all orders using the Bethe-Salpeter equation. It was pointed out that in the covariant calculation of the loop function appearing in the Bethe-Salpeter equation, one loses the heavy-quark spin and flavor symmetry [104]. We study this problem in detail and propose a new renormalization scheme, similar in spirit to the EOMS scheme widely used in the one-baryon sector [58, 59, 110] and also used in Refs. [49, 78, 109], to recover heavy-quark spin and flavor symmetry up to $1/m_H$ corrections, where m_H is a generic heavy-light meson mass. We apply our approach to describe the most recent fully dynamical LQCD simulations for the scattering lengths of Nambu-Goldstone bosons off the D mesons [12] and fix the relevant low-energy and subtraction constants. We then solve the corresponding Bethe-Salpeter equations and search for poles in the complex energy plane, identified as dynamically generated states. We show that a number of 0^+ and 1^+ states emerge naturally, including the $D_{s0}^*(2317)$, the $D_{s1}^*(2460)$ and their bottom-quark counterparts².

This chapter is organized as follows. In Section 5.2 we give the basic ingredients of unitarized chiral perturbation theory (UChPT). Starting from Section 5.3 we apply this theory to the scattering of Nambu-Goldstone bosons off heavy-light mesons. Subsections 5.3.1 and 5.3.2 give the driving potentials up to NLO. In Subsection 5.4.1 we propose a new renormalization scheme to be used in the Bethe-Salpeter equation, which manifestly satisfies the chiral power counting rules and heavy-quark spin and flavor symmetries. We discuss the advantage of this scheme in comparison with others widely used in unitarized ChPT in Subsection 5.4.2. In this subsection we give also predictions for a number of dynamically generated resonances in both the charm and the bottom sectors. In Section 5.5 we finally investigate off-shell effects on the scattering of Nambu-Goldstone bosons off D mesons.

²A similar strategy was adopted in Refs. [12, 111], but both studies are limited to the 0^+ charm sector, and in addition Ref. [111] studied the preliminary LQCD results of Ref. [112].

5.2 The T-matrix, unitarity, and the Bethe-Salpeter equation

5.2.1 The S- and T-matrix

The operator S -matrix is defined through [18]

$$\langle \mathbf{p}_3 \mathbf{p}_4 | \mathbf{p}_1 \mathbf{p}_2 \rangle_{\text{out}} \equiv \langle \mathbf{p}_3 \mathbf{p}_4 | S | \mathbf{p}_1 \mathbf{p}_2 \rangle, \quad (5.1)$$

where two-particle initial and final states are chosen for better readability. The generalization to more particles is straight forward. The *in* and *out* states are defined in the Heisenberg picture, i.e. the two states have a nontrivial overlap. The states $|\mathbf{p}_1 \mathbf{p}_2\rangle$ and $\langle \mathbf{p}_3 \mathbf{p}_4|$ represent states in the interaction picture, where the S matrix serves as the time evolution operator. Previous definition implies the unitarity of the S matrix, $S^\dagger S = \mathbf{1}$, which is equivalent to the conservation of probability.

The S -matrix is related to the T -matrix by

$$S = \mathbf{1} - iT, \quad (5.2)$$

where $\mathbf{1}$ represents the part where the two initial particles pass each other without interaction. The part that is responsible for the interaction is denoted as T . This definition together with the unitarity condition, $S^\dagger S = \mathbf{1}$, gives

$$i((T - T^\dagger) = T^\dagger T). \quad (5.3)$$

Due to momentum conservation, the matrix elements of T can be expressed as

$$\langle \mathbf{p}_3 \mathbf{p}_4 | T | \mathbf{p}_1 \mathbf{p}_2 \rangle = (2\pi)^4 \delta^{(4)}(p_1 + p_2 - p_3 - p_4) \mathcal{T}(p_1 p_2 \rightarrow p_3 p_4), \quad (5.4)$$

where \mathcal{T} is the invariant matrix element or scattering amplitude. Using this definition in Eq. (5.3) gives the identity

$$\begin{aligned} & \mathcal{T}(p_1 p_2 \rightarrow p_3 p_4) - \mathcal{T}^*(p_3 p_4 \rightarrow p_1 p_2) \\ &= -i \sum_n \left(\prod_{i=1}^n \int \frac{d^3 q_i}{(2\pi)^3} \frac{1}{2E_i} \right) \mathcal{T}^*(p_3 p_4 \rightarrow \{q_i\}) \mathcal{T}(p_1 p_2 \rightarrow \{q_i\}) (2\pi)^4 \delta^{(4)}(p_1 + p_2 - \sum_i q_i), \end{aligned} \quad (5.5)$$

where we have inserted a complete set of intermediate states with particle number n and momenta q_i for $i = 1, \dots, n$. It relates the imaginary part of the forward scattering amplitude to the total cross section³. This special case of equation (5.5) is known as optical theorem.

We concentrate on two particle intermediate states with momenta $q_1 \equiv -\tilde{Q}$ and $q_2 \equiv \tilde{Q} + P$. Then Eq.

³Our normalization of \mathcal{T} is chosen such that the differential cross section in the center of mass frame is given by $\frac{d\sigma}{d\Omega_{\text{CM}}} = \frac{1}{64\pi^2 s} \frac{p_f}{p_i} |\mathcal{T}(p_1 p_2 \rightarrow p_3 p_4)|^2$, where p_i and p_f are the center of mass momenta of the initial and final particles, $p_i = \frac{1}{2\sqrt{s}} \lambda^{1/2}(s, m_1^2, m_2^2)$ and $p_f = \frac{1}{2\sqrt{s}} \lambda^{1/2}(s, m_3^2, m_4^2)$, with the mass m_k of particle k . The total momentum squared is denoted as $s = P^2$ and $\lambda(x, y, z) = x^2 + y^2 + z^2 - 2xy - 2xz - 2yz$ is the Källén function.

(5.5) reads

$$\begin{aligned}
& \mathcal{T}(p_1 p_2 \rightarrow p_3 p_4) - \mathcal{T}^*(p_3 p_4 \rightarrow p_1 p_2) \\
&= -i \int \frac{d^4 \tilde{Q}}{(2\pi)^4} \mathcal{T}^*(p_3 p_4 \rightarrow -\tilde{Q}, \tilde{Q} + P) \mathcal{T}(p_1 p_2 \rightarrow -\tilde{Q}, \tilde{Q} + P) \\
& \quad \times (2\pi)^2 \delta^+((P + \tilde{Q})^2 - m^2) \delta^+((-\tilde{Q})^2 - M^2), \tag{5.6}
\end{aligned}$$

with $\delta^+(q_i^2 - m^2) = \Theta(q_i^0) \delta(q_i^2 - m^2)$ for $i = 1, 2$. The total momentum is $P = p_1 + p_2 = p_3 + p_4$ and the masses of the particles with momenta q_1 and q_2 are denoted as M and m . This relation is the two-particle unitarity requirement. As will be shown, this relation is fulfilled by solutions of the Bethe-Salpeter (BS) equation. In other words: solutions of the BS equation conserve probability to all orders, not only on a perturbative level.

5.2.2 The Bethe-Salpeter equation

BS equation for $P\phi$ scattering

The Bethe-Salpeter equation [113] for scattering a Nambu-Goldstone boson ϕ off a pseudoscalar heavy-light meson P reads

$$\mathcal{T}_P(q, Q) = \mathcal{V}_P(q, Q) - i \int \frac{d^4 \tilde{Q}}{(2\pi)^4} \mathcal{V}_P(q, \tilde{Q}) \Delta_h(\tilde{Q}) \Delta_l(\tilde{Q} + P) \mathcal{T}_P(\tilde{Q}, Q), \tag{5.7}$$

where the propagator of the heavy-light meson is denoted by Δ_h and the propagator of the light Nambu-Goldstone boson by Δ_l . The scattering amplitude is abbreviated as $\mathcal{T}_P(q, Q) \equiv \mathcal{T}(P(p_1)\phi(p_2) \rightarrow P(p_3)\phi(p_4))$, where the momenta are related by $p_1 = -q$, $p_2 = q + P$, $p_3 = -Q$ and $p_4 = Q + P$. In accordance with this convention the potential is denoted by $\mathcal{V}_P(q, Q)$. Diagrammatically, the BS equation is shown in Figure 5.1. It is straight forward to include channel coupling effects by promoting \mathcal{T}_P and \mathcal{V}_P to matrices. The multiplication in (5.7) is then understood as matrix multiplication and the propagators become diagonal matrices. Explicitly, equation (5.7) becomes

$$\left(\mathcal{T}_P(q, Q) \right)_{ij} = \left(\mathcal{V}_P(q, Q) \right)_{ij} - i \int \frac{d^4 \tilde{Q}}{(2\pi)^4} \left(\mathcal{V}_P(q, \tilde{Q}) \right)_{ik} \Delta_{h,k}(\tilde{Q}) \Delta_{l,k}(\tilde{Q} + P) \left(\mathcal{T}_P(\tilde{Q}, Q) \right)_{kj}, \tag{5.8}$$

where $\Delta_{h,k}$ and $\Delta_{l,k}$ are the propagators corresponding to the two-particle state k . From now on channel coupling effects are treated implicitly as far as possible.

Inserting the exact propagators together with the exact two-particle irreducible amplitude (the potential) into equation (5.7) gives access to the exact scattering amplitude. However, since both are not exactly known, one has to rely on approximations. We use the free propagators

$$\Delta_h(q) = \frac{i}{q^2 - M^2 + i\epsilon}, \quad \Delta_l(q) = \frac{i}{q^2 - m^2 + i\epsilon}, \tag{5.9}$$

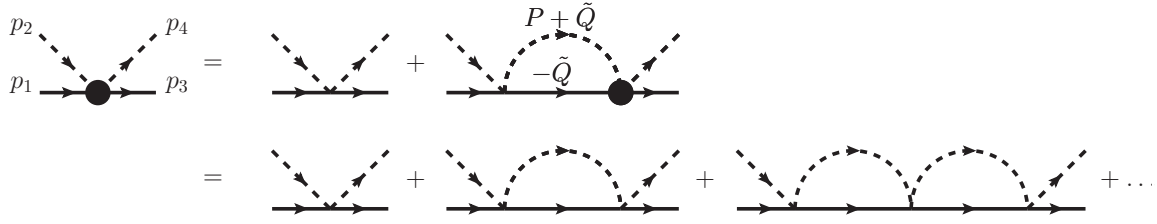


FIGURE 5.1: Diagrammatical representation of the Bethe-Salpeter equation. The solid lines correspond to pseudoscalar heavy-light mesons and the dashed lines to Nambu-Goldstone bosons. The left side represents the scattering amplitude and the first term on the right side the potential.

where M stands for the mass of heavy-light meson and m for the mass of the Nambu-Goldstone boson. For the potential no further assumptions are necessary at the moment. Using these propagators, we can proof the unitarity requirement (5.6) for the solution \mathcal{T}_P of equation (5.7). Obviously, the scattering amplitude is real for total momentum \sqrt{s} smaller than the lightest possible mass for the intermediate state. In this case no denominator vanishes and one can ignore the $i\epsilon$ prescription for treating the poles in the propagators. Hence, for $\sqrt{s} < m + M$, we can write

$$\mathcal{T}_P(q, Q) \Big|_{P^2=s} = \left[\mathcal{T}_P(q, Q) \Big|_{P^2=s^*} \right]^* . \quad (5.10)$$

Since the scattering amplitude is an analytical function depending on s , it can be continued to the entire complex s plane by

$$\begin{aligned} \operatorname{Re} \mathcal{T}_P(q, Q) \Big|_{P^2=s+i\epsilon} &= \operatorname{Re} \mathcal{T}_P(q, Q) \Big|_{P^2=s-i\epsilon} \\ \operatorname{Im} \mathcal{T}_P(q, Q) \Big|_{P^2=s+i\epsilon} &= -\operatorname{Im} \mathcal{T}_P(q, Q) \Big|_{P^2=s-i\epsilon} \end{aligned} \quad (5.11)$$

near the real s axis for $\sqrt{s} > M + m$. The discontinuity across the cut is given by

$$\operatorname{Disc}_s \left[\mathcal{T}_P(q, Q) \Big|_{P^2=s} \right] = 2i \operatorname{Im} \left[\mathcal{T}_P(q, Q) \Big|_{P^2=s+i\epsilon} \right] . \quad (5.12)$$

Inserting equation (5.7) into the left side of the two-particle unitarity requirement (5.6) gives

$$\begin{aligned} \operatorname{Disc}_s \left[-i \int \frac{d^4 \tilde{Q}}{(2\pi)^4} \mathcal{V}_P(q, \tilde{Q}) \Delta_h(\tilde{Q}) \Delta_l(\tilde{Q} + P) \mathcal{T}_P(\tilde{Q}, Q) \right] = \\ -i \int \frac{d^4 \tilde{Q}}{(2\pi)^2} \mathcal{T}_P(q, \tilde{Q}) \delta^+((-\tilde{Q})^2 - M^2) \delta^+((\tilde{Q} + P)^2 - m^2) \mathcal{T}_P^*(Q, \tilde{Q}) , \end{aligned} \quad (5.13)$$

where we have used time reversal invariance, $\mathcal{T}_P(q, Q) = \mathcal{T}_P(Q, q)$. In the following we proof that solutions of the BS equation fulfill this relation. First, we realize that the BS equation can be understood as an iteration of loop diagrams. Then the discontinuity of each diagram can be directly evaluated. For the one-loop correction this is straight forward. One has to shift to the center of mass frame $P^\mu = (P^0, \mathbf{0})$, then all poles in \tilde{Q}^0 can be identified and finally the discontinuity is obtained by use of Cauchy's integral formula. The result, however, is

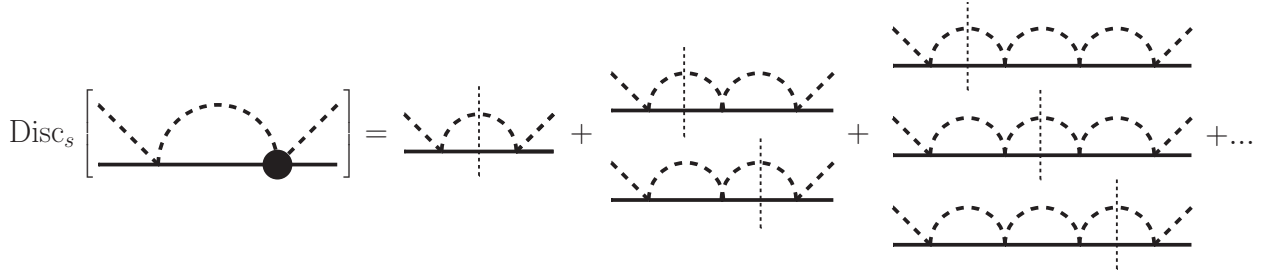


FIGURE 5.2: Diagrammatic proof of equation (5.13) by use of Cutkosky's rule.

equivalent to “cutting” the diagram as shown in the first term on the right side of Figure 5.2, and replacing the cut propagators by

$$\frac{i}{p^2 - m^2 \pm i\epsilon} \rightarrow \pm 2\pi\delta^+(p^2 - m^2). \quad (5.14)$$

This prescription is known as Cutkosky's cutting rules. These rules can be generalized to arbitrary Feynman diagrams as shown in [114]. For various applications see also [115]. Due to Cutkosky all possible cuts have to be drawn to evaluate the discontinuity of a given Feynman diagram. Applying this to the left side of equation (5.13) gives the cuts shown in Figure 5.2. Now one has to take into account that all propagators right to the cut are replaced according to the rule $i/(p^2 - m^2 + i\epsilon) \rightarrow -i/(p^2 - m^2 - i\epsilon)$, whereas the propagators left to the cut keep as they are. Finally, the vertices $i\mathcal{V}_P$ right to the cut are replaced by their complex conjugated $-i\mathcal{V}_P^*$ and the total sign of the cut Feynman diagram is flipped. This yields immediately the right side of equation (5.13). As should be clear from this proof, the potential should no longer enter the expression, whereas the scattering amplitude has to appear twice, once of it as its complex conjugated. It is important to notice that we have not made any further assumptions on the potential and scattering amplitude, except that we do not include more than two-particle intermediate states, in accordance with the two-particle unitarity requirement. One should also note that off-shell parts in the potential do not alter the previous statements. This is of relevance for the off-shell resummation proposed in Section 5.5.

BS equation for $P^*\phi$ scattering

Similar to the BS equation for scattering pseudoscalar mesons, we can write down an equation for the scattering of vector mesons P^* off pseudoscalar mesons ϕ . This reads

$$T_P^{\mu\nu}(q, Q) = \mathcal{V}_P^{\mu\nu}(q, Q) - i \int \frac{d^4\tilde{Q}}{(2\pi)^4} \mathcal{V}_P^{\mu\sigma}(q, \tilde{Q}) \Delta_{h,\sigma\bar{\sigma}}(\tilde{Q}) \Delta_l(\tilde{Q} + P) T_P^{\bar{\sigma}\nu}(\tilde{Q}, Q), \quad (5.15)$$

where the potential $\mathcal{V}_P^{\mu\nu}$ and the scattering amplitude $T_P^{\mu\nu}$ carry Lorentz indices μ and ν , corresponding to the ingoing and outgoing vector meson fields $P^{*\nu}$ and $P^{*\mu}$. The free vector-meson propagator is

$$\Delta_{h,\mu\nu}(q) = \left(-g^{\mu\nu} + \frac{q^\mu q^\nu}{M^2} \right) \frac{i}{q^2 - M^2 + i\epsilon}, \quad (5.16)$$

and the free Nambu-Goldstone propagator Δ_l is given in equation (5.9). The momenta are assigned as previously. Equation (5.7) is shown diagrammatically in Figure 5.3.

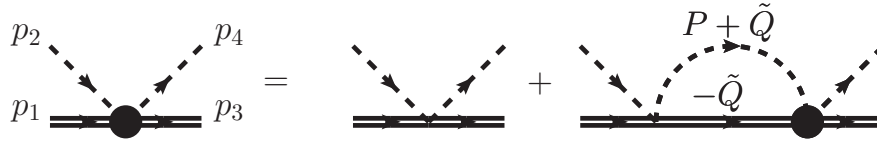


FIGURE 5.3: Diagrammatic representation of the Bethe-Salpeter equation for $P^*\phi \rightarrow P^*\phi$. The dashed lines correspond to Nambu-Goldstone bosons and the double lines to the heavy-light vector meson.

The two-particle unitarity requirement (5.6) becomes

$$\begin{aligned} \text{Disc}_s \left[-i \int \frac{d^4 \tilde{Q}}{(2\pi)^4} \mathcal{V}_P^{\mu\sigma}(q, \tilde{Q}) \Delta_{h,\sigma\bar{\sigma}}(\tilde{Q}) \Delta_l(\tilde{Q} + P) \mathcal{T}_P^{\bar{\sigma}\nu}(\tilde{Q}, Q) \right] &= -i \int \frac{d^4 \tilde{Q}}{(2\pi)^2} \\ &\times \mathcal{T}_P^{\mu\sigma}(q, \tilde{Q}) \left(\sum_{\lambda} \epsilon_{\sigma}(-\tilde{Q}, \lambda) \epsilon_{\bar{\sigma}}^{\dagger}(-\tilde{Q}, \lambda) \right) \delta^{+}((-\tilde{Q})^2 - M^2) \delta^{+}((P + \tilde{Q})^2 - m^2) \mathcal{T}_P^{*\bar{\sigma}\nu}(Q, \tilde{Q}). \end{aligned} \quad (5.17)$$

This equation can be proven analogously to Eq. (5.13) by use of Cutkosky's rules together with the identification $-g^{\mu\nu} + q^{\mu}q^{\nu}/M^2 = \sum_{\lambda} \epsilon^{\mu}(q, \lambda) \epsilon^{\dagger\nu}(q, \lambda)$.

Finally, we want to emphasize that we have introduced the vector particles in the conventional way by using vector fields. A different method is by use of antisymmetric tensor fields. The equivalence of both approaches has been shown in [116] for some special cases. For a unitarized chiral perturbation theory approach to $P^*\phi$ scattering using the tensor representation, we refer to [102].

5.2.3 Partial-wave and isospin decomposition

$P\phi$ scattering

Taking the momenta on the mass shell enables us to express the scattering amplitude in terms of Mandelstam variables $s = P^2$ and $t = (Q - q)^2$,

$$T^I(s, t)_{ij} \equiv \mathcal{T}_P^I(q, Q)_{ij}, \quad (5.18)$$

where the index I stands for the total isospin and the indices i and j denote the two-particle initial and final states. Isospin-breaking effects, i.e. $m_u \neq m_d$, are neglected. As previously, the channel indices will be treated implicitly. The s -channel partial wave decomposition reads

$$T^I(s, t) = \sum_{J=0}^{\infty} (2J+1) T^{IJ}(s) P_J(\cos \theta), \quad (5.19)$$

where P_J are the Legendre polynomials and T^{IJ} is the scattering amplitude for total angular momentum J . These amplitudes can be projected out of equation (5.19) by use of the orthogonality relation for Legendre

polynomials. This yields

$$T^{IJ}(s) \equiv \frac{1}{2} \int_{-1}^{+1} d(\cos \theta) P_J(\cos \theta) T^I(s, t(\cos \theta)), \quad (5.20)$$

where t is expressed in the center of mass frame in terms of the scattering angle θ between \mathbf{q} and \mathbf{Q} . Explicitly, t is given by

$$t(x) = (E_3^2 - q_f^2) + (E_1^2 - q_i^2) - 2E_1E_3 + 2q_iq_f x, \quad (5.21)$$

where $E_1 = (s + M_1^2 - m_2^2)/(2\sqrt{s})$ and $E_3 = (s + M_3^2 - m_4^2)/(2\sqrt{s})$. In accordance with the momentum assignments in Figure 5.1, the subscript 1 (2) and 3 (4) stand for the initial and final heavy-light meson (Nambu-Goldstone boson). The center of mass momenta of initial and final particles are given by $q_i = |\mathbf{q}|$ and $q_f = |\mathbf{Q}|$, c.f. footnote ³.

$P^* \phi$ scattering

In analogy to the previous paragraph we define

$$T^{I,\mu\nu}(s, t)_{ij} \equiv \mathcal{T}_P^{I,\mu\nu}(q, Q)_{ij}. \quad (5.22)$$

To project on partial waves we choose explicit polarization vectors $\epsilon_\mu(-Q, \bar{\lambda})$ and $\epsilon_\nu(-q, \lambda)$ in the center of mass frame, where λ and $\bar{\lambda}$ are the helicities of the vector mesons with momenta $-q$ and $-Q$. Then the corresponding scattering amplitude can be expressed through partial wave amplitudes $\langle \bar{\lambda} | \mathcal{T}^{IJ} | \lambda \rangle$ of given total angular momentum J . The whole procedure is explained in detail in Appendix A.2. Here we state only the result for the $J^P = 1^+$ and 1^- partial waves taken between parity eigenstates $|1_+\rangle = (|+1\rangle - |-1\rangle)/\sqrt{2}$ and $|1_-\rangle = (|+1\rangle + |-1\rangle)/\sqrt{2}$:

$$\langle 1_+ | \mathcal{T}^{I,J=1} | 1_+ \rangle = \int_{-1}^1 dx \frac{1}{4} (q_f q_i x (x^2 - 1) \mathcal{F}_5(s, t(x)) - (x^2 + 1) \mathcal{F}_1(s, t(x))) \quad (5.23)$$

$$\langle 1_- | \mathcal{T}^{I,J=1} | 1_- \rangle = \int_{-1}^1 dx \frac{1}{4} (q_f q_i (x^2 - 1) \mathcal{F}_5(s, t(x)) - 2x \mathcal{F}_1(s, t(x))) \quad (5.24)$$

The functions \mathcal{F}_1^I and \mathcal{F}_5^I originate from a decomposition of the scattering amplitude $\mathcal{T}_P^{I,\mu\nu}$ into the complete set of Lorentz structures $l_i^{\mu\nu}$ of Eq. (A.7). The functions \mathcal{F}_1^I and \mathcal{F}_5^I are the coefficients of the Lorentz structures $l_{1,P}^{\mu\nu} = g^{\mu\nu} - P^\mu P^\nu / P^2$ and $l_{5,P}^{\mu\nu} = \left(Q^\mu - \frac{Q \cdot P}{P^2} P^\mu \right) \left(q^\nu - \frac{q \cdot P}{P^2} P^\nu \right)$, respectively.

One comment is in order: as shown in Appendix A.2, there may be non-vanishing transition matrix elements $\langle 1_+ | \mathcal{T}^{IJ} | 0 \rangle$ and $\langle 0 | \mathcal{T}^{IJ} | 1_+ \rangle$. As a consequence, the potential projected on partial waves with quantum numbers $J^P = 1^+, 2^-, 3^+, \dots$ acquires a matrix structure that has to be taken into account if used in the BS equation. This is in contrast to the $J^P = 1^-, 2^+, 3^-, \dots$ projections, where no transitions between $|1_-\rangle$ and $|0\rangle$ states are

possible. For completeness we give here also the remaining $J^P = 1^+$ matrix elements

$$\begin{aligned}
\langle 0 | \mathcal{T}^{I,J=1} | 1_+ \rangle &= \int_{-1}^1 dx \frac{(1-x^2) \left(\omega_f (q_f q_i x \mathcal{F}_5(s, t(x)) - \mathcal{F}_1(s, t(x))) + q_f^2 \mathcal{F}_3(s, t(x)) \right)}{2\sqrt{2}M_3}, \\
\langle 1_+ | \mathcal{T}^{I,J=1} | 0 \rangle &= \int_{-1}^1 dx \frac{(1-x^2) \left(\omega_i (q_f q_i x \mathcal{F}_5(s, t(x)) - \mathcal{F}_1(s, t(x))) + q_i^2 \mathcal{F}_4(s, t(x)) \right)}{2\sqrt{2}M_1}, \\
\langle 0 | \mathcal{T}^{I,J=1} | 0 \rangle &= \int_{-1}^1 dx \frac{x}{2M_1 M_3} \left\{ (x\omega_f (\mathcal{F}_4(s, t(x))q_i^2 - \omega_i \mathcal{F}_1(s, t(x))) \right. \\
&\quad \left. + q_f q_i (\mathcal{F}_5(s, t(x))x^2\omega_i\omega_f + \mathcal{F}_2(s, t(x))) + \mathcal{F}_3(s, t(x))x\omega_i q_f^2 \right\}, \tag{5.25}
\end{aligned}$$

where $\omega_i = \sqrt{q_i^2 + M_1^2}$ and $\omega_f = \sqrt{q_f^2 + M_3^2}$, and \mathcal{F}_2 , \mathcal{F}_3 and \mathcal{F}_4 are introduced in Appendix A.2.

5.3 Chiral potentials

5.3.1 Off-shell potentials

In order to solve the BS equation (5.7) we have to rely on approximated potentials and propagators. This is done formally in the spirit of chiral perturbation theory by expanding in the small Nambu-Goldstone boson momentum p ,

$$\begin{aligned}
\Delta_l(p) &= \Delta_l^{(-2)}(p) + \Delta_l^{(-1)}(p) + \dots \\
\Delta_h(p) &= \Delta_h^{(-1)}(p) + \Delta_h^{(0)}(p) + \dots \\
\mathcal{V}_P(q, Q) &= \mathcal{V}_P^{(1)}(q, Q) + \mathcal{V}_P^{(2)}(q, Q) + \dots, \tag{5.26}
\end{aligned}$$

where the chiral order is indicated by the superscript (-2) , (-1) , (0) , (1) . . . , corresponding to $\mathcal{O}(p^{-2})$, $\mathcal{O}(p^{-1})$, $\mathcal{O}(1)$, $\mathcal{O}(p)$ The propagators at lowest chiral order are the bare propagators (5.9), and the leading order potential is given by $\mathcal{T}_P^{(1)}(q, Q)$, which is of chiral order $\mathcal{O}(p)$. It originates directly from the Weinberg-Tomozawa term of Lagrangian (3.21) and is given by

$$\mathcal{V}_{\text{WT}}(P(p_1)\phi(p_2) \rightarrow P(p_3)\phi(p_4)) = \frac{1}{4f_0^2} \mathcal{C}_{\text{LO}} (p_1 \cdot p_2 + p_1 \cdot p_4 + p_2 \cdot p_3 + p_3 \cdot p_4), \tag{5.27}$$

where the coefficients \mathcal{C}_{LO} for different strangeness and isospin combinations (S, I) are listed in Table 5.1⁴. The channels shown in Table 5.1 correspond to pseudoscalar D mesons scattering off Nambu-Goldstone bosons. To obtain an analogues table for B mesons, one has to replace $D_{(s)} \rightarrow \bar{B}_{(s)}$. The coefficients remain unchanged since the chiral sector of the theory is the same for D and \bar{B} mesons. Formally also s and u channel exchange corrections enter at this order. These corrections are postponed to Subsection 5.3.2.

For a reasonable description of the available data [12] it is necessary to include higher-order corrections.

⁴The coefficient \mathcal{C}_{LO} indicates already at this level a stronger attraction for $(S, I) = (1, 0)$ and $DK \rightarrow DK$ compared to other channels. Its size is the reason for the dynamical generation of the $D_{s_0}^*(2317)$ state in many previous approaches [96, 102, 117].

The NLO potential derived from Lagrangian (3.23) is

$$\begin{aligned}
\mathcal{V}_{\text{NLO}}(P(p_1)\phi(p_2) \rightarrow P(p_3)\phi(p_4)) &= -\frac{8}{f_0^2} \mathcal{C}_{24} \left(c_2 p_2 \cdot p_4 - \frac{c_4}{m_P^2} (p_1 \cdot p_4 p_2 \cdot p_3 + p_1 \cdot p_2 p_3 \cdot p_4) \right) \\
&\quad -\frac{4}{f_0^2} \mathcal{C}_{35} \left(c_3 p_2 \cdot p_4 - \frac{c_5}{m_P^2} (p_1 \cdot p_4 p_2 \cdot p_3 + p_1 \cdot p_2 p_3 \cdot p_4) \right) \\
&\quad -\frac{4}{f_0^2} \mathcal{C}_6 \frac{c_6}{m_P^2} (p_1 \cdot p_4 p_2 \cdot p_3 - p_1 \cdot p_2 p_3 \cdot p_4) \\
&\quad -\frac{8}{f_0^2} \mathcal{C}_0 c_0 + \frac{4}{f_0^2} \mathcal{C}_1 c_1, \tag{5.28}
\end{aligned}$$

with the coefficients \mathcal{C}_i listed in Table 5.1 and the low-energy constants c_0, \dots, c_6 introduced in Section 3.3. The sets c_i for two different kind of heavy-light mesons, P and P' , are related by $c_{i,P}/m_P = c_{i,P'}/m_{P'}$, as a consequence of heavy-quark flavor symmetry. This equality holds up to corrections in $1/m_H$, where m_H is the lighter of the two masses m_P and $m_{P'}$. As has been shown in Eq. (3.24), a similar statement can be drawn between pseudoscalar and vector heavy-light mesons, P and P^* , by use of heavy-quark spin symmetry. As a consequence the relations $c_i \equiv c_{i,P} = c_{i,P^*} \equiv \tilde{c}_i$ and $m_P = m_{P^*}$ hold up to corrections in $1/m_P$. With this identity we can relate the potential $\mathcal{V}(P^*(p_1)\phi(p_2) \rightarrow P^*(p_3)\phi(p_4))$ for Nambu-Goldstone bosons scattering off heavy-light vector mesons to $\mathcal{V}(P(p_1)\phi(p_2) \rightarrow P(p_3)\phi(p_4))$ by⁵

$$\mathcal{V}_{\text{LO(NLO)}}(P^*(p_1)\phi(p_2) \rightarrow P^*(p_3)\phi(p_4)) = -\epsilon_3^* \cdot \epsilon_1 \mathcal{V}_{\text{LO(NLO)}}(P(p_1)\phi(p_2) \rightarrow P(p_3)\phi(p_4)). \tag{5.29}$$

in accordance with the arguments presented in Section 2.

If heavy-quark symmetry breaking effects on the low-energy constants are neglected, we are left with seven NLO constants c_0, \dots, c_6 describing $D\phi$, $D^*\phi$, $\bar{B}\phi$ and $\bar{B}^*\phi$ scattering. Therefore, one can fix the constants in one sector, here $D\phi$, and can then use them to give predictions for the other sectors, $D^*\phi$, $\bar{B}\phi$ and $\bar{B}^*\phi$, as will be shown in Subsection 5.4.2. Obviously, heavy-quark symmetry breaking effects on the low-energy constants can be substantial and make predictions for the other sectors less reliable.

Not all of the NLO constants are unknown. In Section 3.3 the constant $c_1(\tilde{c}_1)$ has been determined from the mass splitting of strange and non-strange heavy-light pseudoscalar (vector) mesons for the charmed and bottomed mesons independently. Those constants will be used throughout our analysis. Further, the NLO mass formulas Eq.(3.25)-(3.28) depend on c_0 and \tilde{c}_0 . To extract c_0 we employ the light-quark mass dependence of the D and D_s meson masses from [12]. Using this data is most reasonable since it corresponds to the charmed meson scattering lengths investigated later in this analysis. The data are shown in Figure 5.4. Given the LQCD results on m_K , m_π , m_D , and m_{D_s} , for four different data sets and performing a lowest- χ^2 fit, gives $c_0 = 0.015$ and $m_{D,0} = 1920 \text{ MeV}$, with $\chi_{\text{d.o.f}}^2 = 38$.

In order to obtain a reasonable description of the pion-mass dependence we refit the relation of kaon mass to pion mass⁶,

$$2B_0 m_s = 2m_K^2 - m_\pi^2. \tag{5.30}$$

⁵Whenever the Lorentz indices of the potential are dropped, it is understood as contracted with polarization vectors.

⁶later we rely on a simple polynomial fit for the kaon mass to visualize the NLO pion-mass dependence of scattering lengths.

TABLE 5.1: Coefficients entering the LO and NLO potentials for $D\phi$ scattering given in equation (5.27) and (5.28). A analogous table holds for $D^*\phi$ potentials by replacing $D \rightarrow D^*$.

(S,I)	Channel	\mathcal{C}_{LO}	\mathcal{C}_0	\mathcal{C}_1	\mathcal{C}_{24}	\mathcal{C}_{35}	\mathcal{C}_6
(2,1/2)	$D_s K \rightarrow D_s K$	1	m_K^2	m_K^2	1	1	-1
(1,1)	$DK \rightarrow DK$	0	m_K^2	0	1	0	0
	$D_s \pi \rightarrow D_s \pi$	0	m_π^2	0	1	0	0
	$DK \rightarrow D_s \pi$	1	0	$\frac{1}{2}(m_K^2 + m_\pi^2)$	0	1	-1
(1,0)	$DK \rightarrow DK$	-2	m_K^2	$2m_K^2$	1	2	2
	$D_s \eta \rightarrow D_s \eta$	0	$\frac{1}{3}(4m_K^2 - m_\pi^2)$	$\frac{4}{3}(2m_K^2 - m_\pi^2)$	1	$\frac{4}{3}$	0
	$DK \rightarrow D_s \eta$	$-\sqrt{3}$	0	$\frac{5m_K^2 - 3m_\pi^2}{2\sqrt{3}}$	0	$\frac{1}{\sqrt{3}}$	$\sqrt{3}$
(0,3/2)	$D\pi \rightarrow D\pi$	1	m_π^2	m_π^2	1	1	-1
(0,1/2)	$D\pi \rightarrow D\pi$	-2	m_π^2	m_π^2	1	1	2
	$D\eta \rightarrow D\eta$	0	$\frac{1}{3}(4m_K^2 - m_\pi^2)$	$\frac{m_\pi^2}{3}$	1	$\frac{1}{3}$	0
	$D_s \bar{K} \rightarrow D_s \bar{K}$	-1	m_K^2	m_K^2	1	1	1
	$D\pi \rightarrow D\eta$	0	0	$-m_\pi^2$	0	-1	0
	$D\pi \rightarrow D_s \bar{K}$	$\sqrt{\frac{3}{2}}$	0	$-\frac{1}{2}\sqrt{\frac{3}{2}}(m_K^2 + m_\pi^2)$	0	$-\sqrt{\frac{3}{2}}$	$-\sqrt{\frac{3}{2}}$
	$D\eta \rightarrow D_s \bar{K}$	$-\sqrt{\frac{3}{2}}$	0	$\frac{3m_\pi^2 - 5m_K^2}{2\sqrt{6}}$	0	$-\frac{1}{\sqrt{6}}$	$\sqrt{\frac{3}{2}}$
(-1,1)	$D\bar{K} \rightarrow D\bar{K}$	1	m_K^2	m_K^2	1	1	-1
(-1,0)	$D\bar{K} \rightarrow D\bar{K}$	-1	m_K^2	$-m_K^2$	1	-1	1

This gives $B_0 m_s = 0.31 \text{ GeV}^2$ and $\chi_{\text{d.o.f}}^2 = 4$. The data for m_K in dependence of the pion mass m_π are shown by the red points in Figure 5.5. Their chiral extrapolation is shown as solid orange line. This should be compared to the solid black line, obtained for $B_0 m_s = 0.24 \text{ GeV}^2$, as derived from the isospin averaged physical pion and kaon mass taken from PDG [1]. The observed discrepancy translates to deviations from the chirally extrapolated D and D_s meson masses, the solid and dashed orange lines in Figure 5.4, to the experimental values represented by the black dot and square, respectively.

Interestingly we observe the hierarchy: $|c_0| \ll |c_1|$. As discussed in detail in [118], there is a deeper reason behind this: low energy constants multiplying single flavor traces, as in the case of c_1 , should have larger values than constants that multiply multiple flavor traces, as for c_0 . The argument behind this is a counting in $1/N_c$, where N_c is the number of colors in QCD. As shown in [118], each additional flavor trace in a chiral Lagrangian implies a suppression of the corresponding low-energy constant by a factor $1/N_c$. This implies the hierarchy

$$|c_0| \ll |c_1|, \quad |c_2| \ll |c_3|, \quad |c_4| \ll |c_5|, |c_6|, \quad (5.31)$$

for the NLO low-energy constants.

Finally, we proof that the c_6 contribution in equation (5.28) is suppressed by $1/m_P$ or the small Nambu-Goldstone boson momentum p . This feature has already been pointed out by [103]. Consider the Lorentz

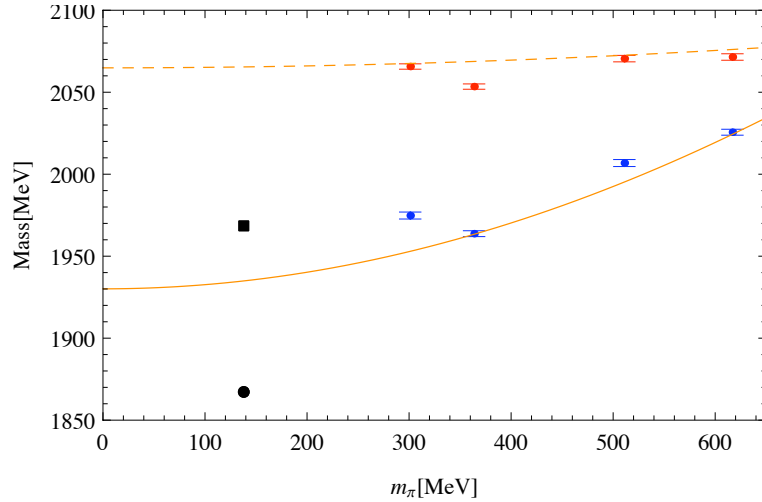


FIGURE 5.4: Pion-mass dependence of the D and D_s meson masses, m_D and m_{D_s} . The blue and red data points are IQCD results for m_D and m_{D_s} , taken from [12]. The solid and dashed orange lines are their chiral extrapolation. The experimental values [1] for m_D and m_{D_s} are represented by the black dot and the black square.

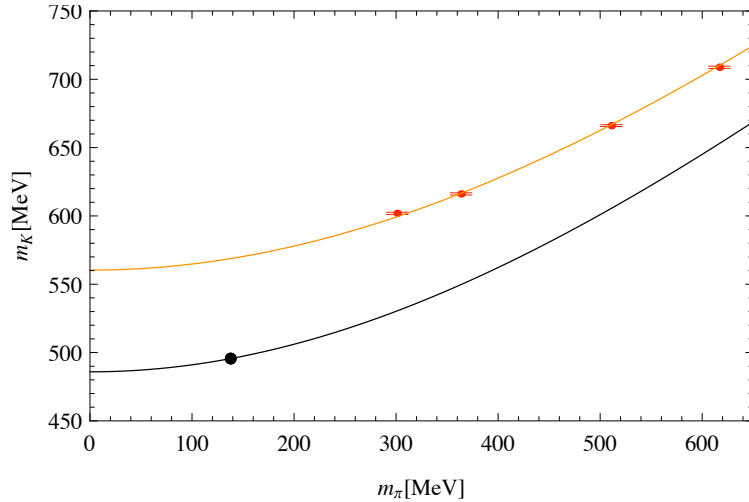


FIGURE 5.5: Pion-mass dependence of the kaon mass, m_K . The red data points are IQCD results taken from [12] and the solid orange line is their chiral extrapolation. The experimental value for m_K [1] and its predicted pion-mass dependence is shown by the black dot and the solid black line.

structure

$$p_1 \cdot p_4 p_2 \cdot p_3 - p_1 \cdot p_2 p_3 \cdot p_4, \quad (5.32)$$

that multiplies the low-energy constant c_6 in equation (5.28). Now the reasoning is the same as in heavy-meson chiral perturbation theory [17] and heavy-quark effective theory [15, 17, 119]. The momenta p_1 and p_3 of the heavy-light mesons can be decomposed as

$$p_1 = m_{P,1}v + k_1 \quad \text{and} \quad p_3 = m_{P,3}v + k_3, \quad (5.33)$$

where v is the velocity of the heavy-light meson with $v^2 = 1$, and k_i is a small residual momentum counted as

order $\mathcal{O}(p)$. Using $p_3 = p_1 + p_3 - p_1 \equiv p_1 + \Delta_p$ with $\Delta_p = (m_{P,1} - m_{P,3})v + k_1 - k_3$ in equation (5.32) gives

$$\Delta_p \cdot (p_2(p_1 \cdot p_4) - p_4(p_1 \cdot p_2)). \quad (5.34)$$

We can state $m_{P,1} = m_{P,3}$ up to higher order corrections in p or $1/m_P$. Hence, also the momentum difference Δ_p should be suppressed. Since p_2 and p_4 are counted as order $\mathcal{O}(p)$, we see that this contribution starts at next-to-next-to leading order (NNLO). For this reason we neglect the c_6 term in (5.28) from now on.

5.3.2 Partial-wave projected on-shell potentials

$J^P = 0^+$ potential for $D\phi \rightarrow D\phi$

In this subsection we present the S-wave projected LO and NLO potentials for on-shell kinematics, as they are finally used in the BS equation, Eq. (5.7). For this Eq. (5.27) and (5.28) are rewritten in terms of Mandelstam variables $s = (p_1 + p_2)^2$, $t = (p_1 - p_3)^2$ and $u = (p_1 - p_4)^2$, with momenta assigned as in Figure 5.6. Using the relation $u + s + t = M_1^2 + m_2^2 + M_3^2 + m_4^2$ eliminates one of them, u , from our expressions. Equation (5.20) for $J = 0$ with $t(x)$ from Eq. (5.21) gives then the LO and NLO potentials

$$\mathcal{V}_{\text{LO}}^{\text{on-shell},0^+}(D(p_1)\phi(p_2) \rightarrow D(p_3)\phi(p_4)) = -\frac{C_{\text{LO}}}{8f_0^2}(m_2^2 + m_4^2 + M_1^2 + M_3^2 + \frac{(M_1^2 - m_2^2)(M_3^2 - m_4^2)}{s} - 3s) \quad (5.35)$$

and

$$\mathcal{V}_{\text{NLO}}^{\text{on-shell},0^+}(D(p_1)\phi(p_2) \rightarrow D(p_3)\phi(p_4)) = -\frac{1}{2} \int_{-1}^1 dx \mathcal{F}_1^{\text{NLO}}(s, t(x)), \quad (5.36)$$

where

$$\begin{aligned} \mathcal{F}_1^{\text{NLO}}(s, t) &= 8\frac{c_0 C_0}{f_0^2} - 4\frac{c_1 C_1}{f_0^2} + 8\frac{C_{24}}{f_0^2} \left\{ -\frac{1}{4} \frac{c_4}{m_P^2} (-m_4^2 - M_1^2 + s + t) (-m_2^2 - M_3^2 + s + t) \right. \\ &\quad \left. - \frac{1}{4} \frac{c_4}{m_P^2} (-m_2^2 - M_1^2 + s) (-m_4^2 - M_3^2 + s) + \frac{1}{2} c_2 (m_2^2 + m_4^2 - t) \right\} \\ &\quad + 4\frac{C_{35}}{f_0^2} \left\{ \frac{1}{2} c_3 (m_2^2 + m_4^2 - t) - \frac{c_5}{m_P^2} \left[\frac{1}{4} (-m_4^2 - M_1^2 + s + t) (-m_2^2 - M_3^2 + s + t) \right. \right. \\ &\quad \left. \left. + \frac{1}{4} (-m_2^2 - M_1^2 + s) (-m_4^2 - M_3^2 + s) \right] \right\} \\ &\quad + 4\frac{c_6 C_6}{f_0^2 m_P^2} \left\{ \frac{1}{4} (-m_4^2 - M_1^2 + s + t) (-m_2^2 - M_3^2 + s + t) \right. \\ &\quad \left. - \frac{1}{4} (-m_2^2 - M_1^2 + s) (-m_4^2 - M_3^2 + s) \right\}, \quad (5.37) \end{aligned}$$

where the mass m_P is chosen as \hat{m}_D for charmed mesons and as \hat{m}_B for bottomed mesons. The masses M_i (m_i) corresponding to heavy-light mesons (Nambu-Goldstone bosons) with momenta p_i . So far we have only discussed LO and NLO contact interactions. Applying the chiral counting rules to diagrams Figure 5.6 (b) and (c) gives $n_\chi = 1$ and hence they are formally of the same order as the Weinberg-Tomozawa term. However, an explicit evaluation shows that they are of second chiral order and can be absorbed into the available $\mathcal{O}(p^2)$ LECs at threshold, as noticed in [49]. Diagram (b) is the s -channel exchange and (c) the u -channel exchange

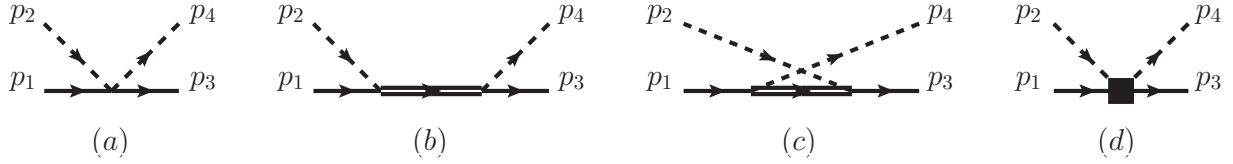


FIGURE 5.6: Feynman diagram (a) is the LO contact interaction, (b) and (c) are the exchange corrections for s and u channel, and (d) stands for NLO contact interactions. The pseudoscalar D mesons are represented by the solid lines and the D^* mesons by the double lines, as previously.

diagram. The s -channel diagram gives

$$\mathcal{V}_{s\text{-Ex}}^{\text{on-shell},0^+}(D(p_1)\phi(p_2) \rightarrow D(p_3)\phi(p_4)) = \sum_{m_h \in \{m_{D^*}, m_{D_s^*}\}} \mathcal{A}_{m_h\text{-Ex}} \frac{\tilde{g}_{PP^*\phi}^2 (m_2^2 - M_1^2 + s)(m_4^2 - M_3^2 + s)}{2f_0^2 s m_h^2} \quad (5.38)$$

where m_h is the D^* (D_s^*) meson mass corresponding to intermediate D^* (D_s^*) mesons. The coefficients $\mathcal{A}_{D^*\text{-Ex}}$ and $\mathcal{A}_{D_s^*\text{-Ex}}$ for different strangeness and isospin combinations can be found in Table 5.2. The intermediate D^* (D_s^*) meson has isospin $I = 1/2$ ($I = 0$) and as a consequence the coefficient $\mathcal{A}_{D^*\text{-Ex}}$ ($\mathcal{A}_{D_s^*\text{-Ex}}$) has to be zero except for $I = 1/2$ ($I = 0$). Analogously, the u -channel exchange diagram gives

$$\begin{aligned} \mathcal{V}_{u\text{-Ex}}^{\text{on-shell},0^+}(D(p_1)\phi(p_2) \rightarrow D(p_3)\phi(p_4)) = & \\ & \sum_{m_h \in \{m_{D^*}, m_{D_s^*}\}} \int_{-1}^1 dx \frac{\tilde{g}_{PP^*\phi}^2 \mathcal{B}_{m_h\text{-Ex}}}{4f_0^2 m_h^2 (-m_2^2 - m_4^2 - M_1^2 - M_3^2 + s + m_h^2 + t(x))} \\ & \times \left\{ - (2m_2^2 + m_4^2 + M_1^2 - s - t(x)) (m_2^2 + 2m_4^2 + M_3^2 - s - t(x)) \right. \\ & \left. + 2m_h^2 (m_2^2 + m_4^2 - t(x)) \right\}, \end{aligned} \quad (5.39)$$

with coefficients $\mathcal{B}_{D_{(s)}^*\text{-Ex}}$ listed in Table 5.2. Note that, in contrast to the s -channel diagram, the u -channel can contribute to all possible isospin combinations. Finally, the potential up to NLO reads

$$\mathcal{V}_{\text{LO}}^{(S,I)}(s) \equiv \mathcal{V}_{\text{LO}}^{\text{on-shell},0^+} + \mathcal{V}_{s\text{-Ex}}^{\text{on-shell},0^+} + \mathcal{V}_{u\text{-Ex}}^{\text{on-shell},0^+} + \mathcal{V}_{\text{NLO}}^{\text{on-shell},0^+} \Big|_{s \equiv P^2 = (p_1 + p_2)^2}, \quad (5.40)$$

$J^P = 1^+$ **potential for** $D^*\phi \rightarrow D^*\phi$

This subsection gives the potentials for the scattering of D^* mesons off Nambu-Goldstone bosons for on-shell kinematics and $J^P = 1^+$. As shown in detail in Appendix A.2, the potential acquires a matrix structure due to the mixing of different helicity states. Therefore we define the potential

$$\hat{\mathcal{M}}_{J^P=1^+} \equiv \begin{pmatrix} \langle 1_+ | \mathcal{T}^{J=1} | 1_+ \rangle & \langle 1_+ | \mathcal{T}^{J=1} | 0 \rangle \\ \langle 0 | \mathcal{T}^{J=1} | 1_+ \rangle & \langle 0 | \mathcal{T}^{J=1} | 0 \rangle \end{pmatrix}, \quad (5.41)$$

TABLE 5.2: Coefficients entering the s and u channel exchange contributions Figure 5.6 (b) and (c).

(S,I)	Channel	$\mathcal{A}_{D^*-\text{Ex}}$	$\mathcal{A}_{D_s^*-\text{Ex}}$	$\mathcal{B}_{D^*-\text{Ex}}$	$\mathcal{B}_{D_s^*-\text{Ex}}$
(2,1/2)	$D_s K \rightarrow D_s K$	0	0	1	0
(1,1)	$DK \rightarrow DK$	0	0	0	0
	$D_s \pi \rightarrow D_s \pi$	0	0	0	0
	$DK \rightarrow D_s \pi$	0	0	1	0
(1,0)	$DK \rightarrow DK$	0	2	0	0
	$D_s \eta \rightarrow D_s \eta$	0	$\frac{2}{3}$	0	$\frac{2}{3}$
	$DK \rightarrow D_s \eta$	0	$\frac{2}{\sqrt{3}}$	$-\frac{1}{\sqrt{3}}$	0
(0,3/2)	$D\pi \rightarrow D\pi$	0	0	1	0
(0,1/2)	$D\pi \rightarrow D\pi$	$\frac{3}{2}$	0	$-\frac{1}{2}$	0
	$D\eta \rightarrow D\eta$	$\frac{1}{6}$	0	$\frac{1}{6}$	0
	$D_s \bar{K} \rightarrow D_s \bar{K}$	1	0	0	0
	$D\pi \rightarrow D\eta$	$-\frac{1}{2}$	0	$-\frac{1}{2}$	0
	$D\pi \rightarrow D_s \bar{K}$	$-\sqrt{\frac{3}{2}}$	0	0	0
	$D\eta \rightarrow D_s \bar{K}$	$\frac{1}{\sqrt{6}}$	0	0	$-\sqrt{\frac{2}{3}}$
(-1,1)	$D\bar{K} \rightarrow D\bar{K}$	0	0	0	1
(-1,0)	$D\bar{K} \rightarrow D\bar{K}$	0	0	0	-1

where the matrix elements are obtained directly from equation (5.23) and (5.25). One should notice that the inclusion of channel coupling effects is straight forward by promoting the entries $\langle \dots | \mathcal{T}^{J=1} | \dots \rangle$ to matrices.

The functions F_i entering Eq. (5.23) and (5.25) are decomposed in terms of LO, exchange and NLO contributions

$$\mathcal{F}_i(s, t) = \mathcal{F}_i^{\text{LO}}(s, t) + \sum_{\{m_h, m_h^*\} = \begin{cases} \{m_D, m_{D^*}\} \\ \{m_{D_s}, m_{D_s^*}\} \end{cases}} \left(\mathcal{A}_{m_h^*-\text{Ex}} \mathcal{F}_i^{s-\text{Ex}}(s, t) + \mathcal{B}_{m_h^*-\text{Ex}} \mathcal{F}_i^{u-\text{Ex}}(s, t) \right) + \mathcal{F}_i^{\text{NLO}}(s, t), \quad (5.42)$$

where the coefficients $\mathcal{A}_{D_{(s)}^*-\text{Ex}}$ and $\mathcal{B}_{D_{(s)}^*-\text{Ex}}$ can be found in Table 5.2. The leading order functions are

$$\mathcal{F}_1^{\text{LO}}(s, t(x)) = \mathcal{F}_2^{\text{LO}}(s, t(x)) = \frac{C_{\text{LO}}}{4f_0^2} (m_2^2 + m_4^2 + M_1^2 + M_3^2 - 2s - t) \quad (5.43)$$

and $\mathcal{F}_3^{\text{LO}} = \mathcal{F}_4^{\text{LO}} = \mathcal{F}_5^{\text{LO}} = 0$. At next-to-leading order $\mathcal{F}_3^{\text{NLO}} = \mathcal{F}_4^{\text{NLO}} = \mathcal{F}_5^{\text{NLO}} = 0$ and $\mathcal{F}_1^{\text{NLO}} = \mathcal{F}_2^{\text{NLO}}$, where $\mathcal{F}_1^{\text{NLO}}$ is introduced in Eq. (5.36).

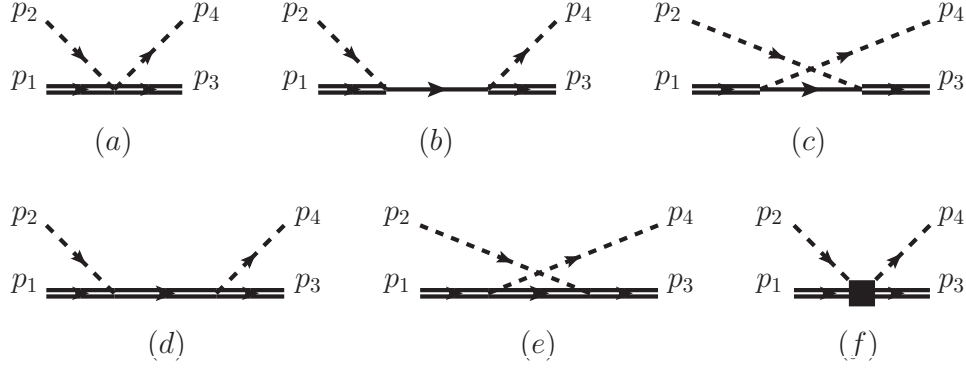


FIGURE 5.7: Feynman diagram (a) is the LO contact interaction, (b) and (c) are the exchange corrections for s and u channel with an intermediate D meson, (d) and (e) are the exchange corrections for s and u channel with an intermediate D^* meson and diagram (f) is the contribution from NLO contact interactions. The propagators are assigned as in Figure 5.6.

The u -channel diagrams, Figure 5.7 (c) and (e), give

$$\begin{aligned}
\mathcal{F}_1^{u\text{-Ex}}(s, t(x)) &= \frac{-g_{P^*P^*\phi}^2}{2f_0^2 (-m_2^2 - m_4^2 - M_1^2 - M_3^2 + s + m_h^{*2} + t(x))} \\
&\times \left\{ M_1^2 (m_2^2 - M_3^2 + s - t(x)) - (m_4^2 + M_3^2) t(x) \right. \\
&\left. + m_4^2 M_3^2 - m_2^2 (m_4^2 - s + t(x)) + m_4^2 s + M_3^2 s - s^2 + t(x)^2 \right\}, \quad (5.44)
\end{aligned}$$

$$\begin{aligned}
\mathcal{F}_2^{u\text{-Ex}}(s, t(x)) &= \frac{-g_{P^*P^*\phi}^2}{4f_0^2 s (-m_2^2 - m_4^2 - M_1^2 - M_3^2 + s + m_h^{*2} + t(x))} \\
&\times \left\{ -m_2^2 \left[-m_4^2 (M_1^2 + M_3^2 + 4s + t(x)) \right. \right. \\
&\left. \left. + m_4^4 + (M_3^2 + 3s) (s + t(x)) + M_1^2 (M_3^2 - s) \right] \right. \\
&\left. - m_4^2 (M_1^2 (M_3^2 + s + t(x)) + s (3(s + t(x)) - M_3^2)) + m_2^4 (-m_4^2 + M_3^2 + s) \right. \\
&\left. + m_4^4 (M_1^2 + s) + (M_1^2 (M_3^2 - s) + s (5s - M_3^2)) t(x) \right. \\
&\left. + 2s (s (s - M_3^2) - M_1^2 (3M_3^2 + s)) + 2st(x)^2 \right\} \\
&\frac{\tilde{g}_{P^*P^*\phi}^2 (m_2^2 - M_1^2 + s) (m_4^2 - M_3^2 + s)}{2f_0^2 s (m_h^2 - m_2^2 - m_4^2 - M_1^2 - M_3^2 + s + t(x))}, \quad (5.45)
\end{aligned}$$

$$\begin{aligned}
\mathcal{F}_3^{u\text{-Ex}}(s, t(x)) &= \frac{-g_{P^*P^*\phi}^2 (M_1^2 (m_2^2 + m_4^2 + 2s - t(x)) - (m_2^2 - s) (m_2^2 + m_4^2 - 2s - t(x)))}{2f_0^2 \sqrt{s} (-m_2^2 - m_4^2 - M_1^2 - M_3^2 + s + m_h^{*2} + t(x))} \\
&\frac{\tilde{g}_{P^*P^*\phi}^2 (m_2^2 - M_1^2 + s)}{f_0^2 \sqrt{s} (m_h^2 - m_2^2 - m_4^2 - M_1^2 - M_3^2 + s + t(x))}, \quad (5.46)
\end{aligned}$$

$$\begin{aligned}
\mathcal{F}_4^{u\text{-Ex}}(s, t(x)) &= \frac{-g_{P^*P^*\phi}^2}{2f_0^2\sqrt{s}(-m_2^2 - m_4^2 - M_1^2 - M_3^2 + s + m_h^{*2} + t(x))} \\
&\quad \times (M_3^2(m_4^2 + 2s - t(x)) + m_2^2(-m_4^2 + M_3^2 + s) - (m_4^2 - s)(m_4^2 - 2s - t(x))) \\
&\quad - \frac{\tilde{g}_{P^*P^*\phi}^2(m_4^2 - M_3^2 + s)}{f_0^2\sqrt{s}(m_h^2 - m_2^2 - m_4^2 - M_1^2 - M_3^2 + s + t(x))}, \tag{5.47}
\end{aligned}$$

$$\begin{aligned}
\mathcal{F}_5^{u\text{-Ex}}(s, t(x)) &= \frac{-g_{P^*P^*\phi}^2(m_2^2 + m_4^2 - t(x))}{f_0^2(m_2^2 + m_4^2 + M_1^2 + M_3^2 - s - m_h^{*2} - t(x))} \\
&\quad - \frac{2\tilde{g}_{P^*P^*\phi}^2}{f_0^2(m_h^2 - m_2^2 - m_4^2 - M_1^2 - M_3^2 + s + t(x))}. \tag{5.48}
\end{aligned}$$

and the s -channel diagrams do not contribute for $J^P = 1^+$, as can be confirmed by an explicit calculation.

Potentials in heavy-meson χ PT

In the HM χ PT, the LO potential reduces to

$$\mathcal{V}_{\text{LO}}^{\text{on-shell}, 0^+} = \frac{1}{4f_0^2} 2\dot{M}(E_2 + E_4)\mathcal{C}_{\text{LO}} \tag{5.49}$$

after S -wave projection, with \dot{M} chosen as \dot{m}_D for charmed mesons and as \dot{m}_B for bottomed mesons, c.f. Table 4.1. At NLO, with the on-shell approximation and for S -wave interactions, effectively only four of the six low-energy constants contribute, i.e.,

$$\mathcal{V}_{\text{NLO}}^{\text{on-shell}, 0^+} = -\frac{8}{f_0^2} C_{24} c_{24} E_2 E_4 - \frac{4}{f_0^2} C_{35} c_{35} E_2 E_4 - \frac{8}{f_0^2} C_0 c_0 + \frac{4}{f_0^2} C_1 c_1, \tag{5.50}$$

where $c_{24} = c_2 - 2c_4$ and $c_{35} = c_3 - 2c_5$ (see, e.g., Ref. [104]). The LO exchange diagrams start contributing at NLO and hence do not have to be considered within HM χ PT.

The potential for the scattering of Nambu-Goldstone bosons off heavy-light vector meson can be easily derived by Eq.(5.41). In the infinite heavy-quark limit we have $\epsilon_3^* \cdot \epsilon_1 = -1$, which leads to

$$\mathcal{V}_{\text{LO(NLO)}}(P^*(p_1)\phi(p_2) \rightarrow P^*(p_3)\phi(p_4)) = \mathcal{V}_{\text{LO(NLO)}}(P(p_1)\phi(p_2) \rightarrow P(p_3)\phi(p_4)) \tag{5.51}$$

(see also, e.g., Ref. [120]). One should notice that the different helicity states do not mix in the heavy-quark limit, reducing the potentials to the simplified form Eq. (5.51).

5.4 The scattering of Nambu-Goldstone bosons off heavy-light mesons in the HQS scheme

5.4.1 Renormalization scheme motivated by heavy-quark symmetry

It is well known that perturbation theory at any finite order cannot generate bound states or resonances. One way to proceed is to perform an infinite summation of a leading subclass of diagrams to all orders using the Bethe-Salpeter (or Lippmann-Schwinger) equation, Eq. (5.7). In combination with coupled-channels dynamics, this approach has turned out to be quite successful in describing a multitude of low-energy strong-interaction phenomena (see, e.g., Refs. [121–129] for early references and Refs. [100, 101] for some recent applications). To simplify the calculations, the so-called on-shell approximation [122, 123] is often introduced, with the argument that the off-shell effects are relegated to higher orders. Schematically, the Bethe-Salpeter equation (5.7) can then be written as

$$T = V + VGT, \quad (5.52)$$

where V is the potential and G is a loop function defined in the following way

$$G(s, M^2, m^2) \equiv i \int \frac{d^n q}{(2\pi)^n} \frac{1}{[(P - q)^2 - m^2 + i\epsilon](q^2 - M^2 + i\epsilon)}, \quad (5.53)$$

where $P = (\sqrt{s}, 0, 0, 0)$ is the total momentum of the two particles. M and m are the masses of the heavy-light meson and of the Nambu-Goldstone boson, respectively, in the two-particle intermediate state. According to the power counting rule specified in Section 4, the loop function G counts as of $\mathcal{O}(p)$. An explicit evaluation in $n = 4$ dimensions with the modified minimal subtraction scheme yields

$$\begin{aligned} G_{\overline{\text{MS}}}(s, M^2, m^2) = & \frac{1}{16\pi^2} \left\{ \frac{m^2 - M^2 + s}{2s} \log \left(\frac{m^2}{M^2} \right) \right. \\ & - \frac{q}{\sqrt{s}} \left\{ \log[2q\sqrt{s} + m^2 - M^2 - s] + \log[2q\sqrt{s} - m^2 + M^2 - s] \right. \\ & \left. - \log[2q\sqrt{s} + m^2 - M^2 + s] - \log[2q\sqrt{s} - m^2 + M^2 + s] \right\} \\ & \left. + \left(\log \left(\frac{M^2}{\mu^2} \right) - 2 \right) \right\}, \quad (5.54) \end{aligned}$$

where $q = \frac{\sqrt{(s-(m+M)^2)(s-(m-M)^2)}}{2\sqrt{s}}$ is the centre of mass (three) momentum. It is easily seen that the underlined term in the loop function (5.54) breaks the chiral power counting. In addition, the heavy-quark flavor symmetry and, to a less extent, the heavy-quark spin symmetry are also broken in the covariant loop function, as noticed in Ref. [104]. The ambiguity in choosing the finite part of the loop function is reflected in the appearance of the renormalization scale μ . In perturbation theory up to some given order, these ambiguities are well understood. All divergent parts can be absorbed into the low-energy constants of the theory and the dependence on the renormalization scale is compensated by the scale dependence of the low-energy constants. However, our solution of the BS equation does not correspond to a consistent perturbation theory calculation. As a consequence, the ambiguity of the loop integral is reflected in the final results, i.e. the scattering amplitude depends

on the renormalization scale μ . There are different approaches to arrive at reasonable predictions anyway. The most common way is to consider μ as an additional parameter of the theory. This is usually done by replacing the underlined term -2 in Eq. (5.54) by the so-called subtraction constant, $a(\mu)$, which we will refer to as the $\overline{\text{MS}}$ scheme from now on. Another method is the χ -BS(3) approach proposed by [121, 130], as has been applied to heavy-light mesons in [96, 131]. This approach has the appealing feature that crossing symmetry is restored at a given kinematical point.

In the following we propose a renormalization scheme that restores the chiral power counting and ensures that the loop function G has a well defined behavior in the $M \rightarrow \infty$ limit. To achieve this, we turn to the HM ChPT. In the static limit the momentum of the heavy-light meson is decomposed as $p_P = m_P v + k$, where v is the constant velocity ($v^2 = 1$) and m_P the mass of the heavy-light meson in the chiral limit. The small residual momentum is denoted by k . Using momentum conservation and expanding in $1/m_P$ gives for the heavy-light meson propagator the replacement

$$\frac{1}{p_P^2 - M^2 + i\epsilon} \rightarrow \frac{1}{2m_P v \cdot k + 2m_P \Delta_P + i\epsilon} \quad (5.55)$$

at leading order in $1/m_P$. The mass splitting Δ_P is defined as $\Delta_P \equiv m_P - M$. This gives the loop function in HM χ PT, (see, e.g., Refs. [23, 104]),

$$G_{\text{HM}}(s, M^2, m^2) = \frac{1}{16\pi^2 \overset{\circ}{M}} \left\{ 2\sqrt{\Delta_{\text{HM}}^2 - m^2} \left(\text{arccosh} \left(\frac{\Delta_{\text{HM}}}{m} \right) - \pi i \right) + \Delta_{\text{HM}} \left(\log \left(\frac{m^2}{\mu^2} \right) + a \right) \right\}, \quad (5.56)$$

where $\overset{\circ}{M}$ is the chiral limit value of the heavy-light meson mass appearing in the loop and $\Delta_{\text{HM}} = \sqrt{s} - M$. Comparing G_{HM} with the loop function of Eq. (5.54) expanded up to order $1/\overset{\circ}{M}$,

$$G(s, M^2, m^2) = \frac{1}{16\pi^2} \left(\log \left(\frac{\overset{\circ}{M}^2}{\mu^2} \right) - 2 \right) + \frac{1}{16\pi^2 \overset{\circ}{M}} \left\{ 2\sqrt{\Delta_{\text{HM}}^2 - m^2} \left(\text{arccosh} \left(\frac{\Delta_{\text{HM}}}{m} \right) - \pi i \right) + \Delta_{\text{HM}} \log \left(\frac{m^2}{\overset{\circ}{M}^2} \right) \right\}, \quad (5.57)$$

one is tempted to introduce the following renormalization scheme:

$$G_{\text{HQS}}(s, M^2, m^2) \equiv G(s, M^2, m^2) - \frac{1}{16\pi^2} \left(\log \left(\frac{\overset{\circ}{M}^2}{\mu^2} \right) - 2 \right) + \frac{m_{\text{sub}}}{16\pi^2 \overset{\circ}{M}} \left(\log \left(\frac{\overset{\circ}{M}^2}{\mu^2} \right) + a \right), \quad (5.58)$$

where $m_{\text{sub}} = m$. From now on, we will refer to this loop function as the heavy-quark symmetry (HQS) inspired loop function. It should be noted that in Eq. (5.58) we have chosen to renormalize the loop function at the threshold of $\sqrt{s} = M + m$, where $\Delta_{\text{HM}} = m(m_{\text{sub}})$. It is easily seen that the renormalized loop function G_{HQS} satisfies the chiral power counting and also exhibits a well-defined behavior in the $M \rightarrow \infty$ limit.⁷ At

⁷If we drop the non-perturbative term $\frac{m}{16\pi^2 \overset{\circ}{M}} \left(\log \left(\frac{\overset{\circ}{M}^2}{\mu^2} \right) + a \right)$, it can be easily seen that our proposed renormalization scheme is

fixed \mathring{M} and m_{sub} the ansatz we propose is equivalent to the $\overline{\text{MS}}$ approach widely used in UChPT, but it has the advantage of manifestly satisfying the (approximate) heavy-quark spin and flavor symmetries at threshold.

In our study of the scattering lengths of Nambu-Goldstone bosons off the D mesons, the subtraction constant a can in principle vary from channel to channel, depending on the intermediate Nambu-Goldstone boson. A reasonable alternative is to use for m_{sub} an SU(3) average mass, e.g., $m_{\text{sub}} = (3m_\pi + 4m_K + m_\eta)/8 = 0.3704$ GeV, and have a common subtraction constant a for all channels. A variation of this value from m_π to m_η can serve as an estimate of uncertainties as one tries to connect physics of the D and B sectors. It should be stressed that using the mass of the intermediate Nambu-Goldstone boson in the subtraction but keeping a common subtraction constant for all channels will introduce sizable uncontrolled SU(3) breaking corrections that should be avoided.

In Fig. 5.8, we show the dependence of the loop functions calculated in the HQS, HM and $\overline{\text{MS}}$ schemes with the renormalization scale $\mu = 1$ GeV⁸, $\mathring{M} = M$, $m = m_\pi = 0.138$ GeV, $\sqrt{s} = M + m$, and $m_{\text{sub}} = 0.3704$ GeV. For the sake of comparison, we have plotted the loop function defined in the chiral SU(3) scheme of Ref. [121], which has the following form

$$G_{\chi\text{-SU}(3)} = G_{\overline{\text{MS}}}(s, M^2, m^2) - G_{\overline{\text{MS}}}(M^2, M^2, m^2). \quad (5.59)$$

This approach has the appealing feature that crossing symmetry is restored at a given kinematical point, here for $\sqrt{s} = M$. For this case all loop corrections vanish and only the potential remains, which is obviously crossing symmetric by construction. For Fig. 5.8 the subtraction constants in the HM, HQS, and $\overline{\text{MS}}$ schemes are adjusted to reproduce the $G_{\chi\text{-SU}(3)}$ at $M = 2$ GeV. From Eq. (5.56) one can see that G_{HM} is inversely proportional to M and therefore MG is a constant for the HM loop function. On the other hand, the G function in the HQS scheme is slightly upward curved while the G function in the $\chi\text{-SU}(3)$ downward curved. The naive $\overline{\text{MS}}$ scheme, on the other hand, changes rapidly with M . It is clear that without readjusting a for different M , which could correspond to either a heavy-light B meson or D meson, heavy-quark flavor symmetry is lost as pointed out in Ref. [104].

So far, we have concentrated on the $1/M$ scaling of the loop function G in different schemes, but have not paid much attention to the chiral series or SU(3) breaking effects. In terms of $1/M$ scaling, the HM, HQS, and $\chi\text{-SU}(3)$ approaches all seem reasonable, as shown in Fig. 5.8. On the other hand, compared to the HM ChPT or the $\chi\text{-SU}(3)$ approach, the subtraction constant in the HQS scheme has the simplest form consistent with the chiral power counting and $1/M$ scaling. We will see in the following subsection that such a choice seems to play a non-negligible role in describing the light-quark mass dependence of the scattering lengths of the Nambu-Goldstone bosons off the D mesons.

in the spirit of the EOMS scheme to remove the power-counting-breaking terms.

⁸From a theoretical point of view, the renormalization scale μ should be the chiral-symmetry breaking scale, $\Lambda_\chi \approx 4\pi f_0 \approx 1.2$ GeV, which can be immediately seen by examining the HM ChPT loop function of Eq. (5.56).

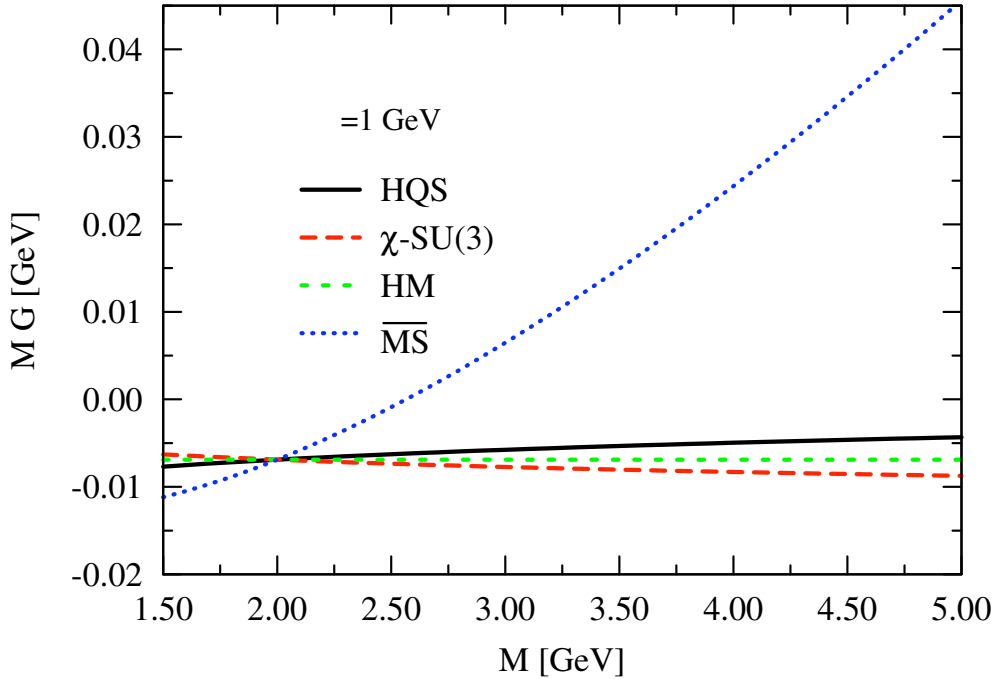


FIGURE 5.8: Dependence of loop functions on the heavy-light meson mass in different schemes with $\mu = 1$ GeV.

5.4.2 Results and discussions

Leading-order predictions

In this subsection we present predictions based on LO potentials, using the heavy-quark symmetry motivated renormalization scheme. In our framework, the scattering length of channel i with strangeness S and isospin I is related to the diagonal T-matrix elements T_{ii} via

$$a_i^{(S,I)} = -\frac{1}{8\pi(M_1 + m_2)} T_{ii}^{(S,I)}(s = (M_1 + m_2)^2). \quad (5.60)$$

At the order we are working, the only free parameter to be fixed is the subtraction constant a . Since our approach might be most reasonable to predict bound states or resonances near threshold we fix this parameter to reproduce the lowest lying strange D meson with $J^P = 0^+$, the $D_{s0}^*(2317)$. This state is well established experimentally [6, 7, 85, 132–134] and has a mass, known with high precision, of 2317.8 MeV [1]. It lies below the DK threshold and hence its S-wave decay mode $D_{s0}^*(2317) \rightarrow DK$ is kinematically forbidden. Reproducing the $D_{s0}^*(2317)$ at its physical mass fixes $a(1 \text{ GeV}) = -4.01$ for $f_0 = f_\pi = 92.21$ MeV, where we have only iterated the Weinberg-Tomozawa term. Using instead of f_0 the isospin-averaged decay constant $F_0 = 1.15 f_\pi$, corresponding to a partial resummation of higher order correction, fixes $a(1 \text{ GeV}) = -4.94$. From now on we use the latter one for the LO predictions, as will be argued in comparison with LQCD data⁹. A subtraction constant of this size might appear large at first, but one should notice that the parameter dependence on the subtraction constant a has been shifted to one order higher within our scheme (it starts to contribute at

⁹For the NLO fits shown later, the standard choice $f_0 = 92.21$ MeV is adopted.

TABLE 5.3: Scattering lengths in units of fm. The column LO shows the tree level results without corrections from exchange diagrams Figure 5.6 (b), (c), whereas LO-Exchange shows the complete LO result. The corresponding unitarized results are denoted by LO_U and LO-Exchange_U.

(S,I)	Channel	LO	LO-Exchange	LO _U	LO-Exchange _U
(2,1/2)	$D_s K \rightarrow D_s K$	-0.28	-0.32	-0.16	-0.18
(1,1)	$DK \rightarrow DK$	0	0	$0.09 + 0.20 i$	$0.09 + 0.26 i$
	$D_s \pi \rightarrow D_s \pi$	0	0	0.01	0.01
(1,0)	$DK \rightarrow DK$	0.55	0.45	-0.89	-1.15
	$D_s \eta \rightarrow D_s \eta$	0	-0.07	$-0.25 + 0.04 i$	$-0.27 + 0.05 i$
(0,3/2)	$D\pi \rightarrow D\pi$	-0.09	-0.09	-0.08	-0.08
(0,1/2)	$D\pi \rightarrow D\pi$	0.18	0.17	0.27	0.26
	$D\eta \rightarrow D\eta$	0	-0.02	$0.41 + 0.23 i$	$0.68 + 0.31 i$
	$D_s \bar{K} \rightarrow D_s \bar{K}$	0.28	0.23	$-0.36 + 0.72 i$	$-0.66 + 0.76 i$
(-1,1)	$D\bar{K} \rightarrow D\bar{K}$	-0.27	-0.32	-0.16	-0.18
(-1,0)	$D\bar{K} \rightarrow D\bar{K}$	0.27	0.32	0.90	1.70

$\mathcal{O}(p^3)$). We cite here also the subtraction constant from [104], $a(m_D) = -3.034$, for comparison (employing $f_0 = 92.4$ MeV). This value, near to ours, implies some similarity between the methods. However, as described in detail in Subsection 5.4.2, this approach leads to significantly different predictions if fitted to LQCD data.

The scattering lengths at physical pion masses are given in Table 5.3 for leading order chiral perturbation theory (LO ChPT) and its unitarized version. For both we show two different scenarios. The first one takes into account only the LO contact interaction from the Weinberg-Tomozawa term. The corresponding results are denoted by LO and LO_U, where the subscript U indicates unitarized ChPT. The second scenario includes also exchange corrections Figure 5.6 (b) and (c). The corresponding columns are denoted as LO-Exchange and LO-Exchange_U. The subtraction constant is fixed for both scenarios to $a(1 \text{ GeV}) = -4.94$, reproducing the $D_{s0}^*(2317)$ for the LO_U scenario, by construction.

The tree level results, columns LO and LO-Exchange, give an impression of the size of exchange corrections. For channels where the Weinberg-Tomozawa term contributes, the inclusion of exchange diagrams shift scattering lengths only slightly, up to 20%. This is indeed small, keeping in mind that both corrections are counted as LO. This can be understood by an explicit calculation, showing that exchange diagrams start at NLO. However, in contrast to the pure contact interaction, these diagrams can also contribute to the channels ($S = 1, I = 0$), $D_s \eta \rightarrow D_s \eta$, and ($S = 0, I = 1/2$), $D\eta \rightarrow D\eta$. However, the corresponding scattering lengths are small and hence the interaction strength near threshold should be small.

As long as the interaction is repulsive, the corrections from the unitarization are quantitatively small, as can be seen by comparing negative scattering length at tree level, columns LO or LO-Exchange, to the resummed results in columns LO_U or LO-Exchange_U. On the other hand, the resummation of an attractive interaction can shift scattering lengths considerably. This becomes evident from the ($S = 1, I = 0$), $DK \rightarrow DK$ channel, where the unitarization flips a sizable positive value to a negative one. This can be observed for both

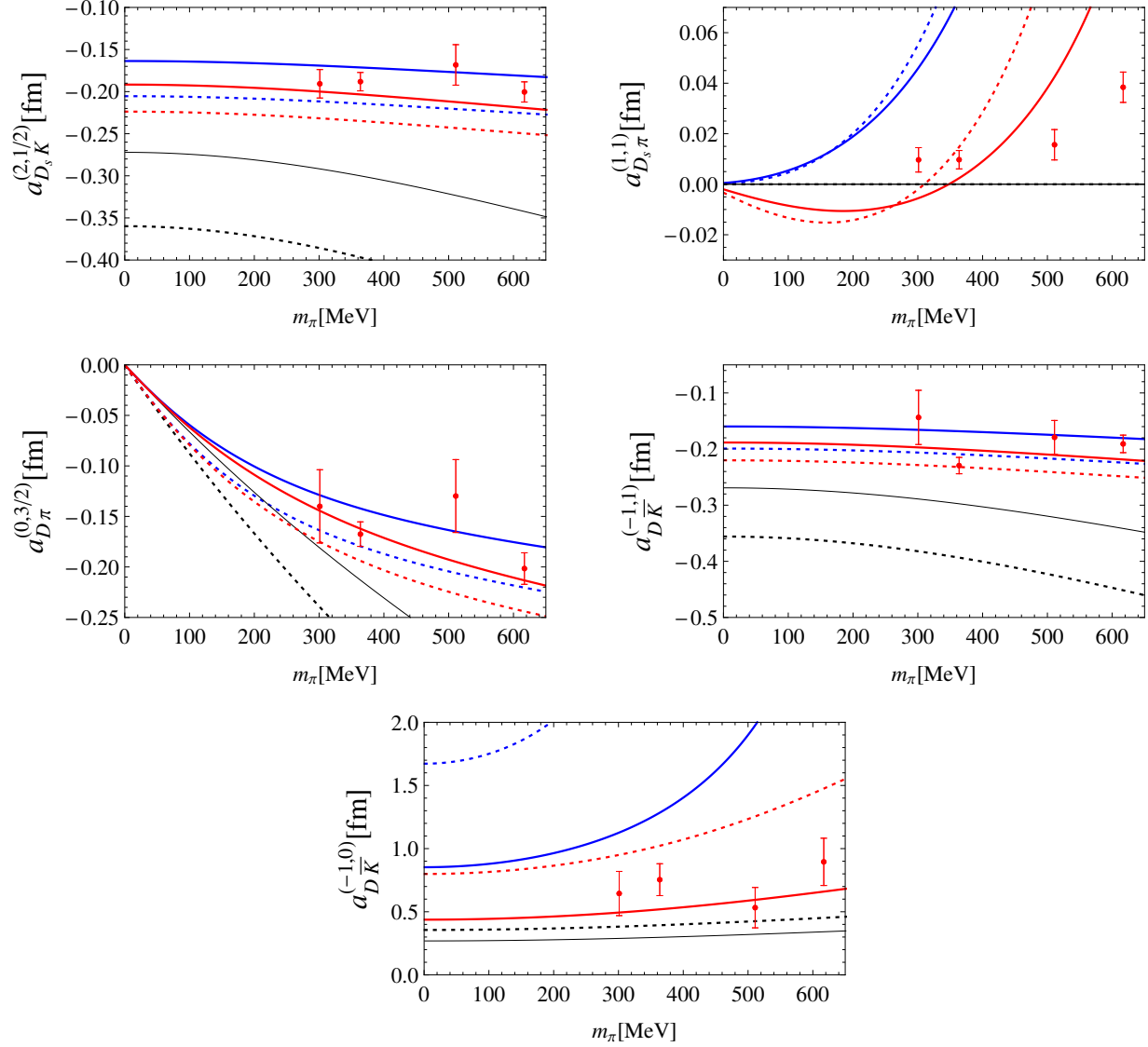


FIGURE 5.9: The $n_f = 2 + 1$ LQCD data [12] vs. LO tree level results (black), LO UChPT in the on-shell approximation (blue), and the LO UChPT taking into account the full off-shellness of the potential (red). The solid and dashed lines always correspond to predictions employing F_0 and f_0 , respectively.

scenarios, LO_U and LO-Exchange_U . This effect even persists if channel coupling effects are switched off, as we have verified explicitly. The large negative scattering length reflects the appearance of a bound state, the $D_{s0}^*(2317)$.¹⁰

In Fig. 5.9, the LQCD data [12] are contrasted with predictions of our approach (shown by the blue lines). We present in addition the pion-mass dependence for the strangeness and Isospin combinations ($S = 0, I = 1/2$) and ($S = 1, I = 0$) in Figure 5.10, where almost no LQCD data is available. The solid lines correspond to the scenario with F_0 , the dashed lines to the scenario with f_0 . Obviously the first one gives a more reasonable

¹⁰One should notice that even the exchange corrections contribute little at tree level, they can be of some relevance in the unitarized framework. However, since they do not improve the description of data and since they are also suppressed by one order, we neglect them from now on.

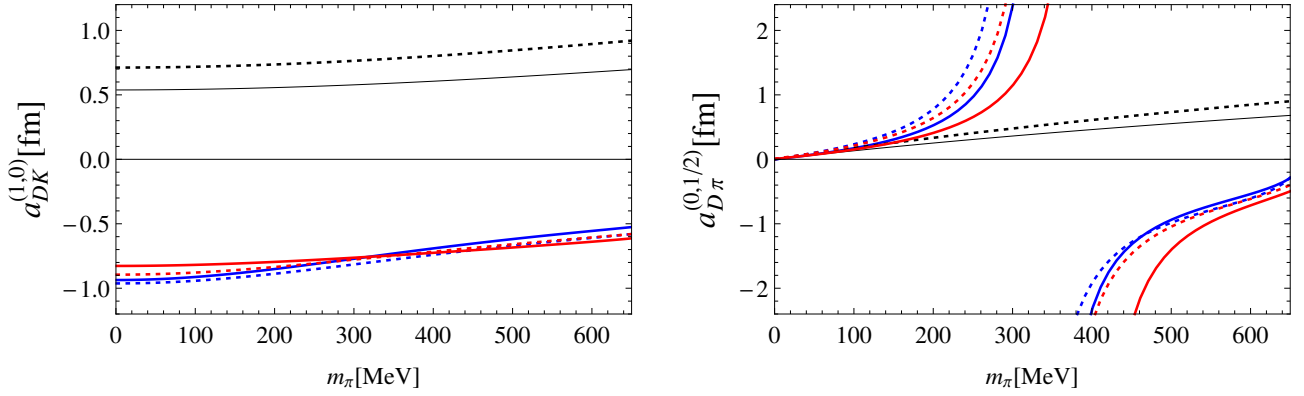


FIGURE 5.10: Predictions for scattering lengths of strangeness and isospin combinations ($S = 1, I = 0$) (left panel) and ($S = 0, I = 1/2$) (right panel) from the LO tree level (black), LO UChPT in the on-shell approximation (blue), and from the LO UChPT taking into account the full off-shellness of the potential (red). The solid and dashed lines always correspond to the scenarios employing F_0 and f_0 .

description of the available data and hence we rely on it in this subsection. The pion mass dependences have been obtained by employing leading order chiral perturbation theory to express the kaon mass in terms of the pion mass,

$$m_K = \sqrt{\frac{1}{2}(m_\pi^2 + 2B_0 m_s)}, \quad (5.61)$$

with $B_0 = m_\pi^2/(m_u + m_d)$, where m_u, m_d, m_s are the masses of up, down and strange quark. To relate the η meson mass to kaon and pion mass, we have used Eq. (3.8). Further we have employed the NLO mass formula Eq. (3.25) with $c_1 = -0.214$ and $m_{D,0} = 1863$ MeV, reproducing the physical D meson mass. Here we have assumed $c_0 = 0$ in accordance with Subsection 5.3.1.

One should notice that within the present approach all repulsive single channel processes are already reproduced to good accuracy. These are the strangeness, isospin combinations $(S, I) = (2, 1/2), (0, 3/2)$ and $(-1, 1)$. This is especially remarkable if one considers the LO tree level predictions, shown by the solid and dashed black lines, which are still far of the LQCD data. On the other hand the predictions for the attractive channels appear to be incompatible with the LQCD computations. These are the channels $(S, I) = (1, 1)$, $D_s\pi \rightarrow D_s\pi$, and $(S, I) = (-1, 0)$, $D\bar{K} \rightarrow D\bar{K}$. The process $(S, I) = (1, 1)$ is a coupled channels process, where the scattering length for $D_s\pi$ shows a strong dependence on the pion mass. At low m_π , near the physical pion mass, the predicted scattering length is still small, near zero. The lattice data is provided at significantly higher pion masses of about 300 MeV to 600 MeV. At these masses the LO unitarized chiral perturbation theory deviates already significantly from LQCD data. Concerning the coupled channels effects, it is interesting that all pion mass dependence disappears if the channel coupling effects are switched off. In this case the predicted scattering length obviously becomes more compatible with LQCD data.

The other channel in question is $(S, I) = (-1, 0)$, $D\bar{K} \rightarrow D\bar{K}$, which is an attractive single channel process. Through unitarizing the amplitude, the scattering length increases significantly and becomes incompatible with the LQCD data. One should notice that the LO tree level prediction is still in agreement with data. Clearly a possible source of uncertainty are missing higher order corrections to the potential. This is investigated in detail in the next subsection. As elaborated in Section 5.5 and shown by the solid and dashed red lines in Fig.

5.9, a resummation taking into account the full off-shellness of the potential can also significantly reduce this discrepancy.

The reduced scattering amplitudes from our chiral unitary approach are shown in Figure 5.11. The upper part shows the reduced amplitudes with $J^P = 0^+$, where we have restricted us to the most interesting channels, $(S = 1, I = 1)$, $(S = 1, I = 0)$, $(S = 0, I = 1/2)$ and $(S = -1, I = 0)$. All of them, except $(S = -1, I = 0)$, are coupled channels processes. Different channels are indicated by the solid blue, dashed red, and small dashed green lines with assignments given in the figure.

Within our scheme we can use the subtraction constant $a(1\text{GeV}) = -4.95$, determined previously, to give predictions for the scattering of Nambu-Goldstone bosons off heavy-light vector mesons. We concentrate on $J^P = 1^+$. The potential is given by equation (5.41), where the matrices $(\mathcal{M}_{J^P=1^+})_{ab}$ carry now indices $a(b)$ running over both, different channels and different helicity states. Inserting the potential (5.41) into the BS equation (5.15) together with using $-g^{\mu\nu} + q^\mu q^\nu / m_h^2 = \sum_\lambda \epsilon^\mu(q, \lambda) \epsilon^{\dagger\nu}(q, \lambda)$, gives

$$\hat{T}^{(S,I)}(s) = [\hat{\mathbf{1}} - \hat{\mathcal{M}}_{J^P}^{(S,I)}(s) \cdot \hat{G}^{(S,I)}(s)]^{-1} \cdot \hat{\mathcal{M}}_{J^P}^{(S,I)}(s). \quad (5.62)$$

Equivalently, in order to construct projectors free of kinematic singularities, the bare helicity states can be rotated as shown in Appendix A.2. This gives the potential

$$\widetilde{\mathcal{M}}_{J^P=1^+} \equiv \begin{pmatrix} \langle 1_c^{(+)} | \mathcal{T}^{J=1} | 1_c^{(+)} \rangle & \langle 1_c^{(+)} | \mathcal{T}^{J=1} | 2_c^{(+)} \rangle \\ \langle 2_c^{(+)} | \mathcal{T}^{J=1} | 1_c^{(+)} \rangle & \langle 2_c^{(+)} | \mathcal{T}^{J=1} | 2_c^{(+)} \rangle \end{pmatrix}, \quad (5.63)$$

where one should notice that the normalization of the states are now given by

$$N = \begin{pmatrix} \langle 1_c^{(+)} | 1_c^{(+)} \rangle & \langle 1_c^{(+)} | 2_c^{(+)} \rangle \\ \langle 2_c^{(+)} | 1_c^{(+)} \rangle & \langle 2_c^{(+)} | 2_c^{(+)} \rangle \end{pmatrix} = \begin{pmatrix} \frac{3}{2} + \frac{p_{\text{cm}}^2}{2M^2} & \frac{p_{\text{cm}}^2 \sqrt{M^2 + p_{\text{cm}}^2}}{\sqrt{2}M^2} \\ \frac{p_{\text{cm}}^2 \sqrt{M^2 + p_{\text{cm}}^2}}{\sqrt{2}M^2} & \frac{p_{\text{cm}}^4}{M^2} \end{pmatrix}, \quad (5.64)$$

with the centre of mass three-momentum p_{cm} of the interacting pair. We have checked numerically that the matrix elements involving the helicity state $|2_c^{(0)}\rangle$ play a negligible role in our present study. Therefore we only keep the $(\widetilde{\mathcal{M}}_{J^P=1^+})_{11}$ component of the potential, which coincides with the approach of Ref. [135].

The comparison of the upper and lower Figure 5.11, corresponding to $J^P = 0^+$ and $J^P = 1^+$, shows the consequences heavy-quark spin symmetry. The shapes of the curves look qualitatively the same, but all structures are shifted up by about 150 MeV for $J^P = 1^+$ compared to $J^P = 0^+$. This is very natural, since the masses of the D^* mesons lie about 140 MeV above the corresponding D mesons.

Figure 5.11 reveals a number of resonances and bound states. The peak positions in the complex \sqrt{s} plane near the physical Riemann sheet are summarized in Table 5.4 for both, $J^P = 0^+$ and $J^P = 1^+$. As a direct consequence of heavy-quark spin symmetry, a bound state in the $J^P = 1^+$ sector can be observed. Our approach predicts its mass at about 2473 MeV near the mass of the charmed-strange meson D_{s1}^* (2460) of 2459 MeV [1], observed in numerous experiments [7, 85, 132–134]. Its quantum numbers are $J^P = 1^+$ and isospin $I = 0$, and its measured widths is very small (< 3.5 MeV), in accordance with our treatment where the

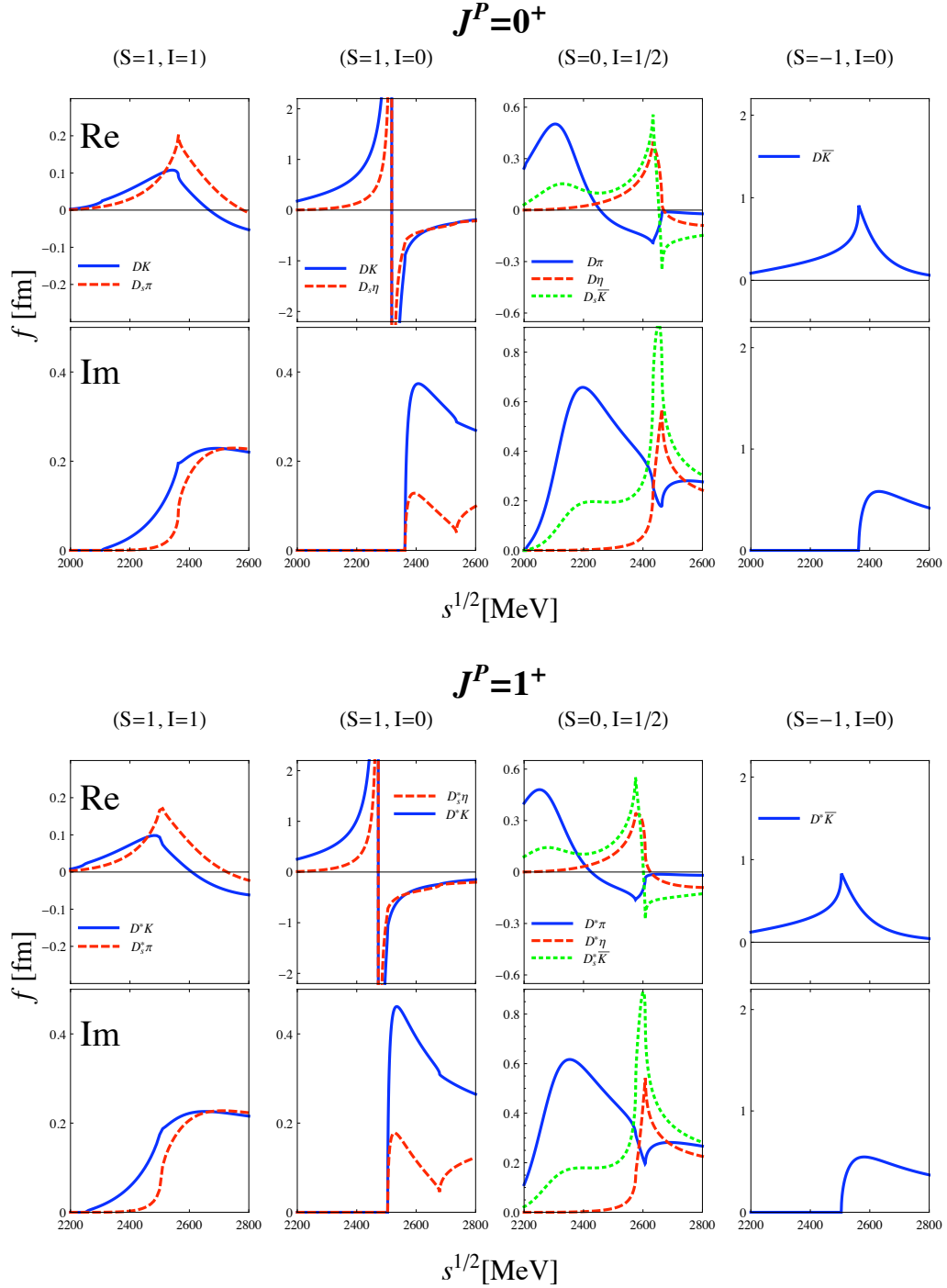


FIGURE 5.11: Predictions for the reduced scattering amplitude $f^{(S,I)}(\sqrt{s}) \equiv -T^{(S,I)}(s)/(8\pi\sqrt{s})$ on the real \sqrt{s} axes for different strangeness and isospin combinations (S, I) . The upper figure shows predictions for $D\phi$ scattering, where the $J^P = 0^+$ potential, Eq. (5.35), was used. The lower figure shows the $J^P = 1^+$ counterpart, where the first entry of Eq. (5.63) was iterated, for details see text. In both figures the upper (lower) row shows the real (imaginary) part of f .

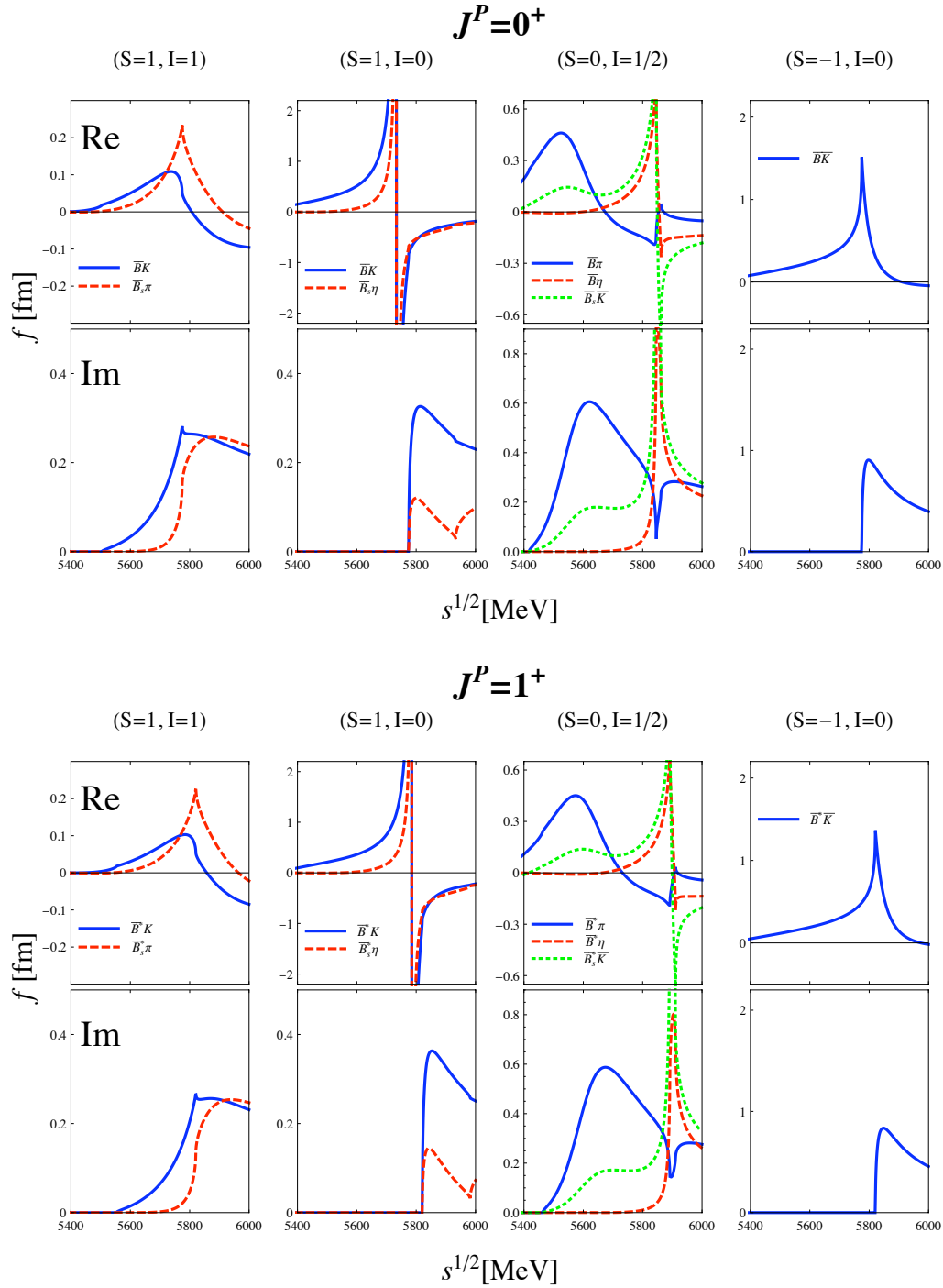


FIGURE 5.12: Reduced scattering amplitude $f^{(S,I)}(\sqrt{s}) \equiv -T^{(S,I)}(s)/(8\pi\sqrt{s})$. The figures are to be understood analogously to Figure 5.11, The upper figure shows predictions for $\bar{B}\phi$ scattering, the lower figure for $\bar{B}^*\phi$ scattering.

state lies below threshold.

Additionally, resonances in the channel $(S, I) = (0, 1/2)$ are found. For $J^P = 0^+$, a broad state with width $\Gamma \sim 228$ MeV and mass 2132 MeV is predicted. It lies on the second Riemann sheet above the $D\pi$ threshold of 2005 MeV. On the other hand, a sharp resonances at 2471 MeV is found near the $D\eta$ threshold. Both states are not in accordance with experiment [1], where the $D_0^*(2400)^0$ and $D_0^*(2400)^\pm$ have been determined to have masses of (2318 ± 29) MeV and $(2403 \pm 14 \pm 35)$ MeV, both with broad widths, $\Gamma = (267 \pm 40)$ MeV and $\Gamma = (283 \pm 24 \pm 34)$ MeV. One should note that these masses contradict each other, assuming that $D_0^*(2400)^0$ and $D_0^*(2400)^\pm$ are isospin partners. The underlying measurements can be found in [138–140]. Interestingly, [138] predicts both states at roughly 2400 MeV, whereas [139, 140] agree on a mass of roughly 2300 MeV for $D_0^*(2400)^0$. The charged state $D_0^*(2400)^\pm$ has not been investigated by [139, 140].

Considering the $J^P = 1^+$ results for $(S, I) = (0, 1/2)$ we see that they are strongly related to $J^P = 0^+$. All masses appear to be shifted up by about 150 MeV and the widths remain of the same order of magnitude. States with appropriate quantum numbers from experiment [1] are $D_1(2420)^0$ and $D_1(2430)^0$ with masses (2420.9 ± 0.8) MeV and $(2427 \pm 26 \pm 25)$ MeV, and widths (27.1 ± 2.7) MeV and $(384_{-75}^{+107} \pm 74)$ MeV, respectively. As previously, we can not clearly relate our predictions to these states. However, of more interest should be the state $D_1(2430)^0$, since it is expected to be an S-wave, in contrast to $D_1(2420)^0$, which should be a D-wave [140]. In our treatment the D-wave is neglected.

As a consequence of heavy-quark flavor symmetry we can also give predictions for bottomed mesons. The reduced scattering amplitudes are shown in Figure 5.12 and the observed resonances and bound states can be found in Table 5.5. Bound states are observed for $(S, I) = (1, 0)$ with $J^P = 0^+$ and $J^P = 1^+$. These can be understood as bottomed partners to $D_{s0}^*(2317)$ and $D_{s1}^*(2460)$. From experiment only little is known about excited B mesons. A sharp resonance with $J^P = 1^+$ was observed in [141]. It is expected to be a D-wave and therefore not favored for a comparison to our prediction.

TABLE 5.4: Pole positions $\sqrt{s} = M - i\frac{\Gamma}{2}$ (in units of MeV) of charm mesons dynamically generated in the leading order HQS UChPT. The * indicates the peak position that is used as an input to fix the subtraction constant to $a(1 \text{ GeV}) = -4.94$.

(S,I)	$J^P = 0^+$	$J^P = 1^+$
(1,0)	2317.8*	2473
(0,1/2)	2132 - i 114	2278 - i 125
	2471 - i 51	2624 - i 45

TABLE 5.5: Pole positions $\sqrt{s} = M - i\frac{\Gamma}{2}$ (in units of MeV) of bottom mesons dynamically generated in the leading order HQS UChPT.

(S,I)	$J^P = 0^+$	$J^P = 1^+$
(1,0)	5734	5786
(0,1/2)	$5559 - i 120$	$5608 - i 126$
	$5843 - i 27$	$5898 - i 28$

Fits to the LQCD results for scattering lengths

Now we are in a position to study the latest fully dynamical LQCD data of Ref. [12]. Up to NLO¹¹, we have six unknown LECs and in the case of the UChPT also the unknown subtraction constant. As explained in Subsection 5.3.1, the constant c_1 can be determined from the mass splitting of the strange and non-strange D mesons, which yields $c_1 = -0.214$. The constant c_0 can be fixed by fitting the NLO mass formulas to the LQCD data of Ref. [12]. This yields $c_0 = 0.015$. Therefore, we have four LECs to be determined in the ChPT and five in the UChPT.

First, we perform fits to the 15 LQCD data¹² with the NLO HMChPT and covariant ChPT. The results are shown in Table 5.6. It seems that both approaches fail to achieve a $\chi^2/\text{d.o.f}$ of about 1, but covariant ChPT describes the LQCD data better than HMChPT. The smaller $\chi^2/\text{d.o.f}$ in the covariant ChPT should be attributed to the terms with the coefficients, c_4 and c_5 . These two terms cannot be distinguished from the terms with coefficients c_2 and c_3 in the HMChPT, as mentioned earlier.

Next we perform fits using the NLO HM approach and covariant UChPT with the loop function regularized in the HQS scheme and in the χ -SU(3) scheme. The results are shown in Table 5.7. A few points are noteworthy. First, the NLO UChPT describes the LQCD data better than the NLO ChPT. Second, the covariant UChPT describes the LQCD data much better than the HM UChPT. The χ -SU(3) approach gives a $\chi^2/\text{d.o.f}$ value in-between those of the HM UChPT and the covariant UChPT.

These results are consistent with the findings from the studies of the decay constants of the heavy-light mesons [78] and the ground-state octet baryon masses in the one-baryon sector [52]. That is to say, the covariant ChPT appears to be superior in describing the light-quark mass evolution of physical observables as compared to its non-relativistic counterpart.

In Fig. 5.13, the LQCD data are contrasted with the NLO UChPT. The theoretical bands are generated from the uncertainties of the LECs. The D (D_s) masses are described with the NLO mass relations of Eqs. (3.25,3.26), where the LECs $m_{D,0}$, c_0 , and c_1 are fixed by fitting to the LQCD masses of Ref. [12]. In addition, the kaon masses are expressed as $m_K^2 = am_\pi^2 + b$ with a and b determined by the LQCD data of Ref. [12] as well. However, one should notice that such a comparison is only illustrative because the NLO

¹¹It should be noted that the scattering lengths of the Nambu-Goldstone bosons off the D mesons have been calculated up to N³LO in both the covariant ChPT [49] and HMChPT [136].

¹²Unless otherwise specified, to ensure that the NLO (U)ChPT is applicable to the LQCD data, we restrict ourselves to the LQCD data obtained with m_π ranging from 301 MeV to 510 MeV and excluding the heaviest point of $m_\pi = 611$ MeV.

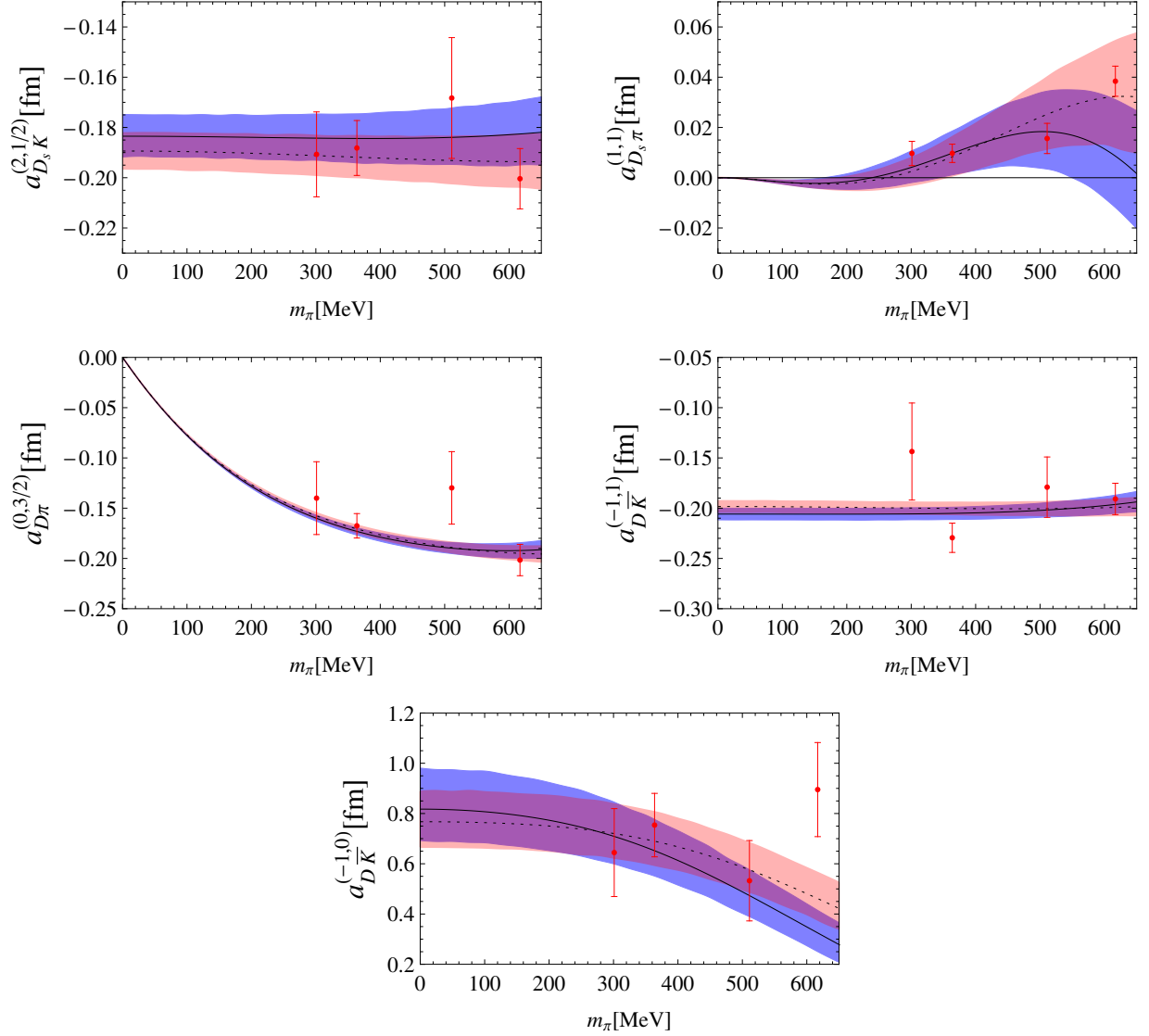


FIGURE 5.13: The $n_f = 2 + 1$ LQCD data [12] vs. the NLO covariant UChPT. The black solid and dashed lines show the best fits to the 15 LQCD points and to the 20 LQCD points, with the blue and red bands covering the uncertainties propagated from those of the LECs within one standard deviation, respectively.

mass formulae cannot describe simultaneously both the LQCD D and D_s masses and their experimental counterparts, as mentioned in Subsection 5.3.1 and as noticed in Ref. [12]. In fact, the $\chi^2/\text{d.o.f}$ shown in Tables 5.6 and 5.7 are calculated with the D and D_s mass data taken directly from LQCD and not with the fitted masses of the NLO ChPT. For the sake of comparison, we show also in Fig. 5.13 the theoretical results obtained from a fit to all of the 20 LQCD data. Within uncertainties they tend to overlap with those calculated with the LECs from the fit to the 15 LQCD points.

TABLE 5.6: Low-energy constants and the $\chi^2/\text{d.o.f}$ from the best fits to the LQCD data [12] in the covariant ChPT and the HM ChPT up to NLO, where $c_{24} = c_2 - 2c_4$ and $c_{35} = c_3 - 2c_5$. The uncertainties of the LECs given in the parentheses correspond to one standard deviation.

	c_{24}	c_{35}	c_4	c_5	$\chi^2/\text{d.o.f}$
Covariant ChPT	0.153(35)	-0.126(71)	0.760(186)	-1.84(39)	2.01
HM ChPT	0.012(6)	0.167(17)	-	-	3.10

TABLE 5.7: Low-energy constants, the subtraction constants, and the $\chi^2/\text{d.o.f}$ from the best fits to the LQCD data [12] in the HQS UChPT, the χ -SU(3) UChPT, and the HM UChPT. The renormalization scale μ is set at 1 GeV. The uncertainties of the LECs given in the parentheses correspond to one standard deviation.

	a	c_{24}	c_{35}	c_4	c_5	$\chi^2/\text{d.o.f}$
HQS UChPT	-4.13(40)	-0.068(21)	-0.011(31)	0.052(83)	-0.96(30)	1.23
χ -SU(3) UChPT	-	-0.096(19)	-0.0037(340)	0.22(8)	-0.53(21)	1.57
HM UChPT	2.52 (11)	4.86(30)	-9.45(60)	-	-	2.69

Dynamically generated heavy-light mesons

Once the subtraction constant and the LECs are fixed, one can utilize the UChPT to study whether the interactions between heavy-light mesons and Nambu-Goldstone bosons are strong enough to generate bound states or resonances, by searching for poles in the complex \sqrt{s} plane. We notice that the subtraction constant in the HM UChPT given in Table 5.7 is positive, and as a result, there is no bound state generated in the $(S, I) = (1, 0)$ channel. On the other hand, using covariant UChPT, a bound state is found at $\sqrt{s} = 2317 \pm 10$ MeV in the complex plane. We identify this bound state as the $D_{s0}^*(2317)$. In addition, one more state is generated in the $(S, I) = (0, 1/2)$ channel. All of them are tabulated in Table 5.8. In calculating the positions of these states, we have used the physical masses listed in Table 4.1. The uncertainties in the positions of these states are estimated by changing the LECs and the subtraction constant within their $1\text{-}\sigma$ uncertainties given in Table 5.7. Furthermore, we predict the heavy quark spin partners of the 0^+ states as well. The counterpart of the $D_{s0}^*(2317)$ appears at $\sqrt{s} = 2457 \pm 17$ MeV¹³, which we identify as the $D_{s1}(2460)$. It is clear that the heavy-quark spin symmetry is approximately conserved in the HQS ChPT approach.

One appealing feature of the renormalization scheme we propose in this work is that the heavy quark flavor symmetry is conserved up to $1/M_{\text{HL}}$, in contrast to the naive $\overline{\text{MS}}$ subtraction scheme. As such, we can calculate the bottom partners of the $D_{s0}^*(2317)$ and $D_{s1}(2460)$ in reasonable confidence. We tabulate in Table 5.9 the bottom counterparts of the charm states of Table 5.8. It should be noted that the absolute positions of these resonances are subject to corrections of a few tens of MeV because of the uncertainty related to the evolution of the UChPT from the charm sector to the bottom sector. On the other hand, the mass differences between the 1^+ states and their 0^+ counterparts should be more stable, as has been argued in a number of different studies (see, e.g., Ref. [104]).

¹³The uncertainties are propagated from the uncertainties of the LECs and the subtraction constant. In addition, we have assigned a 10% uncertainty for relating the LECs in the D^* sector with those in the D sector by use of heavy-quark spin symmetry. To relate the LECs between D and B sectors, a 20% uncertainty is assumed, and m_{sub} is varied from m_π to m_η .

TABLE 5.8: Pole positions $\sqrt{s} = M - i\frac{\Gamma}{2}$ (in units of MeV) of charm mesons dynamically generated in the HQS UChPT.

(S,I)	$J^P = 0^+$	$J^P = 1^+$
(1,0)	2317 ± 10	2457 ± 17
(0,1/2)	$(2105 \pm 4) - i(103 \pm 7)$	$(2248 \pm 6) - i(106 \pm 13)$

TABLE 5.9: Pole positions $\sqrt{s} = M - i\frac{\Gamma}{2}$ (in units of MeV) of bottom mesons dynamically generated in the HQS UChPT.

(S,I)	$J^P = 0^+$	$J^P = 1^+$
(1,0)	5726 ± 28	5778 ± 26
(0,1/2)	$(5537 \pm 14) - i(118 \pm 22)$	$(5586 \pm 16) - i(124 \pm 25)$

TABLE 5.10: Dynamically generated 0^+ and 1^+ bottom states in $(S, I) = (1, 0)$ from different formulations of the UChPT. Masses of the states are in units of MeV.

J^P	present work	NLO HMChPT [104]	LO UChPT [97]	LO χ -SU(3) [96]
0^+	5726 ± 28	5696 ± 36	5725 ± 39	5643
1^+	5778 ± 26	5742 ± 36	5778 ± 7	5690

In Table 5.10 we compare the predicted 0^+ and 1^+ states from several different formulations of UChPT in the bottom sector. It is seen that the absolute positions can differ by as much as 80 MeV, which is not surprising because the heavy-quark flavor symmetry was implemented differently.

It has been argued that the light-quark mass evolution of the masses of mesons and baryons can provide important hints about their nature (see, e.g., Refs. [104, 142]). In the left panel of Fig. 5.14, we show how the pole positions of the D_{s0}^* (2317) and the D_{s1} (2460) evolve as a function of m_π . The strange-quark mass is fixed to its physical value using leading-order ChPT. The light-quark mass dependences of the $D(D_s)$ and $D^*(D_s^*)$ are given by the NLO ChPT formulas of Eqs. (3.25 to 3.28). The right panel of Fig. 5.14 shows the evolution of the D_{s0}^* (2317) and D_{s1} (2460) pole position as a function of the kaon mass (or equivalently the strange-quark mass) as we fix the pion mass to its physical value. As has been argued in Ref. [104], the feature of being dynamically generated dictates that the dependence of the masses of these states on m_K are linear with a slope close to unity, which can be clearly seen from Fig. 5.14.

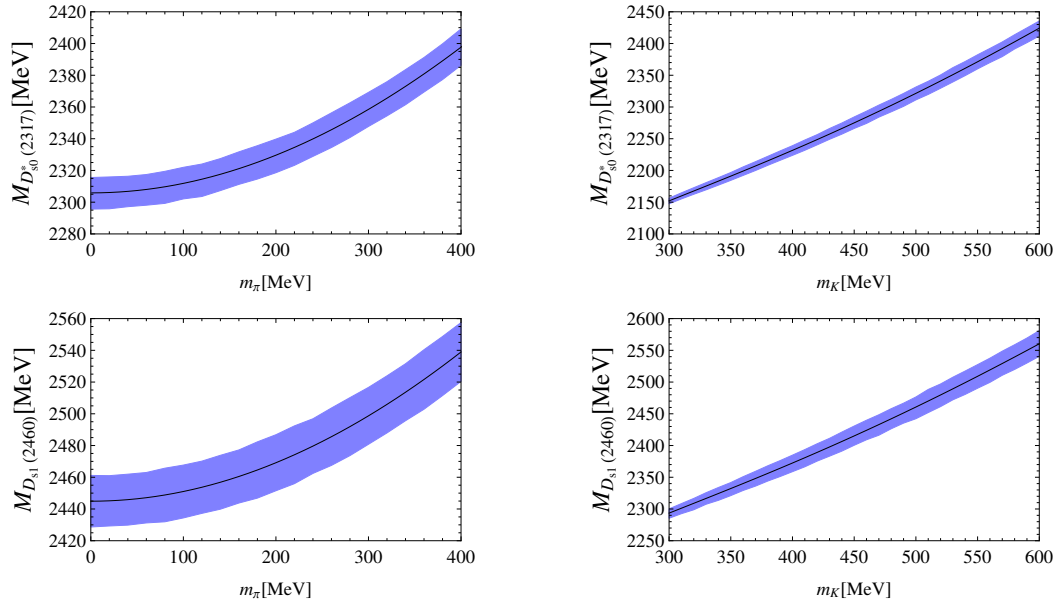


FIGURE 5.14: Pion and kaon mass evolution of the pole positions of the $D_{s0}^*(2317)$ and the $D_{s1}(2460)$.

5.5 Off-shell effects on the light-quark mass evolution of scattering lengths

At the heart of unitary chiral theories are the interaction kernels provided by chiral Lagrangians, which are constrained by QCD and its approximate symmetries, such as chiral symmetry and heavy quark spin/flavor symmetry and their breaking pattern. By solving the BS equation we are able to implement exact two-body (s-channel) unitarity, as proven in Subsection 5.2.2. In contrast to conventional chiral perturbation theory, however, one loses exact crossing symmetry, leading to non trivial issues in the renormalization procedure, c.f. [143].

To simplify the solution of the BS equation, the on-shell approximation was adopted in the previous subsection. This is also the approach widely employed, c.f. [122, 123]. It assumes that the interaction kernel can be put on the mass shell with the argument that the off-shell terms can be absorbed by the available coupling constants and physical hadron masses, which is a non-trivial assumption keeping in mind the loss of crossing symmetry. A vast amount of applications have shown that such an approximation works very well. Nevertheless, from a formal point of view, one may prefer to take into account the full off-shell effects to have an order by order correspondence with the underlying results of chiral perturbation theory. Such off-shell effects have been studied for pion-pion interactions up to NLO [143, 144] and for interactions between the pseudoscalar meson octet and the ground state baryon octet up to LO [145–148] and NLO [149, 150]. These studies mainly focused on the description of physical observables such as phase shifts over a wide range of energies, except Ref. [147] where the contribution to the nucleon mass as a function of the pion mass was discussed.

In the present section, off-shell effects in UChPT for the scattering of Nambu-Goldstone bosons off D mesons are explored. We show that they lead to an improved description of the light-quark mass dependence of the latest $n_f = 2 + 1$ LQCD data [12]. To our knowledge, this is the first of such studies performed in the heavy-light sectors [151], thus extending the many previous studies performed with the on-shell approximation [12, 111, 152].

5.5.1 Framework

To solve the BS equation (5.7) with explicit off-shell dependence, we introduce the following matrix notation for the LO potential

$$\begin{aligned}
 \begin{array}{c} p_2 \\ \diagdown \\ \\ \diagup \\ p_4 \end{array} & \begin{array}{c} \\ \diagup \\ \\ \diagdown \\ p_3 \end{array} \\
 \hline
 p_1 & \longrightarrow
 \end{array}
 \quad = \quad \frac{\mathcal{C}_{\text{LO}}}{4f_0^2} (p_1 \cdot p_2 + p_1 \cdot p_4 + p_2 \cdot p_3 + p_3 \cdot p_4) \\
 & = \frac{\mathcal{C}_{\text{LO}}}{4f_0^2} (2P^2 - 2(P+q) \cdot (P+Q) - q^2 - Q^2) \\
 & = B(q, \nu, \tilde{\nu})^T \cdot \hat{V}_{\text{LO}}(\nu, \tilde{\nu}, \mu, \tilde{\mu}) \cdot B(Q, \mu, \tilde{\mu}), \tag{5.65}
 \end{aligned}$$

where we have redefined the momenta by use of momentum conservation: $p_1 = -q$, $p_2 = q + P$, $p_3 = -Q$ and $p_4 = Q + P$. The vectors in the last line are defined as

$$B(q, \mu, \tilde{\mu}) = \left(\frac{q^2 - M^2}{f_0^2}, \frac{(P_\mu + q_\mu)(P_{\tilde{\mu}} + q_{\tilde{\mu}})}{f_0^2}, \frac{P_\mu + q_\mu}{f_0}, 1 \right)^T, \quad (5.66)$$

where the mass M is chosen as M_1 if B appears on the left of Eq. (5.65) and as M_3 if it appears on the right. The matrix in the last line is defined as

$$\hat{V}_{\text{LO}}(\nu, \tilde{\nu}, \mu, \tilde{\mu}) = \mathcal{C}_{\text{LO}} \begin{pmatrix} 0 & 0 & 0 & -\frac{1}{4} \\ 0 & 0 & 0 & 0 \\ 0 & 0 & -\frac{g^{\mu\nu}}{2} & 0 \\ -\frac{1}{4} & 0 & 0 & \frac{1}{2} \left(\frac{P^2}{f_0^2} - \frac{M_1^2}{2f_0^2} - \frac{M_3^2}{2f_0^2} \right) \end{pmatrix}. \quad (5.67)$$

The NLO potential can be rewritten analogously by using the matrix

$$\hat{V}_{\text{NLO}}(\nu, \tilde{\nu}, \mu, \tilde{\mu}) = -f_0^2 \begin{pmatrix} A_1 & 0 & \frac{P^\mu A_1}{f_0} & \frac{A_1(M_3^2 - P^2)}{f_0^2} \\ 0 & -g^{\mu\tilde{\nu}} g^{\tilde{\mu}\nu} (A_1 + A_2) & \frac{P^\nu g^{\mu\tilde{\nu}} (A_1 + A_2)}{f_0} & 0 \\ \frac{P^\nu A_1}{f_0} & \frac{P^\mu g^{\tilde{\mu}\nu} (A_1 + A_2)}{f_0} & \frac{4(2C_{24}c_2 + C_{35}c_3)g^{\mu\nu} - P^\mu P^\nu A_2}{f_0^2} & \frac{P^\nu A_1 (M_3^2 - P^2)}{f_0^3} \\ \frac{A_1(M_1^2 - P^2)}{f_0^2} & 0 & \frac{P^\mu A_1 (M_1^2 - P^2)}{f_0^3} & \frac{8C_0c_0 - 4C_1c_1 + A_1(P^2 - M_1^2)(P^2 - M_3^2)}{f_0^4} \end{pmatrix}, \quad (5.68)$$

where we have used the abbreviations $A_1 = -\frac{4}{m_P^2}(2c_4C_{24} + c_5C_{35} + c_6C_6)$ and $A_2 = \frac{8}{m_P^2}(2c_4C_{24} + c_5C_{35})$.

With previous definitions, the NNLO loop diagram of Eq. (5.7) reads

$$\begin{aligned}
&= B(q, \nu, \tilde{\nu})^T \cdot \hat{V}_{\text{LO}}(\nu, \tilde{\nu}, \rho, \tilde{\rho}) \cdot \hat{G}(\rho, \tilde{\rho}, \sigma, \tilde{\sigma}) \cdot \hat{V}_{\text{LO}}(\sigma, \tilde{\sigma}, \mu, \tilde{\mu}) \cdot B(Q, \mu, \tilde{\mu}) \\
&\equiv B(q)^T \cdot \hat{V}_{\text{LO}} \cdot \hat{G} \cdot \hat{V}_{\text{LO}} \cdot B(Q), \quad (5.69)
\end{aligned}$$

where we have defined the loop function as

$$\begin{aligned} \hat{G}(\nu, \tilde{\nu}, \mu, \tilde{\mu}) &\equiv i \int \frac{d^n \tilde{Q}}{(2\pi)^n} \frac{1}{[(P + \tilde{Q})^2 - m^2]} \frac{1}{(\tilde{Q}^2 - M^2)} B(\tilde{Q}, \nu, \tilde{\nu}) \cdot B(\tilde{Q}, \mu, \tilde{\mu})^T \\ &= \begin{pmatrix} G^{1,1}(s) & G_{\mu\tilde{\mu}}^{1,2}(s) & 0 & G^{1,4}(s) \\ G_{\nu\tilde{\nu}}^{1,2}(s) & G_{\nu\tilde{\nu}\mu\tilde{\mu}}^{2,2}(s) & G_{\nu\tilde{\nu}\mu}^{2,3}(s) & G_{\nu\tilde{\nu}}^{2,4}(s) \\ 0 & G_{\nu\mu\tilde{\mu}}^{2,3}(s) & G_{\nu\mu}^{3,3}(s) & G_{\nu}^{3,4}(s) \\ G^{1,4}(s) & G_{\mu\tilde{\mu}}^{2,4}(s) & G_{\mu}^{3,4}(s) & G^{4,4}(s) \end{pmatrix}, \end{aligned} \quad (5.70)$$

with the Functions $G(s = P^2)$ listed in Appendix A.1, Eq. (A.3) to (A.5). In the last step we have introduced a brief notation, keeping in mind that a summation over Lorentz indices is implicit.

An arbitrary diagram generated by the BS equation is simply calculated as

$$B(q)^T \cdot \hat{V}_{(N)LO} \cdot \hat{G} \cdot \hat{V}_{(N)LO} \cdot \hat{G} \cdot \dots \cdot \hat{V}_{(N)LO} \cdot B(Q). \quad (5.71)$$

For instance, the loop integral of Eq.(5.7) reads

$$\begin{aligned} B(q, \nu, \tilde{\nu})^T \cdot \hat{V}_{LO,NLO}(\nu, \tilde{\nu}, \rho, \tilde{\rho}) \cdot \hat{G}(\rho, \tilde{\rho}, \sigma, \tilde{\sigma}) \cdot \hat{T}(\sigma, \tilde{\sigma}, \mu, \tilde{\mu}) \cdot B(Q, \mu, \tilde{\mu}) \\ \equiv B(q)^T \cdot \hat{V}_{LO,NLO} \cdot \hat{G} \cdot \hat{T} \cdot B(Q). \end{aligned} \quad (5.72)$$

The complete BS equation becomes

$$B(q)^T \cdot \hat{T} \cdot B(Q) = B(q)^T \cdot (\hat{V} + \hat{V} \cdot \hat{G} \cdot \hat{T}) \cdot B(Q), \quad (5.73)$$

with $\hat{V} = V_{LO} + V_{NLO}$. As Ansatz for the scattering amplitude \hat{T} we use

$$\begin{aligned} \hat{T}(\nu, \nu', \mu, \mu') &\equiv \\ &\begin{pmatrix} t_{11} & g^{\mu\mu'} t_{12a} + P^\mu P^{\mu'} t_{12b} & P^\mu t_{13} & t_{14} \\ g^{\nu\nu'} t_{21a} + P^\nu P^{\nu'} t_{21b} & P^\mu P^\nu P^{\mu'} P^{\nu'} t_{22a} + A^{\nu\nu'\mu\mu'} + C^{\nu\nu'\mu\mu'} & P^\mu P^\nu P^{\nu'} t_{23a} + B_{23}^{\mu\nu\nu'} & P^\nu P^{\nu'} t_{24a} + g^{\nu\nu'} t_{24b} \\ P^\nu t_{31} & P^\mu P^\nu P^{\mu'} t_{32a} + B_{32}^{\nu\mu\mu'} & g^{\mu\nu} t_{33a} + P^\mu P^\nu t_{33b} & P^\nu t_{34} \\ t_{41} & P^\mu P^{\mu'} t_{42a} + g^{\mu\mu'} t_{42b} & P^\mu t_{43} & t_{44} \end{pmatrix}, \end{aligned} \quad (5.74)$$

with the abbreviations

$$\begin{aligned}
C^{\nu\nu'\mu\mu'} &= g^{\mu\mu'} g^{\nu\nu'} t_{22b} + g^{\nu\mu'} g^{\nu'\mu} t_{22c} + g^{\nu\mu} g^{\nu'\mu'} t_{22d} \\
B_{23}^{\mu\nu\nu'} &= P^{\nu'} g^{\nu\mu} t_{23b} + P^\nu g^{\nu'\mu} t_{23c} + P^\mu g^{\nu\nu'} t_{23d} \\
B_{32}^{\nu\mu\mu'} &= P^{\mu'} g^{\nu\mu} t_{32b} + P^\nu g^{\mu'\mu} t_{32c} + P^\mu g^{\nu\mu'} t_{32d} \\
A^{\nu\nu'\mu\mu'} &= P^{\mu'} P^{\nu'} g^{\nu\mu} t_{22e} + P^\nu P^{\nu'} g^{\mu\mu'} t_{22f} + P^\nu P^{\mu'} g^{\nu'\mu} t_{22g} \\
&\quad + P^\mu P^{\nu'} g^{\nu\mu'} t_{22h} + P^\mu P^{\mu'} g^{\nu\nu'} t_{22i} + P^\mu P^\nu g^{\nu'\mu'} t_{22j}.
\end{aligned} \tag{5.75}$$

We have introduced a set of functions t_i that depend on the total momentum squared s . These functions have to be determined by solving the set of linear equations

$$\hat{T} = \hat{V} + \hat{V} \cdot \hat{G} \cdot \hat{T}. \tag{5.76}$$

As previously, the whole calculation can be simply extended to include coupled channels effects by increasing the dimension of the matrices. The form of Eq. (5.73) makes obvious that the solutions of the BS equation, Eq. (5.7), still correspond to a geometric series, even if off-shell effects are taken into account. Explicitly, the matrix \hat{T} becomes

$$\hat{T} = (\mathbf{1} - \hat{V} \cdot \hat{G})^{-1} \cdot \hat{V}. \tag{5.77}$$

Some comments are in order: first, the potentials Eq. (5.67) and (5.68) could have been also written as a 3×3 matrix. This can be achieved by using the metric tensors $g^{\mu\tilde{\mu}}$ ($g^{\nu\tilde{\nu}}$) in the definition of $\hat{V}_{\text{LO,NLO}}$. Then the two vectors $(q + P)^\mu$ and $(q + P)^{\tilde{\mu}}$, $((Q + P)^\nu$ and $(Q + P)^{\tilde{\nu}}$), entering Eq. (5.66), are contracted with each other and Lorentz structures like q^2 (Q^2) can be created. Hence, the first component of the vector Eq. (5.66) is no longer necessary. Performing this way, however, requires care in factorizing the potential from the loop function (this should be done consistently in D dimensions!). Secondly, our summation does not exactly correspond to the result obtained in dimensional regularization, i.e. we insert the T matrix in four space-time (not D) dimensions into the BS equation. This subtlety plays only a role for the contributions originating from the c_4 , c_5 and c_6 terms in the NLO potential. As a last comment: usually one solves the BS equation for potentials with off-shellness by some specific ansatz. Due to the previous subtleties in the dimensional regularization of the loop integral, this can lead to a loss of time-reversal invariance. This happens only for the iteration of the c_4 , c_5 and c_6 terms. All similar approaches listed so far circumvent this issue by either stopping at sufficiently low order, or not relying on dimensional regularization. Our approach, on the other hand, keeps time reversal invariance. This is an advantage of performing the resummation explicitly by iterating matrices.

Concerning the computation of the loop function, a few words are in order. Relativistic loop functions involving a heavy particle, whose mass does not vanish in the chiral limit, contain power-counting-breaking (PCB) term, as already encountered numerous times in this theses. In the one-baryon sector, various approaches have been proposed to remove PCB terms, such as the heavy-baryon formulation [153], the infrared formulation [154], and the extended-on-mass-shell approach [59] (see, Ref. [110] for a short review for their respective advantages and limitations). Traditionally, in the UChPT with the on-shell approximation, no attention is paid

to this particular fact since the effects of the PCB terms are effectively absorbed by the so-called subtraction constants (for a recent discussion see [152]). In the studies taking into account the off-shellness of the chiral potentials, the heavy-baryon formalism is adopted in Refs. [145, 146], the infrared formulation in Ref. [147], and an approach similar in spirit to the EOMS formulation was adopted in Ref. [148–150]. One should note that, however, because of the loss of exact crossing symmetry in principle one cannot remove the PCB terms by a redefinition of the available LECs at the working order in the UChPT. Therefore, all the three formulations, the HB, the IR, and the EOMS, should be viewed only as an ansatz to calculate the loop function.

In the present work, in order to compare with the results of the on-shell approximation, we calculate the loop function in the modified minimal subtraction ($\overline{\text{MS}}$) scheme as for the on-shell approximation [152]. Furthermore, we set the regularization scale at 1 GeV and add one single subtraction constant to the one-loop scalar 1-point and 2-point functions for all the channels, i.e., replacing $\log(\mu^2)$ by $\log(\mu^2) + a$. As we will see later, the limited LQCD data do not allow us to adopt more sophisticated subtraction schemes such as those of Refs. [145, 146] and Refs. [149, 150], though they do have certain appealing features.

In the following, we want to elaborate on the renormalization of the loop function in more detail. We define the renormalized loop matrix as $\hat{G}_r = \hat{G} - \hat{R}_{\text{Div}}$. The matrix \hat{R}_{Div} absorbs all divergent parts and is defined as

$$\hat{R}_{\text{Div}} = \begin{pmatrix} -\frac{m^2 R(m^2 + 2M\Delta(s))}{16\pi^2 f_0^4} & -\frac{m^4 R g_{\mu\bar{\mu}}}{64\pi^2 f_0^4} & 0 & -\frac{m^2 R}{16\pi^2 f_0^2} \\ -\frac{m^4 R g_{\nu\bar{\nu}}}{64\pi^2 f_0^4} & \hat{R}^{2,2}_{\nu\bar{\nu}\mu\bar{\mu}} & \hat{R}^{2,3}_{\nu\bar{\nu}\bar{\mu}} & \hat{R}^{2,4}_{\nu\bar{\nu}} \\ 0 & \hat{R}^{2,3}_{\nu\mu\bar{\mu}} & -\frac{R(4P_\mu P_\nu + g_{\mu\nu}(-M^2 - 2\Delta(s)M + 3(m^2 + M^2)))}{192\pi^2 f_0^2} & -\frac{R P_\nu}{32\pi^2 f_0} \\ -\frac{m^2 R}{16\pi^2 f_0^2} & \hat{R}^{2,4}_{\mu\bar{\mu}} & -\frac{R P_\mu}{32\pi^2 f_0} & -\frac{R}{16\pi^2} \end{pmatrix}, \quad (5.78)$$

where

$$\begin{aligned} \hat{R}^{2,2}_{\nu\bar{\nu}\mu\bar{\mu}} &= -\frac{R}{1920\pi^2 f_0^4} (5m^2 + 12M^2 - 6M\Delta(s)) f_{\nu\bar{\nu}\mu\bar{\mu}} - \frac{R P_\mu P_\nu P_{\bar{\mu}} P_{\bar{\nu}}}{80\pi^2 f_0^4} \\ &\quad - \frac{R}{3840\pi^2 f_0^4} (10m^4 + 2M\Delta(s)(-5m^2 - 3M^2 + 2M\Delta(s)) + 5m^2 M^2 + 6M^4) g_{\nu\bar{\nu}\mu\bar{\mu}}, \\ \hat{R}^{2,3}_{\nu\bar{\nu}\mu\bar{\mu}} &= \frac{R(-2m^2 - 3M^2 + 2M\Delta(s))(P_{\bar{\nu}} g_{\nu\mu} + P_\nu g_{\bar{\nu}\mu} + P_\mu g_{\nu\bar{\nu}})}{384\pi^2 f_0^3} - \frac{R P_\mu P_\nu P_{\bar{\nu}}}{64\pi^2 f_0^3}, \\ \hat{R}^{2,4}_{\nu\bar{\nu}} &= -\frac{R(g_{\nu\bar{\nu}}(3(m^2 + M^2) - M^2 - 2M\Delta(s)) + 4P_\nu P_{\bar{\nu}})}{192\pi^2 f_0^2}, \end{aligned} \quad (5.79)$$

where $R = \frac{2}{n-4} - [\log(4\pi) + \Gamma'(1)]$ and $\Delta(s) = (s - M^2)/(2M)$, and $f_{\nu\bar{\nu}\mu\bar{\mu}}$ is given in Appendix A.1. From the statements drawn in Appendix A.3, we deduce that these subtractions are equivalent to using the renormalized potential

$$\hat{V}_r = \hat{V} + \hat{V} \cdot [(1 + \hat{R}_{\text{Div}} \cdot \hat{V})^{-1} - 1], \quad (5.80)$$

instead of \hat{V} in the BS equation (5.73). We note that the absorption of divergent terms requires LECs of arbitrary high order. Hence we are not able to render the BS equation finite by redefining the available LECs on the level

of the Lagrangian. Considering the different strangeness and isospin channels simultaneously shows that it is even impossible to absorb the divergence of the single NNLO diagram (5.69) by adding the NLO tree level. This problem reflects the missing crossing symmetry in solutions of the BS equation.

Similarly we can construct a matrix $\hat{R}_{\text{PCB}}^{(0)}$ as

$$\hat{R}_{\text{PCB}}^{(0)} \equiv \begin{pmatrix} 0 & 0 & 0 & 0 \\ 0 & C_{\nu\bar{\nu}\mu\bar{\mu}} & \frac{D_{\nu\bar{\nu}\mu} (1-2L)m_{D,0}^2 + 2(3-2L)P_\mu P_\nu P_{\bar{\nu}}}{256\pi^2 f_0^3} & \frac{(1-3L)g_{\nu\bar{\nu}} m_{D,0}^2 + 2(4-3L)P_\nu P_{\bar{\nu}}}{288\pi^2 f_0^2} \\ 0 & \frac{D_{\nu\mu\bar{\mu}} (1-2L)m_{D,0}^2 + 2(3-2L)P_\mu P_\nu P_{\bar{\mu}}}{256\pi^2 f_0^3} & \frac{(1-3L)g_{\mu\nu} m_{D,0}^2 + 2(4-3L)P_\mu P_\nu}{288\pi^2 f_0^2} & -\frac{(L-1)P_\nu}{32\pi^2 f_0} \\ 0 & \frac{(1-3L)g_{\mu\bar{\mu}} m_{D,0}^2 + 2(4-3L)P_\mu P_{\bar{\mu}}}{288\pi^2 f_0^2} & -\frac{(L-1)P_\mu}{32\pi^2 f_0} & -\frac{L}{16\pi^2} \end{pmatrix} \quad (5.81)$$

with

$$C_{\nu\bar{\nu}\mu\bar{\mu}} = \frac{g_{\nu\bar{\nu}\mu\bar{\mu}} (1-10L)m_{D,0}^4 + 8f_{\nu\bar{\nu}\mu\bar{\mu}} (3-5L)m_{D,0}^2 + 16(8-5L)P_\mu P_\nu P_{\bar{\mu}} P_{\bar{\nu}}}{6400\pi^2 f_0^4}, \quad (5.82)$$

where we have used the abbreviation $L = 2 + \log(\mu^2/m_{D,0}^2)$. Removing this matrix from the loop matrix is sufficient to eliminate all NLO contributions originating from PCB terms, even if it is not sufficient to render the diagrams of it correct chiral order. Practically we do not perform any subtraction of PCB terms since this can not be done by a redefinition of LECs and hence might cause potentially inconsistencies. However, from this explicit form we can draw some conclusions. We argue in the following that the constants c_0 and c_1 are not renormalized by PCB terms. Hence we can use their values determined in perturbation theory, c.f. Subsection 5.3.

We note that c_0 and c_1 are not renormalized by PCB terms if all of them have a structure different from the NLO tree levels provided by c_0 and c_1 . Hence, since c_0 and c_1 always multiply the squared of the Nambu-Goldstone boson mass m , we have to show that all NLO PCB terms are independent of m . The relevant PCB term can be written in the form

$$B(q)^T \cdot \hat{V}_{\text{LO}} \cdot \hat{R}_{\text{PCB}}^{(0)} \cdot \hat{V}_{\text{LO}} \cdot \hat{R}_{\text{PCB}}^{(0)} \cdot \dots \cdot \hat{V}_{\text{LO}} \cdot B(Q). \quad (5.83)$$

where only the dominant PCB term $\hat{R}_{\text{PCB}}^{(0)}$ is inserted, which is independent of m . One should notice that these terms contain also contribution of order higher than NLO. Since we are only interested in the NLO part of Eq. (5.83), we take the limit $M_1 = M_2 = M$. In this case the Nambu-Goldstone boson mass m appears only explicitly with the coefficients c_0 and c_1 in \hat{V}_{NLO} . However, every term Eq. (5.83) that depends on c_0 or c_1 does not create any PCB terms at NLO¹⁴. Hence, Eq. (5.83) is independent of m at NLO. Since the EOMS renormalization procedure can also be applied without taking the momenta on the mass shell, we can deduce

¹⁴This is very natural since the c_0 and c_1 terms in the potential are momentum independent.

TABLE 5.11: Low-energy constants, the subtraction constants, and the $\chi^2/\text{d.o.f.}$ from the best fits to the LQCD data [12] in the off-shell UChPT.

	a	c_2	c_3	c_4	c_5	$\chi^2/\text{d.o.f.}$
LO	-0.452(11)					17.9
NLO	0.639(131)	0.382(181)	0.653(345)	0.597(92)	-2.084(276)	0.79

TABLE 5.12: Pole positions $\sqrt{s} = M - i\frac{\Gamma}{2}$ (in units of MeV) of charm mesons dynamically generated in the LO UChPT taking into account off-shell effects in the potential. The * indicates the mass that is used as an input to fix the subtraction constant, $a(1 \text{ GeV}) = -0.61$. The numbers are obtained by adopting the isospin averaged decay constant $F_0 = 1.15 f_0$.

(S,I)	$J^P = 0^+$
(1,0)	2318*
(0,1/2)	2155 - i 122

that c_0 and c_1 are not renormalized by PCB terms.

5.5.2 Results and discussions

First, we adjust $a(\mu)$ such that the LO resummation reproduces the mass of the $D_{s0}^*(2317)$ state in the $(S = -1, I = 0)$, $D\bar{K} \rightarrow D\bar{K}$ channel, as done previously in Section 5.4. This requires a subtraction constant $a(1 \text{ GeV}) = -0.49$ for $f_0 = 92.21 \text{ MeV}$ and $a(1 \text{ GeV}) = -0.61$ for the isospin averaged $F_0 = 1.15 f_0$, c.f. Subsection 5.4.2. Interestingly the dominant part in $B_0 = 2 + \log(\frac{\mu^2}{m_{D,0}^2}) + a(\mu) + \mathcal{O}(1/m_{D,0})$, the PCB term, is automatically rendered small for those scales. The peak positions for adopting F_0 are summarized in Table 5.12.

The pion-mass dependences of scattering lengths can be predicted as previously in Subsection 5.4.2. They are shown in Figure 5.9 and 5.10 by the solid and dashed red lines, corresponding to the f_0 and the $F_0 = 1.15 f_0$ scenario, respectively. As has been pointed out in Section 5.4, the LO resummation of the on-shell potential (5.40) partially contradicts the recent lattice computations [12]. For $a_{D_s\pi}^{(S,I)=(1,1)}$ we did observe a stronger dependence on the pion mass than indicated by data. In this approach the dependence is much weaker and hence in better accordance with [12]. Significant deviations are only observed for very large pion masses, $> 500 \text{ MeV}$, where the systematic errors of our approach are out of control. Also no agreement was observed previously for $a_{D\bar{K}}^{(S,I)=(-1,0)}$, c.f. Figure 5.9, where a pretty large scattering length was predicted. In the approach described here, however, the curve is in excellent agreement to the data [12].

Now we proceed to LO/NLO fits of the data [12]. We fix c_0 and c_1 as in Section 5.4 and are left with five LECs to be determined, c_2, c_3, c_4, c_5 and the subtraction constant a . As previously the pseudoscalar decay constant f_0 is fixed to that of the pion, 92.21 MeV [1], unless otherwise stated.

Fitting these unknown LECs to the lightest 15 LQCD data, we obtain the results shown in Fig. 5.15, with the corresponding LECs tabulated in Table 5.11. At LO the $\chi^2/\text{d.o.f.}$ is rather poor, indicating the failure of a quantitative description of the LQCD data. On the other hand, if one would use the $SU(3)$ isospin averaged pseudoscalar decay constant $F_0 = 1.15 f_0$ instead of f_0 , reduces the $\chi^2/\text{d.o.f.}$ to about 5. At NLO, we obtain a

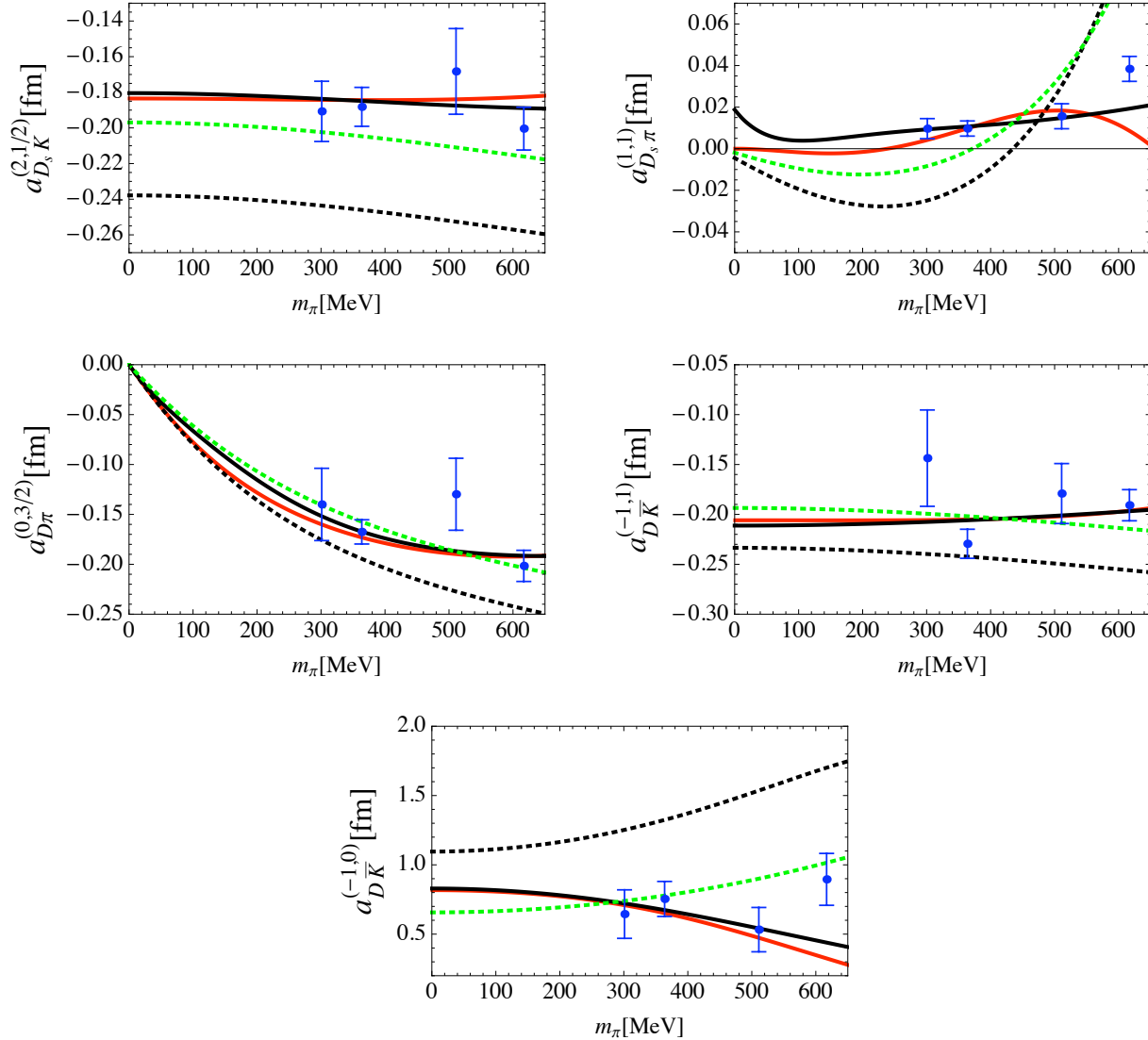


FIGURE 5.15: The $n_f = 2 + 1$ LQCD data [12] are shown by the red points. The black solid and red solid lines show the NLO off-shell and on-shell UChPT fits. The black dashed and green dashed lines are the LO off-shell UChPT fits for $f_0 = 92.21$ MeV and $f_0 = 106.04$ MeV, respectively.

$\chi^2/\text{d.o.f.} = 0.79$, which should be compared to that obtained in the on-shell approximation, $\chi^2/\text{d.o.f.} = 1.23$, Section 5.4.¹⁵

Clearly, the off-shell effects seem to improve significantly the description of the LQCD data of Ref. [12]. This result should not be seen as a total surprise. In Refs. [122, 123], it was pointed out that the off-shell effects, which appear through diagrams renormalizing the vertices, the propagators, etc., can be absorbed by the available LECs and physical masses. Of course, such “renormalizations” are only possible at the physical point, which are the main interest of the majority of the studies performed in the UChPT so far. To study the light-

¹⁵It should be mentioned that one could still obtain a $\chi^2/\text{d.o.f.} \approx 0.89$ fitting the whole 20 LQCD data points in the off-shell approach.

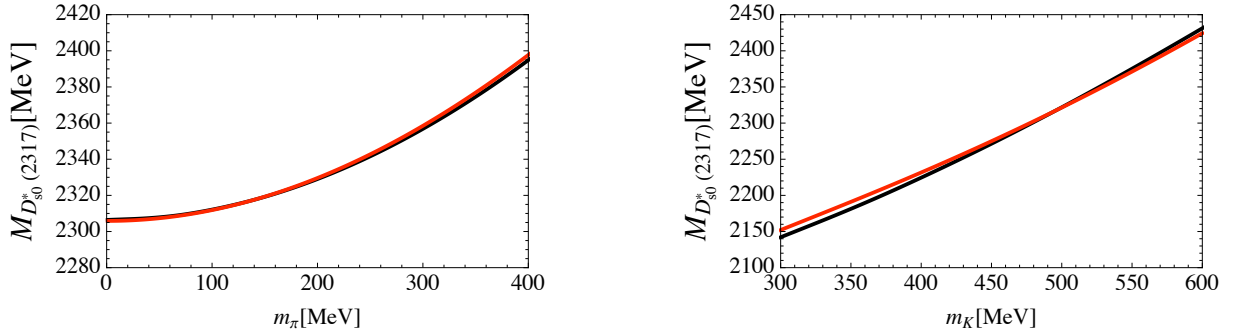


FIGURE 5.16: Pion and kaon mass evolution of the pole positions of the $D_{s0}^*(2317)$. The black and Red solid lines are assigned as in Figure 5.15, while the off-shell results have been shifted to agree with the on-shell results at the physical point.

quark mass evolution of physical observables, one may wish to explicitly keep all the off-shell effects [151]. Our results show that this may indeed improve the description of the light-quark mass dependence. Nevertheless, more studies are needed, before a firm conclusion can be reached.

The LQCD simulations of Ref. [12] did not include the channel where the $D_{s0}^*(2317)$ appears. The studies in Ref. [12] and Section 5.4 show that a fit to the LQCD data yields naturally the $D_{s0}^*(2317)$. It will be interesting to check whether this still holds in the present formalism. Searching for a pole in the complex \sqrt{s} plane, we find a bound state at $\sqrt{s} = 2295$ MeV, which is not so far away from the $D_{s0}^*(2317)$ pole position in the on-shell approach, $\sqrt{s} = 2317$ MeV. The discrepancy of about 22 MeV provides another indicator on the magnitude of the off-shell effects.

In Fig. 5.16 we show the pion mass and kaon mass evolution of the $D_{s0}^*(2317)$. To facilitate the comparison, we have shifted the off-shell results so that the on-shell and off-shell results agree at the physical point. The figure in the left panel is obtained by fixing the strange quark mass to its physical value using LO ChPT, while the figure in the right panel is obtained by fixing the pion mass to its physical value. The dependences of the D and D_s masses on the pion and kaon masses are provided by the NLO ChPT as in Subsection 5.3.1. It is clear that for the light-quark mass evolution of the $D_{s0}^*(2317)$ pole position there is no appreciable difference between the on-shell and off-shell UChPT.

Chapter 6

Summary and conclusions

Lattice QCD computations have made remarkable progress in recent years. Nowadays, they offer an accurate method to calculate a variety of physical quantities governed by non-perturbative strong interaction physics. For “gold plated” quantities, such as the decay constants studied in this work, the overall uncertainties have been reduced to a few percent. Obviously, chiral perturbation theory plays an important role in understanding some of the systematic errors, such as those from finite volume and extrapolations of the light quark masses to their physical values.

In the first part of this theses we have investigated the light-quark mass dependence of the HPQCD lattice QCD data [25] for the decay constants f_D and f_{D_s} . This is done in the framework of covariant chiral perturbation theory (ChPT). This analysis reveals that the covariant ChPT describes the HPQCD extrapolations considerably better than the standard heavy meson ChPT at a given order, although both approaches show improvement when going from next-to-leading to next-to-next-to leading order. Our studies show that if the lattice simulations are performed with relatively large light quark masses (e.g., $m_\pi > 300$ MeV), a covariant formulation of ChPT is a better choice for chiral extrapolations, particularly at low chiral orders.

On the other hand, precise lattice data are valuable to fix some of the low energy constants of our theory. These constants can be used to predict physical observables involving the same low-energy-constants, or constants that are related by symmetries. In the present work, we give predictions for the ratios of f_{B_s}/f_B , $f_{D_s^*}/f_{D^*}$, and $f_{B_s^*}/f_{B^*}$ and their light-quark mass dependencies, where the low-energy-constants have been determined by employing the lattice QCD data of Ref. [25]. These predictions should be testable in the near future. Our results show that the relations $f_{B_s}/f_B > f_{D_s}/f_D$ and $f_{D_s^*}/f_{D^*} < f_{D_s}/f_D$ should hold in a large portion of the allowed parameter space.

The second part of this theses, starting from Chapter 5, has investigated the interactions of the heavy-light mesons (D , D^* , B , B^* and their strange counterparts) with Nambu-Goldstone bosons (the octet of the lightest pseudoscalar mesons). These interactions have been iterated by a unitarization procedure, i.e. solving a Bethe-Salpeter equation, which has the appealing feature that various higher-lying charm/bottom states can be studied. In order to fix the relevant low-energy constant up to next-to-leading order we have fitted the latest fully dynamical lattice QCD simulations for the scattering lengths of Nambu-Goldstone bosons off D mesons of Ref. [12]. As in the first part of this theses we have relied on the covariant formulation of chiral

perturbation theory. This calculation shows, as previously for the study of the decay constants f_D and f_{D_s} , that the covariant (unitarized) ChPT describes the lattice QCD data better than its non-relativistic (heavy-meson) counterpart. In addition, we show that the $D_{s0}^*(2317)$ can be dynamically generated without a priori assumption of its existence, where the predicted mass is in excellent agreement with experiment. This success indicates that the nearby DK threshold can not be neglected in terms of naive constituent quark models.

To employ the determined low-energy constants in other sectors of heavy-light mesons, D^* , B and B^* , we have proposed a new subtraction scheme to ensure that the loop function appearing in the Bethe-Salpeter equation satisfies the chiral power counting rule and has a well defined behavior in the limit of infinite heavy quark mass. It has been shown that this scheme has a similar $1/M_{\text{HL}}$ scaling as the heavy-meson ChPT loop function, but provides a better description of the light-quark mass dependence of the lattice QCD scattering lengths. With such a scheme, we have predicted the counterparts of the $D_{s0}^*(2317)$ in the $J^P = 1^+$ sector and in the bottom sector. The experimental confirmation of the dynamically generated states in the bottom sector can serve as a stringent test of our theoretical model and the interpretation of the $D_{s0}^*(2317)$ as a dynamically generated state from the strong DK interaction.

Apart from the successes of such a unitarization procedure, its range of applicability is very limited. States more distant to the lowest lying threshold are usually not reproduced to good accuracy. These apparent problems motivated us to test the validity of a simplification usually employed in the unitarization procedure. This is the use of potentials taken on the mass shell. This widely accepted approximation is understood to be legitimate, since all effects coming from the off-shellness of the potential should be absorbable into the low-energy constants of the theory, even if these constants enter at arbitrarily high order. This is a highly nontrivial statement since the results produced by unitarization do no longer respect crossing symmetry. A consequence of this is the loss of renormalizability, even at a given chiral order.

In the end of Chapter 5 we have solved the Bethe-Salpeter equation in unitary chiral perturbation theory by taking into account the full off-shellness of the chiral potentials up to next-to-leading order. To quantify the magnitude and impact of the off-shell effects, we have studied the light-quark mass dependence of the scattering lengths of the Nambu-Goldstone bosons off the D mesons from Ref. [12]. In comparison with the widely used on-shell approximation, we have shown that taking into account off-shell effects can indeed improve the description of the lattice QCD data, in terms of light-quark mass evolution. On the other hand, both descriptions look qualitatively similar, at least for the observables we studied. Therefore, unless the lattice QCD data becomes more precise, the on-shell approximation may still be confidently used, given its simplicity. On the other hand we have shown that predictions obtained by employing only the leading order potential can significantly differ within these two approaches, as demonstrated in Section 5.4. There we have observed that the results taking into account the full off-shellness of the potential are clearly favored by the lattice QCD data. So far, even if we can not yet draw a final statement concerning the quality of the on-shell approximation, our procedure can be seen as a step towards improving the standard unitarization techniques.

Chapter 7

Acknowledgements

Finally, I want to thank a number of people that contributed significantly to this theses

- Prof. Dr. Wolfram Weise for giving me the opportunity to write this theses in his group T39, and for numerous discussions and constructive feedback over the last few years.
- Prof. Dr. Lisheng Geng for the fruitful collaboration. I want to thank him for his active contributions, his numerous ideas and the verification of most parts of the present work.
- Prof. Dr. Norbert Kaiser for enlightening discussions.
- all members of T39 for the very nice working atmosphere. I also want to thank a number of former members of T39: Maximilian Duell, Salvatore Fiorilla, Thomas Hell and Alexander Laschka.
- and last but not least my family for supporting me over all the years.

For the financial support, I would like to thank the German Bundesministerium für Bildung und Forschung (BMBF), the DFG Cluster of Excellence “Origin and Structure of the Universe”, and the Sino-German CRC 110 “Symmetries and Emergence of Structure in QCD” by DFG and NSFC.

Appendix A

Appendix

A.1 Loop functions

The functions A_0 and B_0 appearing in the calculation of the D and D_s meson decay constants are defined as:

$$A_0(m^2) = -\frac{1}{16\pi^2} m^2 \log\left(\frac{\mu^2}{m^2}\right), \quad (\text{A.1})$$

$$B_0(p_i^2, m_1^2, m_2^2) = \begin{cases} -\frac{1}{16\pi^2} \left[\log\left(\frac{\mu^2}{m_1^2}\right) - 1 \right] & \text{if } p_i^2 = 0 \text{ and } m_1 = m_2 \\ -\frac{1}{16\pi^2} \left[\frac{m_1^2 \log\left(\frac{\mu^2}{m_1^2}\right) - m_2^2 \log\left(\frac{\mu^2}{m_2^2}\right)}{m_1^2 - m_2^2} \right] & \text{if } p_i^2 = 0 \text{ and } m_1 \neq m_2 \\ -\frac{1}{16\pi^2} \frac{1}{2p_i^2} \left[2p_i^2 \left\{ \log\left(\frac{\mu^2}{m_2^2}\right) + 1 \right\} + (m_2^2 - m_1^2 - p_i^2) \log\left(\frac{m_1^2}{m_2^2}\right) \right. \\ \quad \left. + 2\sqrt{2m_1^2(p_i^2 + m_2^2) - (m_2^2 - p_i^2)^2 - m_1^4} \right. \\ \quad \left. \times \left\{ \tan^{-1}\left(\frac{m_2^2 - m_1^2 - p_i^2}{\sqrt{2m_1^2(p_i^2 + m_2^2) - (m_2^2 - p_i^2)^2 - m_1^4}}\right) - \tan^{-1}\left(\frac{m_2^2 - m_1^2 + p_i^2}{\sqrt{2m_1^2(p_i^2 + m_2^2) - (m_2^2 - p_i^2)^2 - m_1^4}}\right) \right\} \right] \end{cases} \quad (\text{A.2})$$

Unless otherwise specified, the regularization scale μ is set at 1 GeV.

The loop function of Eq. (5.70) is given in terms of $\bar{A}_0 = (-16\pi^2)A_0$ and $\bar{B}_0 = (-16\pi^2)B_0$, where the one- and two-point functions are regularized by the standard $\overline{\text{MS}}$ prescription. Therefore, the definitions A.1 and A.2 have to be used with the replacement $\log(\mu^2) \rightarrow \log(\mu^2) + 1$.

$$\begin{aligned}
G^{1,1}(s) &= -\frac{\bar{A}_0(m^2)(m^2 - M^2 + s)}{16\pi^2 f_0^4} \\
G_{\mu\bar{\mu}}^{1,2}(s) &= -\frac{g_{\mu\bar{\mu}}}{128\pi^2 f_0^4} (2m^2 \bar{A}_0(m^2) + m^4) \\
G^{1,4}(s) &= -\frac{\bar{A}_0(m^2)}{16\pi^2 f_0^2} \\
G_{\nu\bar{\nu}\mu}^{2,3}(s) &= \frac{P_\mu P_\nu P_{\bar{\nu}}}{384\pi^2 f_0^3 s^3} \left\{ -6(m^2 - M^2 + s) \left[(m^2 - M^2)^2 - 2M^2 s + s^2 \right] \bar{B}_0(s, M^2, m^2) \right. \\
&\quad - 6\bar{A}_0(M^2) \left[s(2m^2 - 3M^2) + (m^2 - M^2)^2 + 3s^2 \right] \\
&\quad + 6\bar{A}_0(m^2) \left[m^4 + m^2(s - 2M^2) + (M^2 - s)^2 \right] \\
&\quad \left. + s(3m^4 + 4m^2 s - 3M^4 + 8M^2 s - 2s^2) \right\} \\
&\quad + \frac{P_{\bar{\nu}} g_{\nu\mu} + P_\nu g_{\bar{\nu}\mu} + P_\mu g_{\nu\bar{\nu}}}{2304\pi^2 f_0^3 s^2} \left\{ -2s^2 \left[3(m^2 + 3M^2) \bar{B}_0(s, M^2, m^2) + 3\bar{A}_0(m^2) \right. \right. \\
&\quad \left. \left. + 3\bar{A}_0(M^2) + 4(m^2 + 2M^2) \right] + 6(m - M)^2 (m + M)^2 \left[(m^2 - M^2) \bar{B}_0(s, M^2, m^2) \right. \right. \\
&\quad \left. \left. - \bar{A}_0(m^2) + \bar{A}_0(M^2) \right] - 3s \left[2(m^4 + 2m^2 M^2 - 3M^4) \bar{B}_0(s, M^2, m^2) \right. \right. \\
&\quad \left. \left. - 2\bar{A}_0(m^2)(m^2 + 2M^2) + 6M^2 \bar{A}_0(M^2) + m^4 - M^4 \right] \right. \\
&\quad \left. + 2s^3 (3\bar{B}_0(s, M^2, m^2) + 2) \right\} \\
G_{\nu\bar{\nu}\mu}^{3,3}(s) &= G_{\nu\bar{\nu}\mu}^{2,4}(s) = \frac{g_{\nu\mu}}{576\pi^2 f_0^2 s} \left\{ 3 \left(m^4 - 2m^2(M^2 + s) + (M^2 - s)^2 \right) \bar{B}_0(s, M^2, m^2) \right. \\
&\quad - 3\bar{A}_0(m^2)(m^2 - M^2 + s) + 3\bar{A}_0(M^2)(m^2 - M^2 - s) \\
&\quad \left. + 2s(s - 3(m^2 + M^2)) \right\} \\
&\quad - \frac{P_\nu P_\mu}{288\pi^2 f_0^2 s^2} \left\{ 6 \left(m^4 + m^2(s - 2M^2) + (M^2 - s)^2 \right) \bar{B}_0(s, M^2, m^2) \right. \\
&\quad - 6\bar{A}_0(m^2)(m^2 - M^2 + s) + 6\bar{A}_0(M^2)(m^2 - M^2 + 2s) \\
&\quad \left. + s(s - 3(m^2 + M^2)) \right\} \\
G_\nu^{3,4}(s) &= \frac{P^\nu}{32\pi^2 f_0 s} \left\{ -(m^2 - M^2 + s) \bar{B}_0(s, M^2, m^2) + \bar{A}_0(m^2) - \bar{A}_0(M^2) \right\} \\
G^{4,4}(s) &= -\frac{1}{16\pi^2} \bar{B}_0(s, M^2, m^2) \tag{A.3}
\end{aligned}$$

$$\begin{aligned}
G_{\nu\bar{\nu}\mu\bar{\mu}}^{2,2}(s) = & \frac{P_\mu P_{\bar{\mu}} P_\nu P_{\bar{\nu}}}{4800\pi^2 f_0^4 s^4} \left\{ -60 \left[m^8 + m^6 (s - 4M^2) + m^4 (6M^4 - 6M^2 s + s^2) \right. \right. \\
& - m^2 (M^2 - s)^2 (4M^2 - s) + (M^2 - s)^4 \left. \right] \bar{B}_0(s, M^2, m^2) \\
& + 60 \bar{A}_0(m^2) \left(m^4 - 2m^2 M^2 + (M^2 - s)^2 \right) (m^2 - M^2 + s) \\
& - 60 \bar{A}_0(M^2) \left[3s^2 (m^2 - 2M^2) + (m^2 - M^2)^3 + 2s (m^4 - 3m^2 M^2 + 2M^4) + 4s^3 \right] \\
& + s \left[5s^2 (9m^2 + 29M^2) + 30 (m^2 - M^2)^2 (m^2 + M^2) \right. \\
& \left. + 10s (4m^4 + m^2 M^2 - 11M^4) - 29s^3 \right] \left. \right\} \\
& + \frac{g_{\nu\bar{\nu}\mu\bar{\mu}}}{115200\pi^2 f_0^4 s^2} \left\{ -30 \left(m^4 - 2m^2 (M^2 + s) + (M^2 - s)^2 \right)^2 \bar{B}_0(s, M^2, m^2) \right. \\
& + 30 \bar{A}_0(m^2) (m^2 - M^2 + s) \left[m^4 - m^2 (2M^2 + 5s) + (M^2 - s)^2 \right] \\
& - 30 \bar{A}_0(M^2) (m^2 - M^2 - s) \left[m^4 - 2m^2 (M^2 + s) + M^4 - 5M^2 s + s^2 \right] \\
& + s \left[160s^2 (m^2 + M^2) + 15 (m^2 - M^2)^2 (m^2 + M^2) \right. \\
& \left. - 5s (61m^4 + 64m^2 M^2 + 61M^4) - 32s^3 \right] \left. \right\} \\
& + \frac{f_{\nu\bar{\nu}\mu\bar{\mu}}}{57600\pi^2 f_0^4 s^3} \left\{ 30 \left[((m - M)^2 - s) ((m + M)^2 - s) \right. \right. \\
& \times [3m^4 + m^2 (4s - 6M^2) + 3 (M^2 - s)^2] \bar{B}_0(s, M^2, m^2) \\
& - \bar{A}_0(m^2) (m^2 - M^2 + s) \left(3m^4 - m^2 (6M^2 + 5s) + 3 (M^2 - s)^2 \right) \\
& + \bar{A}_0(M^2) \left(-s^2 (m^2 + 18M^2) + 3 (m^2 - M^2)^3 - 3s^3 \right. \\
& \left. \left. + s (m^4 - 13m^2 M^2 + 12M^4) \right) \right] + s \left[-10s^2 (13m^2 + 33M^2) \right. \\
& \left. - 45 (m^2 - M^2)^2 (m^2 + M^2) + 15s (m^4 + 4m^2 M^2 + 11M^4) + 66s^3 \right] \left. \right\}, \tag{A.4}
\end{aligned}$$

with

$$\begin{aligned}
g^{\nu\nu'\mu\mu'} &= g^{\mu\mu'} g^{\nu\nu'} + g^{\nu\mu'} g^{\nu'\mu} + g^{\nu\mu} g^{\nu'\mu'}, \\
f^{\nu\nu'\mu\mu'} &= P^{\mu'} P^{\nu'} g^{\nu\mu} + P^\nu P^{\nu'} g^{\mu\mu'} + P^\nu P^{\mu'} g^{\nu'\mu} \\
&\quad + P^\mu P^{\nu'} g^{\nu\mu'} + P^\mu P^{\mu'} g^{\nu\nu'} + P^\mu P^\nu g^{\nu'\mu'}, \\
D^{\bar{\nu}\nu\mu} &= P^{\bar{\nu}} g^{\nu\mu} + P^\nu g^{\bar{\nu}\mu} + P^\mu g^{\nu\bar{\nu}}. \tag{A.5}
\end{aligned}$$

A.2 Partial wave decomposition for $P^*\phi$ scattering

The amplitude for a pseudoscalar meson ϕ scattering off a vector meson P^* is denoted by

$$T_P^{\mu\nu}(q, Q) = T^{\mu\nu}(P^*(p_1)\phi(p_2) \rightarrow P^*(p_3)\phi(p_4)), \tag{A.6}$$

where the momenta are related by $p_1 = -q$, $p_2 = q + P$, $p_3 = -Q$ and $p_4 = Q + P$. According to we use covariance, parity and time reversal invariance to decompose $\mathcal{T}_P^{\mu\nu}(q, Q)$ into a complete set of Lorentz structures $l_{i,P}^{\mu\nu}$ and scalar functions \mathcal{F}_i :

$$\begin{aligned} \mathcal{T}_P^{\mu\nu}(q, Q) &= \sum_{i=1}^5 l_{i,P}^{\mu\nu}(q, Q) \mathcal{F}_i(q, Q), \\ l_{1,P}^{\mu\nu} &= g^{\mu\nu} - \frac{P^\mu P^\nu}{P^2}, \quad l_{2,P}^{\mu\nu} = \frac{P^\mu P^\nu}{P^2}, \quad l_{3,P}^{\mu\nu} = \frac{P^\mu}{\sqrt{P^2}} \left(Q^\nu - \frac{Q \cdot P}{P^2} P^\nu \right), \\ l_{4,P}^{\mu\nu} &= \left(q^\mu - \frac{q \cdot P}{P^2} P^\mu \right) \frac{P^\nu}{\sqrt{P^2}}, \quad l_{5,P}^{\mu\nu} = \left(q^\mu - \frac{q \cdot P}{P^2} P^\mu \right) \left(Q^\nu - \frac{Q \cdot P}{P^2} P^\nu \right). \end{aligned} \quad (\text{A.7})$$

We now evaluate the helicity matrix elements in the center of mass frame, $P^\mu = (\sqrt{s}, \mathbf{0})$, and relate them to partial wave amplitudes $\langle \bar{\lambda} | T^J | \lambda \rangle$ with fixed total angular momentum J [155]:

$$\epsilon_\mu^\dagger(p_3, \bar{\lambda}) \mathcal{T}_P^{\mu\nu}(q, Q) \epsilon_\nu(p_1, \lambda) = \sum_J (2J+1) \langle \bar{\lambda} | T^J | \lambda \rangle d_{\lambda\bar{\lambda}}^{(J)}(\theta) \quad (\text{A.8})$$

The functions $d_{\lambda\bar{\lambda}}(\theta)$ are the Wigner rotation functions [156], depending on the scattering angle θ . They have a number of properties that simplify calculations considerable [157]: they are orthogonal with respect to the integration over the angle θ

$$\int_{-1}^1 d(\cos \theta) d_{\lambda\bar{\lambda}}^{\bar{J}}(\theta) d_{\lambda\lambda}^J(\theta) = \frac{2}{2J+1} \delta_{\bar{J}J}, \quad (\text{A.9})$$

and the rows and columns form orthonormal vectors

$$\sum_{\lambda=-J}^J d_{\lambda\sigma}^J(\theta) d_{\lambda\rho}^J(\theta) = \delta_{\sigma\rho} \quad \text{and} \quad \sum_{\lambda=-J}^J d_{\sigma\lambda}^J(\theta) d_{\rho\lambda}^J(\theta) = \delta_{\sigma\rho}. \quad (\text{A.10})$$

Further symmetries are found to be

$$d_{\sigma\rho}^J(\theta) = (-1)^{\sigma-\rho} d_{-\sigma-\rho}^J(\theta) = (-1)^{\sigma-\rho} d_{\rho\sigma}^J(\theta) = d_{-\rho-\sigma}^J(\theta). \quad (\text{A.11})$$

To relate the helicity amplitudes to the partial wave amplitudes we choose explicit polarization vectors in the center of mass frame:

$$\epsilon^\mu(p_1, \pm 1) = \begin{pmatrix} 0 \\ \frac{\mp 1}{\sqrt{2}} \\ \frac{-i}{\sqrt{2}} \\ 0 \end{pmatrix}, \quad \epsilon^\mu(p_1, 0) = \begin{pmatrix} \frac{p}{M} \\ 0 \\ 0 \\ \frac{\omega}{M} \end{pmatrix}, \quad \epsilon^\mu(p_3, \pm 1) = \begin{pmatrix} 0 \\ \frac{\mp \cos \theta}{\sqrt{2}} \\ \frac{-i}{\sqrt{2}} \\ \frac{\pm \sin \theta}{\sqrt{2}} \end{pmatrix}, \quad \epsilon^\mu(p_3, 0) = \begin{pmatrix} \frac{\bar{p}}{M} \\ \frac{\bar{\omega} \sin \theta}{M} \\ 0 \\ \frac{\bar{\omega} \cos \theta}{M} \end{pmatrix} \quad (\text{A.12})$$

with $\omega = \sqrt{M^2 + p^2}$ and $\bar{\omega} = \sqrt{M^2 + \bar{p}^2}$, where the abbreviations $p = |\mathbf{p}_1| = |\mathbf{q}|$ and $\bar{p} = |\mathbf{p}_3| = |\mathbf{Q}|$ are used. The corresponding momenta read

$$P^\mu = \begin{pmatrix} \sqrt{s} \\ 0 \\ 0 \\ 0 \end{pmatrix}, \quad p_1^\mu = -q^\mu = \begin{pmatrix} \omega \\ 0 \\ 0 \\ p \end{pmatrix}, \quad p_3^\mu = -Q^\mu = \begin{pmatrix} \bar{\omega} \\ \bar{p} \sin \theta \\ 0 \\ \bar{p} \cos \theta \end{pmatrix}. \quad (\text{A.13})$$

To solve for the different partial wave amplitudes on the right side of equation (A.8) it is convenient to introduce linear combinations ξ_i of helicity amplitudes,

$$\begin{aligned} \xi_1 &= \epsilon_\mu^\dagger(-Q, +1) \mathcal{T}_P^{\mu\nu}(q, Q) \epsilon_\nu(-q, -1) + \epsilon_\mu^\dagger(-Q, -1) \mathcal{T}_P^{\mu\nu}(q, Q) \epsilon_\nu(-q, +1) \\ \xi_2 &= \epsilon_\mu^\dagger(-Q, +1) \mathcal{T}_P^{\mu\nu}(q, Q) \epsilon_\nu(-q, +1) + \epsilon_\mu^\dagger(-Q, -1) \mathcal{T}_P^{\mu\nu}(q, Q) \epsilon_\nu(-q, -1) \\ \xi_3 &= \epsilon_\mu^\dagger(-Q, 0) \mathcal{T}_P^{\mu\nu}(q, Q) \epsilon_\nu(-q, +1) - \epsilon_\mu^\dagger(-Q, 0) \mathcal{T}_P^{\mu\nu}(q, Q) \epsilon_\nu(-q, -1) \\ \xi_4 &= \epsilon_\mu^\dagger(-Q, +1) \mathcal{T}_P^{\mu\nu}(q, Q) \epsilon_\nu(-q, 0) - \epsilon_\mu^\dagger(-Q, -1) \mathcal{T}_P^{\mu\nu}(q, Q) \epsilon_\nu(-q, 0) \\ \xi_5 &= \epsilon_\mu^\dagger(-Q, 0) \mathcal{T}_P^{\mu\nu}(q, Q) \epsilon_\nu(-q, 0). \end{aligned} \quad (\text{A.14})$$

These linear combination can be easily related to the scalar functions $\mathcal{F}_i(s, t(x)) \equiv F_P(q, Q)$,

$$\begin{pmatrix} \xi_1 \\ \xi_2 \\ \xi_3 \\ \xi_4 \\ \xi_5 \end{pmatrix} = \begin{pmatrix} x-1 & 0 & 0 & 0 & -p(x^2-1)\bar{p} \\ -x-1 & 0 & 0 & 0 & p(x^2-1)\bar{p} \\ \frac{\sqrt{2}\bar{\omega}\sin(\theta)}{M} & 0 & -\frac{\sqrt{2}\bar{p}^2\sin(\theta)}{M} & 0 & -\frac{\sqrt{2}px\bar{p}\bar{\omega}\sin(\theta)}{M} \\ -\frac{\sqrt{2}\omega\sin(\theta)}{M} & 0 & 0 & \frac{\sqrt{2}p^2\sin(\theta)}{M} & \frac{\sqrt{2}px\omega\bar{p}\sin(\theta)}{M} \\ -\frac{x\omega\bar{\omega}}{MM} & \frac{p\bar{p}}{MM} & \frac{x\omega\bar{p}^2}{MM} & \frac{p^2x\bar{\omega}}{MM} & \frac{px^2\omega\bar{p}\bar{\omega}}{MM} \end{pmatrix} \begin{pmatrix} \mathcal{F}_1 \\ \mathcal{F}_2 \\ \mathcal{F}_3 \\ \mathcal{F}_4 \\ \mathcal{F}_5 \end{pmatrix}, \quad (\text{A.15})$$

where the abbreviation $x = \cos \theta$ is used. On the other the ξ_i can be expressed in terms of partial wave amplitudes,

$$\begin{pmatrix} \xi_1 \\ \xi_2 \\ \xi_3 \\ \xi_4 \\ \xi_5 \end{pmatrix} = \sum_J (2J+1) \begin{pmatrix} (\langle 1_+ | \mathcal{T}^J | 1_+ \rangle - \langle 1_- | \mathcal{T}^J | 1_- \rangle) d_{-1+1}^J(\theta) \\ (\langle 1_+ | \mathcal{T}^J | 1_+ \rangle + \langle 1_- | \mathcal{T}^J | 1_- \rangle) d_{+1+1}^J(\theta) \\ \sqrt{2} \langle 0 | \mathcal{T}^J | 1_+ \rangle d_{0+1}^J(\theta) \\ \sqrt{2} \langle 1_+ | \mathcal{T}^J | 0 \rangle d_{+10}^J(\theta) \\ \langle 0 | \mathcal{T}^J | 0 \rangle d_{00}^J(\theta) \end{pmatrix}, \quad (\text{A.16})$$

where parity eigenstates $|1_{\pm}\rangle = (|-1\rangle \pm |1\rangle)/\sqrt{2}$ are used. Using the orthogonality relation together with the explicit form of Wigner rotation functions [158],

$$\begin{aligned} d_{00}^J(\theta) &= P_J(\cos\theta), & d_{\pm 10}(\theta) &= \mp \frac{\sin\theta}{\sqrt{J(J+1)}} P_J'(\cos\theta) = -d_{0\pm 1}^J \\ d_{\pm 1\pm 1}^J(\theta) &= \frac{(1 \pm x)(P_J'(x) \mp (1 \mp x)P_J''(x))}{J(J+1)} = \frac{(1 \mp x)P_J'(x) \pm J(J+1)P_J(x)}{J(J+1)} = d_{1\pm 1}^J(\theta) \end{aligned} \quad (\text{A.17})$$

gives immediately access to the partial wave amplitudes

$$\begin{aligned} \mathcal{M}_{JP_-} &\equiv \langle 1_- | \mathcal{T}^J | 1_- \rangle = \frac{1}{4} \int_{-1}^1 d(\cos\theta) (d_{+1+1}^J(\theta)\xi_2(\theta) - d_{-1+1}^J(\theta)\xi_1(\theta)) \\ &= \int_{-1}^1 dx \frac{1}{2} \left(\frac{\bar{p}p(x^2-1)P_J'(x)\mathcal{F}_5(s, t(x))}{J(J+1)} - P_J(x)\mathcal{F}_1(s, t(x)) \right) \\ (\mathcal{M}_{JP_+})_{11} &\equiv \langle 1_+ | \mathcal{T}^J | 1_+ \rangle = \frac{1}{4} \int_{-1}^1 d(\cos\theta) (d_{+1+1}^J(\theta)\xi_2(\theta) + d_{-1+1}^J(\theta)\xi_1(\theta)) \\ &= \int_{-1}^1 dx \frac{1}{2} \left(\frac{(x^2-1)}{J(J+1)} P_J'(x) (\mathcal{F}_1(s, t(x)) - \bar{p}px\mathcal{F}_5(s, t(x))) \right. \\ &\quad \left. + P_J(x) (\bar{p}p(x^2-1)\mathcal{F}_5(s, t(x)) - x\mathcal{F}_1(s, t(x))) \right) \\ (\mathcal{M}_{JP_+})_{12} &\equiv \langle 1_+ | \mathcal{T}^J | 0 \rangle = \frac{1}{2\sqrt{2}} \int_{-1}^1 d(\cos\theta) d_{+10}^J(\theta)\xi_4(\theta) \\ &= \int_{-1}^1 dx \frac{1}{2\sqrt{J(J+1)M}} (1-x^2) P_J'(x) (-\mathcal{F}_1(s, t(x))\omega + \mathcal{F}_4(s, t(x))p^2 + \mathcal{F}_5(s, t(x))p\bar{p}x\omega) \\ (\mathcal{M}_{JP_+})_{21} &\equiv \langle 0 | \mathcal{T}^J | 1_+ \rangle = \frac{1}{2\sqrt{2}} \int_{-1}^1 d(\cos\theta) d_{0+1}^J(\theta)\xi_3(\theta) \\ &= \int_{-1}^1 dx \frac{1}{2\sqrt{J(J+1)M}} (1-x^2) P_J'(x) (-\mathcal{F}_1(s, t(x))\bar{\omega} + \mathcal{F}_3(s, t(x))\bar{p}^2 + \mathcal{F}_5(s, t(x))p\bar{p}x\bar{\omega}) \\ (\mathcal{M}_{JP_+})_{22} &\equiv \langle 0 | \mathcal{T}^J | 0 \rangle = \frac{1}{2} \int_{-1}^1 d(\cos\theta) d_{00}^J(\theta)\xi_5(\theta) \\ &= \int_{-1}^1 dx \frac{1}{2MM} P_J(x) \left\{ x\bar{\omega} (\mathcal{F}_4(s, t(x))p^2 - \mathcal{F}_1(s, t(x))\omega) \right. \\ &\quad \left. + p\bar{p} (\mathcal{F}_5(s, t(x))x^2\omega\bar{\omega} + \mathcal{F}_2(s, t(x))) + \mathcal{F}_3(s, t(x))x\omega\bar{p}^2 \right\}. \end{aligned} \quad (\text{A.18})$$

The matrix valued potential can be transformed by a non-unitary transformation to new states $|1_c^{(+)}, J\rangle$ and $|2_c^{(+)}, J\rangle$ defined as

$$\begin{aligned} |1_c^{(+)}, J\rangle &= p^{J-1} \left(|1_+, J\rangle + \sqrt{\frac{J}{1+J}} \frac{\omega}{M} |0, J\rangle \right) \\ |2_c^{(+)}, J\rangle &= \frac{p^{J+1}}{M} |0, J\rangle \end{aligned} \quad (\text{A.19})$$

As described in detail in [130] this ensures that projectors to given J^P are free of kinematical singularities. The

new transition matrix elements are given by

$$\begin{aligned}
\langle 1_c^{(+)}, J | \mathcal{T} | 1_c^{(+)}, J \rangle &= \int_{-1}^1 dx \frac{1}{2} (p\bar{p})^{1-J} \left\{ p\bar{p} \mathcal{F}_5(s, t(x)) \left(\frac{x(1-x^2) P'_J(x)}{J(J+1)} - (1-x^2) P_J(x) \right) \right. \\
&\quad \left. + \mathcal{F}_1(s, t(x)) \left(-x P_J(x) - \frac{(1-x^2) P'_J(x)}{J(J+1)} \right) \right\}, \\
\langle 1_c^{(+)}, J | \mathcal{T} | 2_c^{(+)}, J \rangle &= \int_{-1}^1 dx \frac{1}{2} \bar{p}^2 (p\bar{p})^{-J-1} \left\{ \sqrt{\frac{J}{J+1}} \omega p \bar{p} (P_J(x) - x P_{J+1}(x)) \mathcal{F}_5(s, t(x)) \right. \\
&\quad \left. + \sqrt{\frac{J}{J+1}} \omega P_{J+1}(x) \mathcal{F}_1(s, t(x)) + \frac{p^2 (1-x^2) P'_J(x) \mathcal{F}_4(s, t(x))}{\sqrt{J(J+1)}} \right\}, \\
\langle 2_c^{(+)}, J | \mathcal{T} | 1_c^{(+)}, J \rangle &= \int_{-1}^1 dx \frac{1}{2} p^2 (p\bar{p})^{-J-1} \left\{ \sqrt{\frac{J}{J+1}} p \bar{p} \bar{\omega} (P_J(x) - x P_{J+1}(x)) F_5(s, t(x)) \right. \\
&\quad \left. + \sqrt{\frac{J}{J+1}} \bar{\omega} P_{J+1}(x) F_1(s, t(x)) + \frac{\bar{p}^2 (1-x^2) P'_J(x) F_3(s, t(x))}{\sqrt{J(J+1)}} \right\}, \\
\langle 2_c^{(+)}, J | \mathcal{T} | 2_c^{(+)}, J \rangle &= \int_{-1}^1 dx \frac{1}{2} (p\bar{p})^{-J-1} \left\{ (-P_{J+1}(x) (p^2 (-\bar{\omega}) F_4(s, t(x)) - \omega \bar{p}^2 F_3(s, t(x))) + \right. \\
&\quad p \omega \bar{p} \bar{\omega} \left(\frac{(2J+1)x P_{J+1}(x)}{J+1} - \frac{J P_J(x)}{J+1} \right) F_5(s, t(x)) \\
&\quad \left. + p \bar{p} P_J(x) F_2(s, t(x)) - \frac{(2J+1)\omega \bar{\omega} P_{J+1}(x) F_1(s, t(x))}{J+1} \right\} \tag{A.20}
\end{aligned}$$

One should notice that this procedure changes the normalization of the states as given in Eq. (5.64).

A.3 “Renormalization” of the BS equation

The BS equation can be rewritten as

$$\hat{T} = \hat{V} + \hat{V} \cdot \hat{G} \cdot \hat{T} = \hat{V} + \hat{V} \cdot \hat{G} \cdot \hat{V} + \hat{V} \cdot \hat{G} \cdot \hat{V} \cdot \hat{G} \cdot \hat{V} + \dots, \quad (\text{A.21})$$

where we assume that the potential \hat{V} can be factorized from the loop function \hat{G} . Effects from coupled channels and from off-shell terms are encoded in the symbolical way of writing this equation¹. Now we decompose $\hat{V} = \hat{V}_0 + \hat{V}_1$, where \hat{V}_0 is the potential and \hat{V}_1 is a correction up to arbitrary order. In the following we determine \hat{V}_1 such that all divergences from an iteration of \hat{V}_0 are cancelled. We decompose $\hat{G} = \hat{G}_r + \hat{R}$, where \hat{G}_r is the finite renormalized loop function and \hat{R} is the divergent part. We make the Ansatz

$$\hat{V}_1 = \hat{V}_0 \cdot \sum_{i=1}^{\infty} (-\hat{R} \cdot \hat{V}_0)^i = \hat{V}_0 \cdot [(1 + \hat{R} \cdot \hat{V}_0)^{-1} - 1]. \quad (\text{A.22})$$

This sum renormalizes the iteration of the potential \hat{V}_0 , as can be seen as follows

$$\hat{T} = (1 - \hat{V} \cdot \hat{G})^{-1} \cdot \hat{V} \quad (\text{A.23})$$

$$\begin{aligned} &= [1 - (\hat{V}_0 + \hat{V}_1) \cdot (\hat{G}_r + \hat{R})]^{-1} \cdot (\hat{V}_0 + \hat{V}_1) \\ &= \left[(1 + \hat{R} \cdot \hat{V}_0) \cdot \hat{V}_0^{-1} \cdot [1 - \hat{V}_0 \cdot (1 + \hat{R} \cdot \hat{V}_0)^{-1} \cdot (\hat{G}_r + \hat{R})] \right]^{-1} \\ &= \left[[(\hat{V}_0^{-1} + \hat{R}) - (\hat{G}_r + \hat{R})] \right]^{-1} = [1 - \hat{V}_0 \cdot \hat{G}_r]^{-1} \hat{V}_0. \end{aligned} \quad (\text{A.24})$$

Therefore it is practically sufficient to replace the divergent loop matrix \hat{G} by the finite renormalized \hat{G}_r and \hat{V} by \hat{V}_0 .

An equivalent proof can be obtained by demanding

$$\frac{d}{d\bar{\epsilon}} \hat{T} = 0, \quad (\text{A.25})$$

where the part to be subtracted is rewritten as $\hat{R} \equiv \bar{\epsilon} \hat{R}_0$, where \hat{R}_0 is a matrix that contains all divergences. Inserting the solution (A.21) into equation (A.25) gives

$$\hat{V}' + (\hat{V}' \cdot (\hat{G}_r + \bar{\epsilon} \hat{R}_0) + \hat{V} \cdot \hat{R}_0) \cdot [1 - \hat{V} \cdot (\hat{G}_r + \bar{\epsilon} \hat{R}_0)]^{-1} \cdot V = 0 \quad (\text{A.26})$$

where the derivative has been abbreviated by ($\hat{V}' = \frac{d}{d\bar{\epsilon}} \hat{V}$). This identity implies

$$\hat{V} = \hat{c} \cdot (1 + \bar{\epsilon} \hat{R}_0 \cdot \hat{c})^{-1}, \quad (\text{A.27})$$

where $\hat{c} = \hat{V}_0$ in accordance with the right side of equation (A.21). This sum obeys Eq. (A.25), as can be easily seen by using

$$\hat{V}'(\bar{\epsilon}) = -\hat{c} \cdot (1 + \bar{\epsilon} \hat{R}_0 \cdot \hat{c})^{-1} \cdot \hat{R}_0 \cdot \hat{c} \cdot (1 + \bar{\epsilon} \hat{R}_0 \cdot \hat{c})^{-1} = -\hat{V} \cdot \hat{R}_0 \cdot \hat{V} \quad (\text{A.28})$$

¹It should be clear from Section 5.5 that not all potentials can be cast into this factorized form

in Eq. (A.26) to obtain

$$\begin{aligned}
\hat{V}'(\bar{\epsilon}) &= -(\hat{V}' \cdot (\hat{G}_r + \bar{\epsilon}\hat{R}_0) + \hat{V} \cdot \hat{R}_0) \cdot [1 - \hat{V} \cdot (\hat{G}_r + \bar{\epsilon}\hat{R}_0)]^{-1} \cdot V \\
&= (\hat{V} \cdot \hat{R}_0 \cdot \hat{V} \cdot (\hat{G}_r + \bar{\epsilon}\hat{R}_0) - \hat{V} \cdot \hat{R}_0) \cdot [1 - \hat{V} \cdot (\hat{G}_r + \bar{\epsilon}\hat{R}_0)]^{-1} \cdot V \\
&= -\hat{V} \cdot \hat{R}_0 \cdot (1 - \hat{V} \cdot (\hat{G}_r + \bar{\epsilon}\hat{R}_0)) \cdot [1 - \hat{V} \cdot (\hat{G}_r + \bar{\epsilon}\hat{R}_0)]^{-1} \cdot V = -\hat{V} \cdot \hat{R}_0 \cdot \hat{V}.
\end{aligned}
\tag{A.29}$$

Therefore (A.25) is fulfilled.

A.4 Charmed and bottomed mesons from PDG [1]

TABLE A.1: Charmed meson resonances listed in Particle Data Group [1].

	$I(J^P)$	Mass[MeV]	Width Γ	established
D^\pm	$\frac{1}{2}(0^-)$	1869.5 ± 0.4		×
D^0	$\frac{1}{2}(0^-)$	1864.91 ± 0.17		×
$D^*(2007)^0$	$\frac{1}{2}(1^-)$	2006.98 ± 0.15	$< 2.1 \text{ MeV}$	×
$D^*(2010)^\pm$	$\frac{1}{2}(1^-)$	2010.28 ± 0.13	$(96 \pm 4 \pm 22) \text{ keV}$	×
$D_0^*(2400)^0$	$\frac{1}{2}(0^+)$	2318 ± 29	$(267 \pm 40) \text{ MeV}$	×
$D_0^*(2400)^\pm$	$\frac{1}{2}(0^+)$	$2403 \pm 14 \pm 35$	$(283 \pm 24 \pm 34) \text{ MeV}$	
$D_1(2420)^0$	$\frac{1}{2}(1^+)$	2420.9 ± 0.8	$(27.1 \pm 2.7) \text{ MeV}$	×
$D_1(2420)^\pm$	$\frac{1}{2}(?)$	2423.4 ± 3.1	$(25 \pm 6) \text{ MeV}$	
$D_1(2430)^0$	$\frac{1}{2}(1^+)$	$2427 \pm 26 \pm 25$	$(384_{-75}^{+107} \pm 74) \text{ MeV}$	
$D_2^*(2460)^0$	$\frac{1}{2}(2^+)$	2461.8 ± 0.8	$(49.0 \pm 1.4) \text{ MeV}$	×
$D_2^*(2460)^\pm$	$\frac{1}{2}(2^+)$	2464.4 ± 1.9	$(37 \pm 6) \text{ MeV}$	×
$D(2550)^0$	$\frac{1}{2}(0^-)$	$2539.4 \pm 4.5 \pm 6.8$	$(130 \pm 12 \pm 13) \text{ MeV}$	
$D(2600)$	$\frac{1}{2}(?)$	2612 ± 6	$(93 \pm 6 \pm 13) \text{ MeV}$	
$D^*(2640)^\pm$	$\frac{1}{2}(?)$	$2637 \pm 2 \pm 6$	$< 15 \text{ MeV}$	
$D^*(2750)$	$\frac{1}{2}(?)$	2761 ± 5	$(63 \pm 6) \text{ MeV}$	

TABLE A.2: Charmed, strange meson resonances listed in Particle Data Group [1].

	$I(J^P)$	Mass[MeV]	Γ	established
D_s^\pm	$0(0^-)$	1969.0 ± 1.4		×
$D_s^{*\pm}$	$0(?^?)$	2112.3 ± 0.5	$< 1.9 \text{ MeV}$	×
$D_{s0}^*(2317)$	$0(0^+)$	2318.0 ± 1.0	$< 3.8 \text{ MeV}$	×
$D_{s1}(2460)^\pm$	$0(1^+)$	2459.6 ± 0.9	$< 3.5 \text{ MeV}$	×
$D_{s1}^*(2536)^\pm$	$0(1^+)$	2535.18 ± 0.24	$(0.92 \pm 0.03 \pm 0.04) \text{ MeV}$	×
$D_{s2}^*(2573)$	$0(?^?)$	2571.9 ± 0.8	$(17 \pm 4) \text{ MeV}$	×
$D_{s1}^*(2700)^\pm$	$0(1^-)$	2709_{-6}^{+9}	$(125 \pm 30) \text{ MeV}$	
$D_{sJ}^*(2860)$	$0(?^?)$	$2862 \pm 2_{-2}^{+5}$	$(48 \pm 3 \pm 6) \text{ MeV}$	
$D_{sJ}(3040)^\pm$	$0(?^?)$	$3044 \pm 8_{-5}^{+30}$	$(239 \pm 35_{-42}^{+46}) \text{ MeV}$	

TABLE A.3: Bottomed meson resonances listed in Particle Data Group [1].

	$I(J^P)$	Mass[MeV]	Width Γ	established
B^\pm	$\frac{1}{2}(0^-)$	5279.25 ± 0.26		×
B^0	$\frac{1}{2}(0^-)$	5279.55 ± 0.26		×
B^*	$\frac{1}{2}(1^-)$	5325.2 ± 0.4		×
$B_1(5721)^0$	$\frac{1}{2}(1^+)$	5723.5 ± 2.0	?	
$B_J^*(5732)$	$?(?^?)$	5698 ± 8	$(128 \pm 18) \text{ MeV}$	×
$B_2^*(5747)^0$	$\frac{1}{2}(2^+)$	5743 ± 5	$22.7_{-3.2-10.2}^{+3.8+3.2} \text{ MeV}$	×

TABLE A.4: Bottomed, strange meson resonances listed in Particle Data Group [1].

	$I(J^P)$	Mass[MeV]	Width Γ	established
B_s^0	$0(0^-)$	5366.7 ± 0.4		×
B_s^*	$0(1^-)$	5415.8 ± 1.5		×
$B_{s1}(5830)^0$	$0(1^+)$	5829.4 ± 0.7	?	×
$B_{s2}^*(5840)^0$	$0(2^+)$	5839.7 ± 0.6	?	×
$B_{sJ}^*(5850)$	$?(?^?)$	5853 ± 15	$(47 \pm 22) \text{ MeV}$	

Bibliography

- [1] J. Beringer et al. (Particle Data Group), Phys. Rev. D **86**, 010001 (2012)
- [2] E. Blucher and W.J. Marciano, “Vud, Vus, the Cabibbo Angle and CKM Unitarity,” (Particle Data Group), Phys. Rev. D **86**, 010001 (2012)
- [3] J. Laiho, E. Lunghi and R. S. Van de Water, Phys. Rev. D **81** (2010) 034503 [arXiv:0910.2928 [hep-ph]].
- [4] M. Golterman, arXiv:0912.4042 [hep-lat].
- [5] <http://www.lepp.cornell.edu/Research/EPP/CLEO/>, <http://belle.kek.jp/>,
<http://www.slac.stanford.edu/BF/>, <http://lhcb.web.cern.ch/lhcb/> .
- [6] B. Aubert *et al.* [BaBar Collaboration], Phys. Rev. Lett. **90** (2003) 242001 [hep-ex/0304021].
- [7] D. Besson *et al.* [CLEO Collaboration], Phys. Rev. D **68** (2003) 032002 [Erratum-ibid. D **75** (2007) 119908] [hep-ex/0305100].
- [8] S. Godfrey and R. Kokoski, Phys. Rev. D **43**, 1679 (1991); S. Godfrey and N. Isgur, Phys. Rev. D **32**, 189 (1985); M. Di Pierro and E. Eichten, Phys. Rev. D **64**, 114004 (2001).
- [9] J. Brodzicka *et al.* [Belle Collaboration], Phys. Rev. Lett. **100** (2008) 092001 [arXiv:0707.3491 [hep-ex]].
- [10] B. Aubert *et al.* [BaBar Collaboration], Phys. Rev. D **80** (2009) 092003 [arXiv:0908.0806 [hep-ex]].
- [11] B. Aubert *et al.* [BaBar Collaboration], Phys. Rev. Lett. **97** (2006) 222001 [hep-ex/0607082].
- [12] L. Liu, K. Orginos, F. -K. Guo, C. Hanhart and U. -G. Meissner, Phys. Rev. D **87** (2013) 014508 [arXiv:1208.4535 [hep-lat]].
- [13] N. Isgur and M. B. Wise, Adv. Ser. Direct. High Energy Phys. **10** (1992) 549.
- [14] H. Georgi, “Heavy quark effective field theory,” HUTP-91-A039.
- [15] M. Neubert, Phys. Rept. **245** (1994) 259 [hep-ph/9306320].
- [16] F. Hussain and G. Thompson, hep-ph/9502241.
- [17] A. V. Manohar, M. B. Wise, Camb. Monogr. Part. Phys. Nucl. Phys. Cosmol. **10**, 1-191 (2000).

- [18] M. E. Peskin and D. V. Schroeder, Reading, USA: Addison-Wesley (1995) 842 p
- [19] A. F. Falk, B. Grinstein and M. E. Luke, Nucl. Phys. B **357** (1991) 185.
- [20] J. G. Körner and G. Thompson, Phys. Lett. B **264** (1991) 185.
- [21] J. Gasser and H. Leutwyler, Annals Phys. **158** (1984) 142.
- [22] J. Gasser and H. Leutwyler, Nucl. Phys. B **250** (1985) 465.
- [23] S. Scherer, Adv. Nucl. Phys. **27** (2003) 277 [hep-ph/0210398].
- [24] M. Gell-Mann, R. J. Oakes and B. Renner, Phys. Rev. **175** (1968) 2195.
- [25] E. Follana, C. T. H. Davies, G. P. Lepage and J. Shigemitsu [HPQCD Collaboration and UKQCD Collaboration], Phys. Rev. Lett. **100**, 062002 (2008).
- [26] W. J. Marciano and A. Sirlin, Phys. Rev. Lett. **71** (1993) 3629.
- [27] C. Amsler *et al.* [Particle Data Group], Phys. Lett. B **667**, 1 (2008).
- [28] A. Dougall *et al.* [UKQCD Collaboration], Phys. Lett. B **569** (2003) 41 [hep-lat/0307001].
- [29] G. S. Bali, Phys. Rev. D **68** (2003) 071501 [hep-ph/0305209].
- [30] G. S. Bali *et al.* [SESAM Collaboration], Phys. Rev. D **71** (2005) 114513 [hep-lat/0505012].
- [31] K. Terasaki, Phys. Rev. D **68** (2003) 011501 [hep-ph/0305213].
- [32] J. Vijande, F. Fernandez and A. Valcarce, Phys. Rev. D **73** (2006) 034002 [Erratum-ibid. D **74** (2006) 059903] [hep-ph/0601143].
- [33] M. B. Wise, Phys. Rev. D **45**, 2188 (1992).
- [34] B. A. Dobrescu and A. S. Kronfeld, Phys. Rev. Lett. **100**, 241802 (2008).
- [35] J. P. Alexander *et al.* [CLEO Collaboration], Phys. Rev. D **79**, 052001 (2009).
- [36] P. U. E. Onyisi *et al.* [CLEO Collaboration], Phys. Rev. D **79**, 052002 (2009).
- [37] P. Naik *et al.* [CLEO Collaboration], Phys. Rev. D **80**, 112004 (2009).
- [38] J. P. Lee *et al.* [The BABAR Collaboration], arXiv:1003.3063 [hep-ex].
- [39] L. Widhalm *et al.* [Belle Collaboration], Phys. Rev. Lett. **100**, 241801 (2008).
- [40] K. Nakamura *et al.* [Particle Data Group], J. Phys. G **37**, 075021 (2010)
- [41] The Heavy Flavor Averaging Group *et al.*, <http://www.slac.stanford.edu/xorg/hfag>.

- [42] C. T. H. Davies, C. McNeile, E. Follana, G. P. Lepage, H. Na and J. Shigemitsu, arXiv:1008.4018 [hep-lat].
- [43] H. Na, C. T. H. Davies, E. Follana, G. P. Lepage and J. Shigemitsu, arXiv:1008.4562 [hep-lat].
- [44] A. Bazavov *et al.* [Fermilab Lattice and MILC Collaborations], PoS **LAT2009**, 249 (2009).
- [45] B. Blossier *et al.*, JHEP **0907**, 043 (2009).
- [46] T. M. Yan, H. Y. Cheng, C. Y. Cheung, G. L. Lin, Y. C. Lin and H. L. Yu, Phys. Rev. D **46**, 1148 (1992) [Erratum-ibid. D **55**, 5851 (1997)].
- [47] G. Burdman and J. F. Donoghue, Phys. Lett. B **280**, 287 (1992).
- [48] R. Casalbuoni, A. Deandrea, N. Di Bartolomeo, R. Gatto, F. Feruglio and G. Nardulli, Phys. Rept. **281**, 145 (1997).
- [49] L. S. Geng, N. Kaiser, J. Martin-Camalich and W. Weise, Phys. Rev. D **82**, 054022 (2010).
- [50] A. Walker-Loud *et al.*, Phys. Rev. D **79**, 054502 (2009).
- [51] K. I. Ishikawa *et al.* [PACS-CS Collaboration], Phys. Rev. D **80**, 054502 (2009).
- [52] J. Martin Camalich, L. S. Geng and M. J. Vicente Vacas, Phys. Rev. D **82**, 074504 (2010).
- [53] X. H. Guo and A. W. Thomas, Phys. Rev. D **65**, 074019 (2002).
- [54] J. Hein, S. Collins, C. T. H. Davies *et al.*, Phys. Rev. **D62**, 074503 (2000).
- [55] B. Grinstein, E. E. Jenkins, A. V. Manohar, M. J. Savage and M. B. Wise, Nucl. Phys. B **380**, 369 (1992).
- [56] J. L. Goity, Phys. Rev. D **46**, 3929 (1992).
- [57] C. G. Boyd and B. Grinstein, Nucl. Phys. B **442**, 205 (1995).
- [58] J. Gegelia and G. Japaridze, Phys. Rev. D **60**, 114038 (1999).
- [59] T. Fuchs, J. Gegelia, G. Japaridze and S. Scherer, Phys. Rev. D **68**, 056005 (2003).
- [60] L. S. Geng, J. Martin Camalich, L. Alvarez-Ruso and M. J. V. Vacas, Phys. Rev. Lett. **101**, 222002 (2008).
- [61] L. S. Geng, J. Martin Camalich and M. J. Vicente Vacas, Phys. Rev. D **79**, 094022 (2009).
- [62] J. Gasser, M. E. Sainio and A. Svarc, Nucl. Phys. B **307** (1988) 779.
- [63] T. Muta, World Sci. Lect. Notes Phys. **57** (1998) 1.
- [64] A. Abada *et al.*, Nucl. Phys. B **376**, 172 (1992).

- [65] K. C. Bowler, L. Del Debbio, J. M. Flynn, G. N. Lacagnina, V. I. Lesk, C. M. Maynard and D. G. Richards [UKQCD Collaboration], Nucl. Phys. B **619**, 507 (2001).
- [66] H. Ohki, H. Matsufuru and T. Onogi, Phys. Rev. D **77**, 094509 (2008).
- [67] D. Becirevic, B. Blossier, E. Chang and B. Haas, Phys. Lett. B **679**, 231 (2009).
- [68] E. Gamiz *et al.* [HPQCD Collaboration], Phys. Rev. **D80**, 014503 (2009).
- [69] B. Grinstein, Phys. Rev. Lett. **71**, 3067-3069 (1993).
- [70] C. Aubin *et al.*, Phys. Rev. Lett. **95**, 122002 (2005).
- [71] J. Simone *et al.* [Fermilab Lattice and MILC Collaborations], PoS **LATTICE2010** (2010) 317.
- [72] Y. Namekawa *et al.* [PACS-CS Collaboration], arXiv:1104.4600 [hep-lat].
- [73] C. Albertus *et al.*, Phys. Rev. D **82**, 014505 (2010).
- [74] D. Becirevic, P. Boucaud, J. P. Leroy, V. Lubicz, G. Martinelli, F. Mescia and F. Rapuano, Phys. Rev. D **60**, 074501 (1999).
- [75] C. Bernard *et al.*, Phys. Rev. D **65**, 014510 (2002).
- [76] S. Collins, C. T. H. Davies, U. M. Heller, A. Ali Khan, J. Shigemitsu, J. H. Sloan and C. Morningstar, Phys. Rev. D **60**, 074504 (1999).
- [77] C. T. H. Davies, private communication.
- [78] L. S. Geng, M. Altenbuchinger and W. Weise, Phys. Lett. B **696** (2011) 390 [arXiv:1012.0666 [hep-ph]].
- [79] J. Bulava, M. A. Donnellan and R. Sommer [ALPHA Collaboration], PoS **LATTICE2010**, 303 (2010).
- [80] N. Di Bartolomeo, R. Gatto, F. Feruglio and G. Nardulli, Phys. Lett. B **347**, 405 (1995).
- [81] M. E. Bracco, M. Chiapparini, F. S. Navarra and M. Nielsen, arXiv:1104.2864 [hep-ph].
- [82] A. M. Badalian, B. L. G. Bakker and Yu. A. Simonov, Phys. Rev. D **75**, 116001 (2007).
- [83] D. Ebert, R. N. Faustov and V. O. Galkin, Phys. Lett. B **635**, 93 (2006).
- [84] H. -M. Choi, Phys. Rev. **D75**, 073016 (2007).
- [85] P. Krokovny *et al.* [Belle Collaboration], Phys. Rev. Lett. **91**, 262002 (2003) [hep-ex/0308019].
- [86] W. A. Bardeen, E. J. Eichten and C. T. Hill, Phys. Rev. D **68**, 054024 (2003).
- [87] M. A. Nowak, M. Rho and I. Zahed, Acta Phys. Polon. B **35**, 2377 (2004).
- [88] E. van Beveren and G. Rupp, Phys. Rev. Lett. **91**, 012003 (2003).

- [89] Y. B. Dai, C. S. Huang, C. Liu and S. L. Zhu, Phys. Rev. D **68**, 114011 (2003).
- [90] S. Narison, Phys. Lett. B **605**, 319 (2005).
- [91] Y. Q. Chen and X. Q. Li, Phys. Rev. Lett. **93**, 232001 (2004).
- [92] A. P. Szczepaniak, Phys. Lett. B **567**, 23 (2003).
- [93] T. E. Browder, S. Pakvasa and A. A. Petrov, Phys. Lett. B **578**, 365 (2004).
- [94] H. Y. Cheng and W. S. Hou, Phys. Lett. B **566**, 193 (2003).
- [95] T. Barnes, F. E. Close and H. J. Lipkin, Phys. Rev. D **68**, 054006 (2003).
- [96] E. E. Kolomeitsev and M. F. M. Lutz, Phys. Lett. B **582**, 39 (2004).
- [97] F. K. Guo, P. N. Shen, H. C. Chiang and R. G. Ping, Phys. Lett. B **641**, 278 (2006).
- [98] D. Gamermann, E. Oset, D. Strottman and M. J. Vicente Vacas, Phys. Rev. D **76**, 074016 (2007).
- [99] S. -L. Zhu, Int. J. Mod. Phys. E **17**, 283 (2008) [hep-ph/0703225].
- [100] C. Garcia-Recio, L. S. Geng, J. Nieves, L. L. Salcedo, E. Wang and J. -J. Xie, Phys. Rev. D **87**, 096006 (2013) [arXiv:1304.1021 [hep-ph]].
- [101] A. Ozpineci, C. W. Xiao and E. Oset, arXiv:1306.3154 [hep-ph].
- [102] M. F. M. Lutz and M. Soyeur, Nucl. Phys. A **813**, 14 (2008) [arXiv:0710.1545 [hep-ph]].
- [103] F. -K. Guo, C. Hanhart, S. Krewald and U. -G. Meissner, Phys. Lett. B **666**, 251 (2008) [arXiv:0806.3374 [hep-ph]].
- [104] M. Cleven, F. -K. Guo, C. Hanhart, U. -G. Meissner, Eur. Phys. J. **A47**, 19 (2011). [arXiv:1009.3804 [hep-ph]].
- [105] A. M. Torres, L. R. Dai, C. Koren, D. Jido, E. Oset, [arXiv:1109.0396 [hep-lat]].
- [106] J. Hofmann, M. F. M. Lutz, Nucl. Phys. **A733**, 142-152 (2004). [hep-ph/0308263].
- [107] F. -K. Guo, P. -N. Shen, H. -C. Chiang, Phys. Lett. **B647**, 133-139 (2007). [hep-ph/0610008].
- [108] Z. -W. Liu, Y. -R. Liu, X. Liu and S. -L. Zhu, Phys. Rev. D **84**, 034002 (2011) [arXiv:1104.2726 [hep-ph]].
- [109] M. Altenbuchinger, L. S. Geng and W. Weise, Phys. Lett. B **713**, 453 (2012) [arXiv:1109.0460 [hep-ph]].
- [110] L. -S. Geng, Front. Phys. China. **8**, 328 (2013) [arXiv:1301.6815 [nucl-th]].
- [111] P. Wang and X. G. Wang, Phys. Rev. D **86** (2012) 014030 [arXiv:1204.5553 [hep-ph]].

- [112] L. Liu, H. -W. Lin and K. Orginos, PoS LATTICE **2008**, 112 (2008) [arXiv:0810.5412 [hep-lat]].
- [113] E. E. Salpeter and H. A. Bethe, Phys. Rev. **84** (1951) 1232.
- [114] R. E. Cutkosky, J. Math. Phys. **1** (1960) 429.
- [115] G. 't Hooft and M. J. G. Veltman, NATO Adv. Study Inst. Ser. B Phys. **4** (1974) 177.
- [116] G. Ecker, J. Gasser, H. Leutwyler, A. Pich and E. de Rafael, Phys. Lett. B **223** (1989) 425.
- [117] F. -K. Guo, C. Hanhart and U. -G. Meissner, Eur. Phys. J. A **40** (2009) 171 [arXiv:0901.1597 [hep-ph]].
- [118] A. V. Manohar, hep-ph/9802419.
- [119] H. Georgi, Phys. Lett. B **240** (1990) 447.
- [120] L. M. Abreu, D. Cabrera, F. J. Llanes-Estrada and J. M. Torres-Rincon, Annals Phys. **326**, 2737 (2011) [arXiv:1104.3815 [hep-ph]].
- [121] M. F. M. Lutz and E. E. Kolomeitsev, Nucl. Phys. A **700** (2002) 193 [nucl-th/0105042].
- [122] J. A. Oller and E. Oset, Nucl. Phys. A **620** (1997) 438 [Erratum-ibid. A **652** (1999) 407] [hep-ph/9702314].
- [123] E. Oset and A. Ramos, Nucl. Phys. A **635** (1998) 99 [nucl-th/9711022].
- [124] N. Kaiser, P. B. Siegel and W. Weise, Nucl. Phys. A **594**, 325 (1995) [nucl-th/9505043].
- [125] A. Dobado and J. R. Pelaez, Phys. Rev. D **56**, 3057 (1997) [hep-ph/9604416].
- [126] J. A. Oller, E. Oset and J. R. Pelaez, Phys. Rev. D **59**, 074001 (1999) [Erratum-ibid. D **60**, 099906 (1999)] [Erratum-ibid. D **75**, 099903 (2007)] [hep-ph/9804209].
- [127] N. Kaiser, Eur. Phys. J. A **3**, 307 (1998).
- [128] J. A. Oller and E. Oset, Phys. Rev. D **60**, 074023 (1999) [hep-ph/9809337].
- [129] J. A. Oller and U. G. Meissner, Phys. Lett. B **500**, 263 (2001) [hep-ph/0011146].
- [130] M. F. M. Lutz and E. E. Kolomeitsev, Nucl. Phys. A **730**, 392 (2004) [nucl-th/0307039].
- [131] E. E. Kolomeitsev and M. F. M. Lutz, AIP Conf. Proc. **717** (2004) 665 [hep-ph/0311205].
- [132] K. Abe *et al.* [Belle Collaboration], Phys. Rev. Lett. **92** (2004) 012002 [hep-ex/0307052].
- [133] B. Aubert *et al.* [BABAR Collaboration], Phys. Rev. D **69** (2004) 031101 [hep-ex/0310050].
- [134] B. Aubert *et al.* [BABAR Collaboration], Phys. Rev. D **74** (2006) 032007 [hep-ex/0604030].
- [135] L. Roca, E. Oset and J. Singh, Phys. Rev. D **72**, 014002 (2005) [hep-ph/0503273].

- [136] Y. -R. Liu, X. Liu and S. -L. Zhu, Phys. Rev. D **79**, 094026 (2009) [arXiv:0904.1770 [hep-ph]].
- [137] H. -B. Tang, hep-ph/9607436.
- [138] J. M. Link *et al.* [FOCUS Collaboration], Phys. Lett. B **586** (2004) 11 [hep-ex/0312060].
- [139] B. Aubert *et al.* [BABAR Collaboration], Phys. Rev. D **79** (2009) 112004 [arXiv:0901.1291 [hep-ex]].
- [140] K. Abe *et al.* [Belle Collaboration], Phys. Rev. D **69** (2004) 112002 [hep-ex/0307021].
- [141] T. Aaltonen *et al.* [CDF Collaboration], Phys. Rev. Lett. **100** (2008) 082001 [arXiv:0710.4199 [hep-ex]].
- [142] C. Hanhart, J. R. Pelaez and G. Rios, Phys. Rev. Lett. **100**, 152001 (2008) [arXiv:0801.2871 [hep-ph]].
- [143] J. Nieves and E. Ruiz Arriola, Nucl. Phys. A **679** (2000) 57 [hep-ph/9907469].
- [144] J. Nieves and E. Ruiz Arriola, Phys. Lett. B **455** (1999) 30 [nucl-th/9807035].
- [145] J. Nieves and E. Ruiz Arriola, Phys. Rev. D **63** (2001) 076001 [hep-ph/0008034].
- [146] J. Nieves and E. Ruiz Arriola, Phys. Rev. D **64** (2001) 116008 [hep-ph/0104307].
- [147] D. Djukanovic, J. Gegelia and S. Scherer, Eur. Phys. J. A **29** (2006) 337 [hep-ph/0604164].
- [148] B. Borasoy, P. C. Bruns, U. -G. Meissner and R. Nissler, Eur. Phys. J. A **34** (2007) 161 [arXiv:0709.3181 [nucl-th]].
- [149] P. C. Bruns, M. Mai and U. G. Meissner, Phys. Lett. B **697** (2011) 254 [arXiv:1012.2233 [nucl-th]].
- [150] M. Mai, P. C. Bruns and U. -G. Meissner, Phys. Rev. D **86** (2012) 094033 [arXiv:1207.4923 [nucl-th]].
- [151] M. Altenbuchinger and L. -S. Geng, arXiv:1310.5224 [hep-ph].
- [152] M. Altenbuchinger, L. -S. Geng and W. Weise, arXiv:1309.4743 [hep-ph].
- [153] E. E. Jenkins and A. V. Manohar, Phys. Lett. B **255** (1991) 558.
- [154] T. Becher and H. Leutwyler, Eur. Phys. J. C **9** (1999) 643 [hep-ph/9901384].
- [155] M. Jacob and G. C. Wick, Annals Phys. **7** (1959) 404 [Annals Phys. **281** (2000) 774].
- [156] A. R. Edmonds, "Angular Momentum in Quantum Mechanics," Princeton Univ. Press, Princeton, 1957.
- [157] J. Pagarán *et al.*, Computer Physics Communications 174 (2006) 616-630
- [158] D. A. Varshalovich, A. N. Moskalev and V. K. Khersonsky, "Quantum Theory Of Angular Momentum: Irreducible Tensors, Spherical Harmonics, Vector Coupling Coefficients, 3nj Symbols," SINGAPORE, SINGAPORE: WORLD SCIENTIFIC (1988) 514p